Master of Science in Offshore & Dredging Engineering
M.Sc. Graduation Thesis

**PIPELINE ROTATION ANALYSIS & MODELING DURING S-LAY INSTALLATION**

Delft University of Technology
Faculty of Mechanical, Maritime and Materials Engineering (3mE)

Sponsor : Allseas Engineering B.V.

George Katsikogiannis

August, 2015

Master of Science Graduation Thesis

*"Pipeline Rotation Analysis & Modeling during S-lay Installation"*

**Author**
George Katsikogiannis

Contact Info: *Tel: +31 617662659*
*Email: geo.katsikogiannis@gmail.com*

**Thesis Committee**

***Delft University of Technology*** Prof. dr. A.V. Metrikine (Chairman)
Dr. ir. F. P. van der Meer

***Allseas Engineering BV*** Dr. Eng. François Gerspach - Installation Engineer

The work in this thesis was supported by Allseas Engineering B.V. Their cooperation is hereby gratefully acknowledged.

**Delft University of Technology**

Department of
Offshore & Dredging Engineering (ODE)

The undersigned hereby certify that they have read and recommend to the Faculty of Mechanical, Maritime and Materials Engineering (3mE) for acceptance the thesis entitled

*"Pipeline Rotation Analysis & Modeling during S-lay Installation"*

by

G. Katsikogiannis

in partial fulfillment of the requirements for the degree of
Master of Science Offshore and Dredging Engineering.

*August 31, 2015*

**Chairman of the committee** ____________________
*Prof. dr. A.V. Metrikine*

**Members of the committee** ____________________
*Dr. Eng. François Gerspach*

____________________
*Dr. ir. F. P. van der Meer*

# I. ABSTRACT

The safety of offshore pipelines during installation has drawn a great deal of attention due to the combined actions of high external pressure, axial tension and bending moment. Subsea pipelines have the tendency to rotate during installation. This rotation can have multiple causes which are interfering with each other.

During S-lay installation, the pipe is exposed to plastic strains when it passes over the stinger, exceeding a certain curvature. That residual curvature causes the pipeline to rotate along its suspended length. Additional causes which contribute to pipe rotation are possible tensioner misalignments, pipeline curves or vessel offsets. Pipeline rotation is also dependent on other factors such as water depth, pipeline characteristics (bending stiffness, submerged weight, etc) and stinger configuration. Pipe rotation is not permissible if inline structures (valves, connections) are installed with the pipeline, it is therefore important to quantify the safety against roll for a given residual strain in the pipe due to plastic deformations over the stinger.

The goal of this thesis is to accurately quantify pipeline rotation during installation of inline structures with S-lay method. A sequential model is built based on mechanical principles in order to solve the pipelay and rotation problem simultaneously and identify the effect of the plastic strains and residual curvature on the rotation phenomenon. The model includes also mitigation measures (buoyancy modules) and their effect in the reduction of total rotation as well as the effect of soil friction.

The report consists of two main parts. The first part is the analytical mathematical modelling and the numerical solution of the pipe-laying problem, considering the pipeline as tensioned beam and solving the nonlinear bending equation along its suspended length using finite difference method. The second part consists of the rotation problem analysis and solution. Having found the pipeline configuration and its physical quantities along the length, the pipe rotation profile is found based on Hamilton's energy minimization principle using the Lagrangian equation, including soil friction and buoyancy module effect. Finally, a sequential model which simulates the installation of a pipeline including inline structures and buoyancy modules is built in order to investigate the roll profile evolution during real operations.

A number of different cases studied based on actual projects were conducted to determine the pipeline configuration and its physical quantities (bending moment, strain, axial tension) along its suspended length. The validity of the pipe-laying model is verified by means of a comparison with results obtained from the commercial finite element software OFFPIPE. Rotation results are verified by results observed in actual projects



***Keywords:*** *offshore pipeline; S-lay method; overbend ; sagbend ; residual curvature; reversed bending; pipeline rotation; Lagrangian principle ; energy minimization; finite difference method ; bvp4c ; OFFPIPE;*

## II. ACKNOWLEDGEMENTS


The research presented in this report was elaborated in the framework of my M.Sc. graduation thesis, during my postgraduate studies at Offshore & Dredging Engineering Department (Delft University of Technology). The duration of the thesis lasted 9 months (01/12/2014 - 31/08/2015) at Allseas Engineering B.V. (Delft) at the Pipeline Engineering Department.

First of all I would like to thank the supervisor of this work, François Gerspach, who trusted me from the beginning and gave me the chance to be part of Allseas. In addition, I would like to thank him for his cooperation during the whole period of the graduation work and the fact that he was always open for questions and discussion as well as for the freedom he gave me to apply my ideas on the problem whenever was possible. Furthermore, I would like to thank Vikrant Kumar, who was always willing to answer my questions and give me an insight about more practical issues considering offshore pipe laying operations, Dirk Sewdoelare who checked the validity of the code and Hugo Chaves from Innovations Department who was willing to listen to my questions about mathematical and numerical issues. Finally, it should be shame not to mention and thank all the staff of Allseas Engineering B.V. and specially of the Pipeline Engineering Department for the friendly working environment, which was one of the most important factors to be productive in a daily basis.

Except from the people in Allseas Engineering B.V., I have to thank the people from TU Delft who had a considerable contribution to the final result the thesis. First of all I would like to the chairman of the committee, Professor dr. A.V. Metrikine for his cooperation and his valuable suggestions for the improvement of the research. His deep knowledge in the field helped me become better as an engineer and have a more concrete view in the principles which govern structural mechanics. Also, I would like to thank my daily supervisor Dr. ir. Frans P. van der Meer for his interest in the topic and the fact that he was always willing to help me and give me his suggestions for further improvement.

The present work is dedicated to my family, who supports me all these years and to my best friends from the undergraduate years in Greece.

**Georgios E. Katsikogiannis**

**Delft, August 2015**

## TABLE OF CONTENTS

## LIST OF FIGURES

# LIST OF TABLES

## LIST OF SYMBOLS

| | | |
|---|---|---|
| $\mathbf{T_h}$ | Bottom Tension | [N] |
| $\mathbf{w_s}$ | Unit Submerged Weight | [N/m] |
| $\mathbf{w_d}$ | Dry Submerged Weight | [N/m] |
| $\mathbf{D}$ | Water Depth | [m] |
| $\mathbf{T}$ | Axial Tension along the catenary | [N] |
| $\mathbf{T(st)}$ | Axial Tension at the stinger tip | [N] |
| $\mathbf{M}$ | Bending Moment | [Nm] |
| $\mathbf{E}$ | Young's Modulus | $[\mathrm{N/m^2}]$ |
| $\mathbf{I_b}$ | Area moment of inertia | $[\mathrm{m^4}]$ |
| $\mathbf{I_t}$ | Polar moment of inertia | $[\mathrm{m^4}]$ |
| $\mathbf{r}$ | Pipeline radius | [m] |
| $\mathbf{R}$ | Pipeline radius of curvature | [m] |
| $\boldsymbol{\kappa}$ | Sagbend pipeline curvature | $[1/m]$ |
| $\boldsymbol{\kappa_0}$ | Nominal pipeline curvature | $[1/m]$ |
| $\boldsymbol{\kappa_r}$ | Residual curvature | $[1/m]$ |
| $\boldsymbol{\varepsilon_b}$ | Bending strain | $[-]$ |
| $\boldsymbol{\varepsilon_{ax}}$ | Axial strain | $[-]$ |
| $\boldsymbol{\varepsilon_h}$ | Hoop strain | $[-]$ |
| $\boldsymbol{\varepsilon_t}$ | Total strain | $[-]$ |
| $\mathbf{A}$ | Cross sectional area of pipeline | $[\mathrm{m^2}]$ |
| $\mathbf{D_o}$ | Outer diameter of pipeline | [m] |
| $\boldsymbol{t}$ | Pipeline wall thickness | [m] |
| $\boldsymbol{\gamma}$ | Specific weight of sea water | $[\mathrm{N/m^3}]$ |
| $\boldsymbol{L}$ | Pipeline suspended length | $[m]$ |
| $\boldsymbol{s}$ | Arc length along the catenary | $[m]$ |
| $\boldsymbol{\theta}$ | Angle between pipeline & $horizontal$ | $[rad]$ |
| $\boldsymbol{R_s}$ | Stinger Radius of curvature | $[m]$ |
| $\boldsymbol{R_r}$ | Rasidual Radius of curvature | $[m]$ |
| $\boldsymbol{R_{SB}}$ | Sagbend Radius of curvature | $[m]$ |
| $\boldsymbol{\varphi(s)}$ | Rotation Angle function of pipeline along the catenary | $[rad]$ |
| $\boldsymbol{\varphi_{ILS}}$ | Rotation Angle of ILS | $[rad]$ |
| $\boldsymbol{W_T}$ | Total work along the suspended length of the pipe | $[J]$ |
| $\boldsymbol{W_{Ax}}$ | Work due to axial tension | $[J]$ |
| $\boldsymbol{W_B}$ | Work due to bending | $[J]$ |
| $\boldsymbol{W_R}$ | Work due to rotation | $[J]$ |
| $\boldsymbol{T_{ILS}}$ | Overturning moment induced by inline structure | [Nm] |
| $\mathbf{w_{ILS}}$ | Submerged weight of the inline structure | [N] |
| $\mathbf{h_{CoG}}$ | Distance between CoG of the inline structure and the pipe centreline | $[m]$ |
| $\boldsymbol{T_{buoy}}$ | Overturning moment induced by buoyancy module | [Nm] |
| $\boldsymbol{T_{soil}}$ | Linearly distributed soil torque resisting pipe rotation | [Nm/m] |
| $\boldsymbol{L_{slip}}$ | Slip length of pipeline at the seabed | $[m]$ |
| $\boldsymbol{T_{TDP}}$ | Torque at the touchdown point | [Nm] |

## LIST OF ABBREVIATIONS

**ILS** Inline Structure
**TDP** Touchdown Point

# 1.0 INTRODUCTION

This chapter will give a short introduction to the Allseas Group and its activities. Moreover the most common methods of pipe-laying will be presented as a general introduction to the offshore pipe-laying industry.

## 1.1 Allseas Engineering B.V.

This thesis is sponsored by Allseas Engineering B.V. located in Delft, the Netherlands. Allseas Engineering B.V. is part of Swiss-based Allseas Groups S.A., one of the global leaders providing pipelay and subsea construction services in offshore oil & gas industry. Allseas Group was founded in 1985 and nowadays employs more than 2500 people worldwide. Allseas has a versatile of fleet including *Solitaire, Audacia, Lorelay, Calamity Jane,* and *Tog Mor*. Currently, Allseas' largest platform installation/decommissioning and pipelay vessel, *Pioneering Spirit,* is under the last stages of completion in the Alexiahaven, at the port of Rotterdam. The *Pioneering Spirit* is the largest vessel in the world (382 m length and 124 m width) and is to be used for the single-lift platform installation and decommissioning and laying large diameter pipes in unprecedented water depths (~3000 m). Allseas has developed its own automatic welding system Phoenix for welding offshore pipelines on board Allseas' vessels. This welding system, which uses various welding techniques, started operation in 1993.

Allseas uses the S-Lay method for pipeline installations. With this method, pipe joints are lined up on-board in an horizontal orientation. The pipe joints pass through a series of welding, coating and non-destructive testing stations and they leave the vessel, as she moves forward, through the use of a stinger. S-lay installation method allows for fast installation operations over a large range of water depths and pipe characteristics.

## 1.2 Pipe-laying methods

There are many different types of pipelines used in oil and gas industry. Infield lines connect different elements of the field, like satellite wells, subsea templates and production platforms. They are typically between 1 and 30 kilometres in length and range from 6" to 12" in diameter. From the production platforms there are export lines which connect the reservoir to a larger grid of trunk lines. These connecting export lines are up to 70 kilometres in length and range from 10" to 24" in diameter. Finally, there are the trunk lines for the transport of the hydrocarbons to shore. These are the largest pipelines, ranging from 100 to 1000 kilometres in length and 24" to 42" in diameter. Subsea pipeline installation is performed by specialized laying vessels. There are several methods to install a pipeline with the most common being S-lay, J-lay and reeling lay.

With *reeling method* both flexible and small diameter steel pipe can be installed. The steel pipe joints are welded onshore and winded onto a large reel on a vessel. The vessel will reach the offshore location where the pipe will be reeled off and placed on the seabed. Before leaving the reel the pipe is straightened and put under constant tension.

With *S-lay and J-lay* method the pipe is constructed entirely offshore. With J-lay, the pipeline is constructed vertically from 12-meter pipe sections. J-lay barges have a tower in which the new pieces of pipe are lined up for welding. After connecting a new piece, the barge is moved and the pipeline is shifted down the tower, making room for a new joint. With this method, all diameter pipes can be installed, but all welding and coating activities have to take place in the limited space of the vertical tower. With S-lay method, the pipe joints are not constructed vertically but horizontally. The entire length of the vessel can therefore be used as a production line enabling the consecutive execution of several welding-, coating and testing operations. This method increases significantly lay rates in comparison with J-lay. Further description and analysis of S-lay method will be done during later chapters.

Depending on the method, a subsea pipeline is exposed to different loads during installation from a laying vessel with the main of them include the hydrostatic pressure, tension and bending. In the present study, we will focus on the S-lay method. A more detailed description about the main principles of S-lay can be found in Chapter 3.0.

The pipe-laying ability of a laying vessel relates primarily to the submerged weight of the pipeline. As the water depth increases, so does the total weight of the pipeline in free span, between the laying vessel and the seafloor touchdown point; consequently higher tension is required. However, the weight can be reduced by either adding extra external buoyancy or increasing the angle of the departure of the pipeline from the laying vessel.

In order to ensure that the load effects on the pipeline are within the strength design criteria, static and dynamic installation analysis are conducted to estimate the minimum required laying tension for the pipeline for specific stinger configuration (length, radius), water depth and pipe characteristics (diameter, thickness, concrete coating) and structural properties (bending and torsional stiffness).

Structural analysis of pipelines experienced a significant increase of importance in the late 1960's and 1970's, when offshore development moved into deeper waters and more hostile environment. Simple approximations and rules of thumb used in 1950's and early 1960's were no longer adequate, and more complex methods had to be designed. This progress brought with it new and more complex problems in structural evaluation and analysis.

### 1.3 S-lay method

S-lay method is the latest method for installing subsea pipelines in both shallow and deep water, depending on the pipe properties and the laying capacity of the vessel. The method is referred as *S-lay method* because the profile of the pipeline between the stinger and the seabed forms an elongated S shape during the pipe laying operation. Pipeline while passing the firing line (see APPENDIX A for terminology), passes through a number of stations (welding, NDT, coating) and moves across the stern of the lay barge. Pipeline leaves the lay barge supported by a truss like circular structure equipped with rollers, known as a stinger.

In Figure 1-1, the major components and pipe sections of S-lay method are shown.

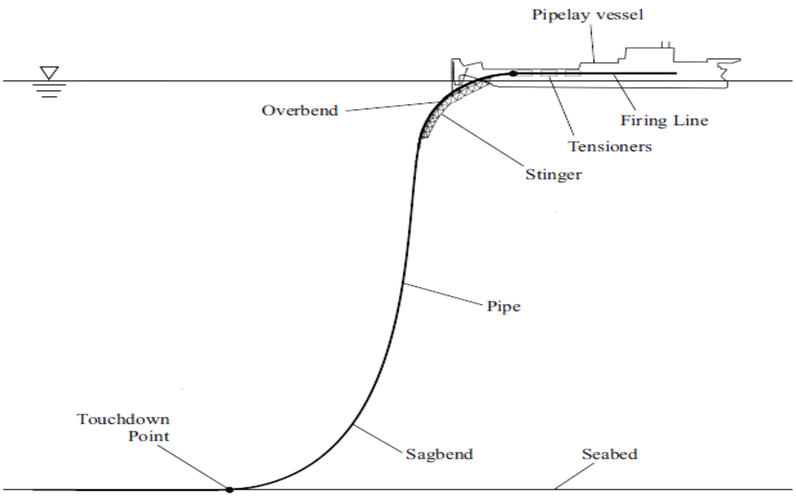


**Figure 1-1 Illustration of S-lay principle**

In general, the installation equipment on S-lay vessels include a dynamic positioning system, 2 or more tensioners which determine the laying capacity of the vessel, pipe cranes and a firing line which contains different stations from which the pipeline passes before leaving the barge through the stinger.

The purpose of the stinger in the S-lay installation is to control the deflection of the pipe in the overbend region. During actual operations, the pipe shall lift off smoothly from the stinger in order to avoid critical damage both to the pipeline and to the stinger due to local buckling. Eventual failure of the pipe joint can cause the complete abandonment of the installation operation. Usually, the pipe leaves the stinger from the second or third last roller box having a gap with the last roller box (stinger tip) of minimum 0.3 meters (for static analysis). This gap of 0.3 meters is well known as the *tip separation criterion* for the pipelay analysis. A global view of the Audacias' stinger is illustrated in Figure 1-2.

**Figure 1-2 Stinger global view (Audacia)**

S-lay method is commonly used in all kinds of deep-water pipe laying projects nowadays. In case of deep or ultra-deep waters, the departure angle of the pipe becomes so steep that the required stinger length may not be feasible. Deeper water depths result in a steeper lift off angle of the suspended pipe span at the stinger tip, which requires the stinger to be longer or more curved to accommodate the larger arc of curvature at the overbend region. Accordingly, more stinger buoyancy or higher structural strength is required to support the increased weight of the suspended pipe span.

### 1.3.1 S-lay Pipeline Configuration

The structural analysis of an offshore pipeline during installation deals with the computation of deformations, internal forces, and stresses as a result of external loads and the structural properties of the pipe. A short pipe section, like a single pipe joint seems to behave like a rigid body, whereas a long pipe of several hundred meters is very elastic and behaves almost like a string. For this reason, pipeline behavior is highly dependent on the water depth.

Figure 1-1 shows a typical static configuration for pipeline with S-lay method.

The static configuration of the pipeline during the pipelay operation depends on the installation method. For the S-lay method, the configuration is governed by the following parameters [4],[5].

1. Tension at the pipelay vessel and departure angle (see APPENDIX A for terminology)
2. Stinger characteristics (Radius-Length)
3. Pipeline characteristics (submerged weight, bending stiffness, etc.)
4. Water depth

The material properties of the pipeline, such as e.g., pipe diameter, wall thickness, weight, coating properties are determined in the design phase of the project in order to meet the operational needs for the pipeline. Once the pipe material properties are determined static and dynamic pipeline installation analysis can be performed.
The deformation of the pipeline from the stern of the pipelay vessel to the seabed, also known as configuration of pipeline, for an S-lay operation is in general split in two sections, namely *overbend* and *sagbend* (see APPENDIX A for terminology) as illustrated in Figure 1-1. A brief description over the different parts of the pipeline is included in the next sections.

### 1.3.2 Overbend Region

The overbend region is the fully supported region from the tension equipment over the stinger and to the stinger tip. The stinger supports the pipe on rollers spaced out along its length and controls the pipe geometry and curvature. From lift-off point and up, the pipe is *displacement-controlled, meaning that* the shape taken up by the pipeline in the overbend is controlled by the pipe supports on the vessel and by the stinger geometry and roller boxes on the stinger. The stinger radius yields a certain overbend strain, this strain has to be checked against allowable strain levels in international codes. The tension applied by the tensioners has almost no effect on the overbend configuration if the stinger is a rigid structure and only a small effect if the stinger is build-up of buoyant segments. During the movement of the vessel the pipeline travels smoothly from the vessel onto the stinger.

Figure 1-3 presents the roller boxes on the stinger of the *Solitaire* and the bending of the pipeline.

**Figure 1-3 Pipeline in the overbend on the stinger (Solitaire)**

### 1.3.3 Sagbend Region

The sagbend is the free span region that extends from the end of the stinger to the touchdown point. In the sagbend, the static load effect is governed by the tension, pipe submerged weight, external pressure and bending stiffness. The equilibrium configuration is load-controlled since there are no physical boundaries for the deformations that the pipeline can experience.

The shape taken up by the pipeline in the sagbend is primarily controlled by the interaction between the applied tension and the submerged weight of the pipeline, and to a lesser extent by the flexural rigidity of the pipeline. If the applied tension is increased, the radius of the pipeline in the sagbend increases, so the sagbend becomes longer and flatter, while the touchdown point moves further from the barge and the lift-off point moves up the stinger. Figure 1-4 presents the schematic view of the change of pipeline curvature. If the applied tension is reduced, the sagbend radius decreases, and the lift-off point moves down the stinger. If the tension is reduced too much the bending radius in the sagbend becomes too small and the lift-off point becomes the same point as the stinger tip. In both the sagbend and the lift-off point the pipeline may buckle. Therefore during pipelay operations, the correct tension is governed by the following two criteria*; the location of the lift-off point and the radius of the sagbend.*

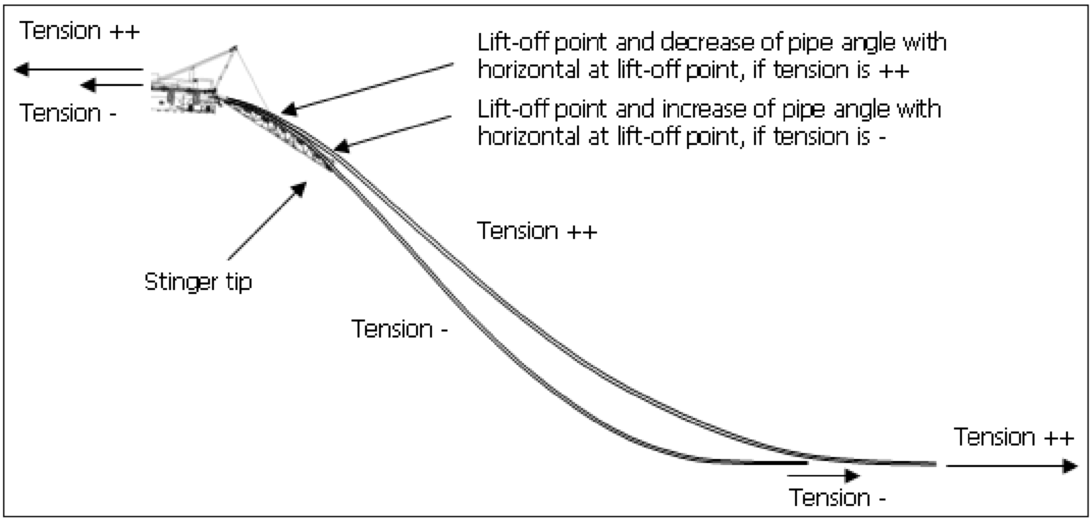


**Figure 1-4 Change of pipeline curvature resulting from changes in the applied tension**

## 2.0 SCOPE OF WORK

### 2.1 Problem Definition

Pipeline rotation is commonly observed during installation with S-lay. Most of the times the phenomenon is harmless for the pipeline itself but it can have serious consequences when installing inline structures. As the word indicates inline structures are attached structures as valves and tees that are welded between normal pipe sections in the main pipeline. When pipe rotation occurs these structures might land rotated over the acceptable limits (i.e. $10^{o}$) on the seabed making them difficult or impossible to access, which leads to very expensive and time consuming operations. Moreover pipe rotation influences stresses and strains in the pipe which should be reckoned with when installation classification demands are considered. Presently, pipeline rotation is still not thoroughly understood and several causes are considered to be influencing the phenomenon as

- Pipe residual curvature due to plastic strains in the overbend.
- Eccentric weight and C.o.G. position of the main line above the pipeline's centreline due to the presence of inline structure.
- Misalignment of the tensioners
- Environmental forces on an inline structure (current and waves)

So far, several attempts have been undertaken to determine the amount of pipe rotation. It was concluded in earlier research [16] that the primary reason for the occurrence of pipe rotation is the plastic deformation of the pipe in the overbend.

Expanding installation activities to deeper waters, requires more tension to carry the larger length of suspended pipeline. Without the appropriate tension the pipeline hanging between the vessel and the seabed can collapse under its own weight because bending strains exceed the acceptable limits and buckling can occur. Furthermore, deep-water installations demand thicker walled, thus heavier pipes to prevent collapse due to high external hydrostatic pressure. Based on the above, the tension required for deep-water projects increases significantly. In order to reduce and keep the tension within the limits of the tensioners capacity, it is common practice to increase the departure angle of the pipeline from the stinger. That happens because, firstly, the vertical component of the tension equals the weight of the suspended pipeline, which makes a steeper departure angle more efficient in carrying the weight and secondly, since the pipeline leaves the vessel at a steeper angle, the suspended length is smaller, which results in less weight hanging from the lay vessel.

Increasing the water depth of the installation requires therefore a steeper, near vertical departure angle of the pipeline from the stinger. Because the length of the stinger is limited, this can only be realized by a decrease in stinger radius, which can have as a consequence the exceedance of the elastic limit of the pipe material and the increase of the plastic strains.

Because of the fact that plastic deformations are non-reversible, pipeline leaves the stinger with a residual curvature. When the pipe joints pass the stinger and move to the sagbend area, are bent in the opposite direction and as a result the residual curvature has to be overcome. It is shown by a minimum energy approach that the configuration of the pipe at the sagbend is taken partially through bending and rotation. As mentioned above an inline structure usually needs to be installed within certain verticality tolerance to allow for future connection or ROV access. For this, the first step is to check the pipeline rotation. If rotation of the pipe is expected, measures are required to keep the structure vertical during -and after- installation. An effective means to install an ILS vertical is to attach buoyancy to the ILS and/or to the pipe using a yoke. For the ILS to remain vertical after installation, foundation has to be sufficient to overcome the possible residual torque from the pipeline.

## 2.2 Objective

The goal of this thesis is to accurately quantify pipeline rotation during installation of inline structures with S-lay method. A sequential model is built based on mechanical principles in order to solve the pipelay and rotation problem simultaneously and identify the effect of the plastic strains and residual curvature on the rotation phenomenon. The model includes also mitigation measures (buoyancy modules) and their effect in the reduction of total rotation as well as the effect of soil friction.

## 2.3 Approach

First of all the theory used in subsea pipeline analysis is discussed, including the definitions of all stresses, strains, and loads applicable to S-lay installation method. The first part of the research consists of the analytical mathematical modelling and the numerical solution of the pipe-laying problem, considering the pipeline as tensioned beam and solving the nonlinear bending equation along its suspended length using finite difference method. A sequential model which simulates the installation of a pipeline including inline structures and buoyancy modules is built in order to investigate the rotation profile evolution later.

The second part consists in the rotation problem analysis and solution. First, an explanation of the mechanism governing pipeline rotation is given, focusing exclusively on rotation induced by pipe residual curvature. Having found the pipe configuration and its physical quantities along the suspended length, the pipe rotation profile is found based on Hamilton's energy minimization principle using the Lagrangian equation. Then the method to determine inline structure stability along the catenary is described taking into account the effect of buoyancy modules and pipe-soil interaction.

Both the pipelay and the rotation problem are modeled and solved in Matlab software.

## 3.0 S-LAY STATIC PIPELAY ANALYSIS

In this chapter the several methods that have been used for the S-lay static analysis will be discussed. Attention will be paid to the nonlinear beam method, its mathematical formulation and numerical implementation for the solution of the pipelay problem.

### 3.1 Mathematical Model

There are several different mathematical models for the analysis of the behaviour of the pipeline free span between the stinger and the touchdown point. The most known are the linear and nonlinear beam method, the natural catenary the stiffened catenary method [8].

#### 3.1.1 Linear Beam Method

Using the linear beam method, the suspended length of the pipeline is considered as a continuous tensioned beam as shown in Figure 3-1.

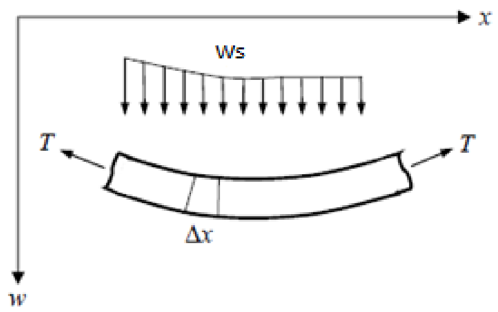


**Figure 3-1 Tensioned Beam**

The main assumption for the method is that the slopes of the beam are assumed to be small, so the following requirement is used

$$\frac{dw}{dx} \ll 0$$

where $dx$ and $dw$ are the increments in the horizontal and vertical direction respectively. Using the equilibrium of forces for a small segment along the suspended length of the pipe, the bending equation can be expressed as follows

$$E \cdot I_b \cdot \frac{d^4 w}{dx^4} - T \cdot \frac{d^2 w}{dx^2} - w_s = 0$$

where *EI* is the bending stiffness of the pipeline, T the acting axial force (tension) and *q1* the submerged weight of the pipeline (distributed external force with density per unit length). The application of this equation is constrained by the requirements that the slopes of the beam are small as mentioned before, the rotational inertia effects are neglected and the Euler-Bernoulli assumptions are not violated significantly. The current method *is applicable only for shallow waters.*

### 3.1.2 Nonlinear Beam Method

The nonlinear beam method considers the pipeline as a continuous beam as the linear beam method. In this model the bending of the pipe span is described by considering the non-linear bending equation of the beam using the equilibrium of forces on a pipe element of length ds. The method is valid for small and large slopes and is applicable to all water depths.
Specifically, is described by the following formula

$$E \cdot I_b \cdot \frac{d}{ds}\left(sec(\theta)\frac{d^2\theta}{ds^2}\right) - T_h \cdot sec^2(\theta) \cdot \frac{d\theta}{ds} + w_s = 0$$

where s is the distance along the pipe span and θ is the angle at distance s.

Boundary conditions may include the displacement at one of the two ends of the span, so the above differential equation can be described with z rather than θ. In order to do that, the following expression can be used

$$sin(\theta) = \frac{dz}{ds}$$

Due to the fact the model can be used for both shallow and deep waters and is valid for small and large slopes, it is considered to be the most suitable for our analysis. A detailed formulation of the model is described in Chapter 3.2.

### 3.1.3 Natural Catenary Method

Using the natural catenary method, the suspended length of the pipeline is considered as a chain, therefore the bending stiffness of the pipeline is neglected. An illustration of the method is illustrated in Figure 3-2.

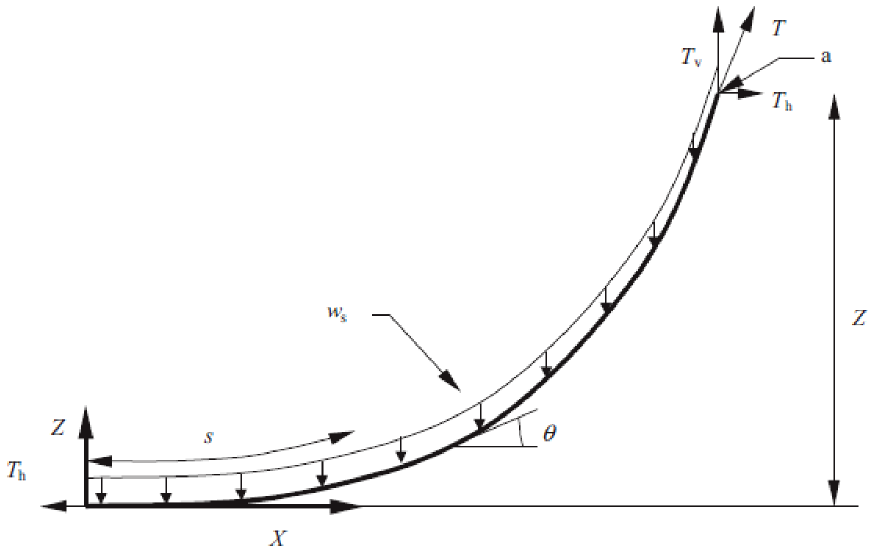


**Figure 3-2 Catenary Model**

The vertical position of the pipe can be obtained using the following equation

$$z = \frac{T_h}{w_s} \cdot \left( cosh\left(\frac{x \cdot w_s}{T_h}\right) - 1 \right)$$

where

x : horizontal distance from touchdown point
z : height above seabed,
$T_h$ : horizontal force at seabed
$w_s$ : submerged weight per unit length

The boundary conditions on pipeline span are not satisfied so this theory is applicable only for parts of the pipeline which are away from the ends. This method *is applicable only to pipelines in deep waters* where the stiffness of the pipe is very small compared to the submerged weight of the pipe and the applied axial tension.

### 3.1.4 Stiffened Catenary Method

Another way to perform calculations on the free span is to use the stiffened catenary method. What makes this method different from the catenary method is that it includes the bending stiffness of the pipeline. In addition the boundary conditions at the end are satisfied. One assumption that has to be made is that the non-dimensional term $\alpha^2$, which is a term depending on the stiffness, the submerged weight and the suspended length of the pipe has to be much lower than unity. This term is given by the following equation

$$a^2 = \frac{E \cdot I_b}{w_s \cdot L^3} \ll 1$$

The stiffened catenary method provides accurate results for the whole pipeline including the regions near the ends but it is mainly limited to deep-water applications.

## 3.2 Nonlinear Beam Method Analysis

In the next chapters, the mathematical model that was used for the solution of the pipelay problem is formulated in detail. In addition, the numerical approach and its implementation is described.

### 3.2.1 Mathematical Formulation

In this section, the nonlinear beam equation that was shown in Chapter 3.1.2 will be derived. Assuming that the pipe has uniform cross-section and weight distribution along its length, the governing equations for the pipeline span can be found by considering the static forces on a short segment of the tensioned pipe at equilibrium, as it can be seen from Figure 3-3.

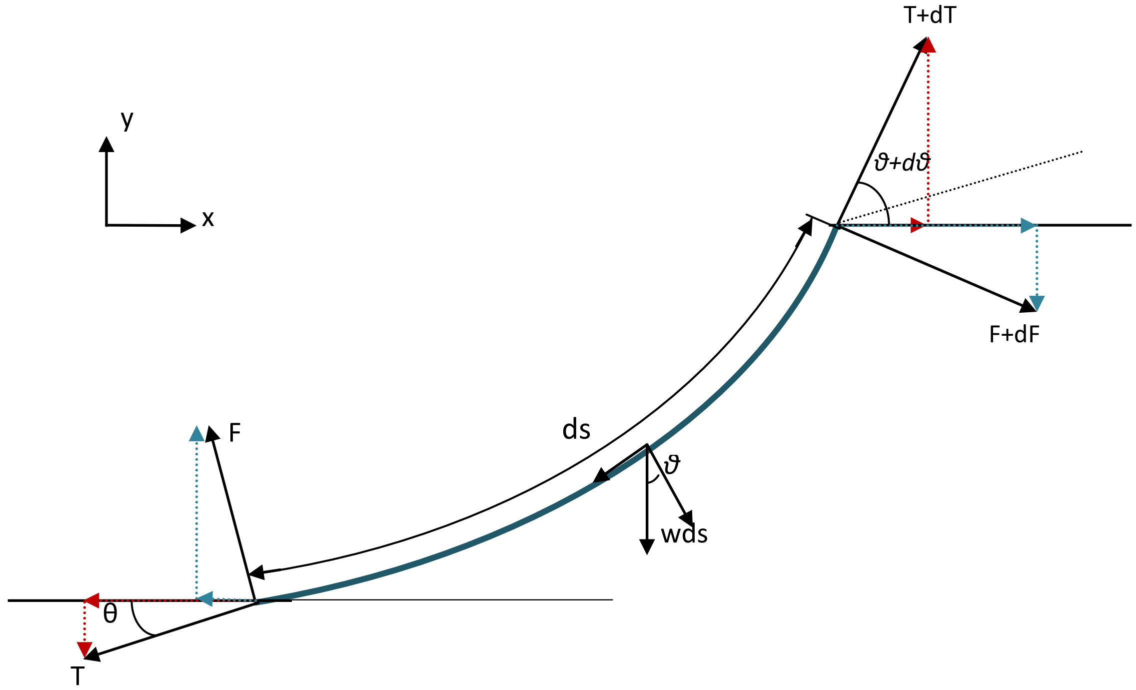


**Figure 3-3 Equilibrium of forces on a pipe element of length ds**

The equilibrium of forces in the vertical direction (y) yields,

$$\Sigma F_y = 0$$

$$(T + dT)sin(\theta + d\theta) - Tsin(\theta) - (F + dF)cos(\theta + d\theta) + Fcos(\theta) - w_s ds = 0 \qquad [\mathbf{3.1}]$$

Respectively, the equilibrium of forces in the horizontal direction (x) yields,

$$\Sigma F_x = 0$$

$$(T + dT)cos(\theta + d\theta) - Tcos(\theta) + (F + dF)sin(\theta + d\theta) - Fsin(\theta) = 0 \qquad [\mathbf{3.2}]$$

where $w_s$ is the submerged weight of the pipeline per unit length. Assuming small changes of the angle θ between the elements, so *dϑ<<1,* the terms of sinuses and cosines can be approximated by the following expressions

$$cos(\theta + d\theta) \approx cos(\theta) - sin(\theta)d\theta$$

$$sin(\theta + d\theta) \approx sin(\theta) + cos(\theta)d\theta$$

Replacing the expressions above into the equations 3.1 and 3.2, based on simple algebraic operations the following equation is derived

$$T\frac{d\theta}{ds} - \frac{dF}{ds} - w_s cos(\theta) = 0 \qquad [\mathbf{3.3}]$$

where dθ/ds is the exact expression for curvature κ. From Euler-Bernoulli beam theory [6],

$$\kappa = \frac{1}{R} = \frac{M}{EI_b} = \frac{d\theta}{ds}$$

Finally, the shear force can be replaced by the following expression [1],

$$F = \frac{dM}{ds}$$

Substituting these expressions into the equation 2.3, yields to the following differential equation which describes the pipelay problem

$$EI_b \frac{d^3\theta}{ds^3} - T\frac{d\theta}{ds} + w_s cos(\theta) = 0 \qquad [\mathbf{3.4}]$$

The forces equilibrium acting in the direction of the pipeline's centerline gives

$$T + w_s sin(\theta)ds = (T + dT)cos(d\theta)$$

Taking into account that for $d\theta << 1$, $cos(d\theta) = 1$, by simple algebraic operations the second equation can be derived

$$\frac{dT}{ds} = w_s sin(\theta) \qquad [\mathbf{3.5}]$$

At the touch down point the horizontal force acting at the pipeline is commonly known as bottom tension, as mentioned in APPENDIX A and is known during the pipe laying process as it depends on the forward motion of the vessel (which is controlled). Assuming that there are no horizontal forces acting along the suspended length of the pipe (e.g. currents), the following equation can be used for the equilibrium in x direction based on Figure 3-3

$$T_h = Tcos(\theta) + Fsin(\theta)$$

where $T_h$is the applied bottom tension. Substituting in the equation above the force F by the following term

$$F = \frac{dM}{ds} = E \cdot I_b \cdot \frac{d^2\theta}{ds^2}$$

we get

$$T_h = T \cdot cos(\theta) + E \cdot I_b \cdot \frac{d^2\theta}{ds^2} sin(\theta) \ \Rightarrow \ T = \frac{T_h}{cos(\theta)} - \frac{E \cdot I_b}{cos(\theta)} \frac{d^2\theta}{ds^2} sin(\theta)$$

Based on the above, the equation 2.4 becomes

$$EI_b \frac{d^3\theta}{ds^3} - \left( \frac{T_h}{cos(\theta)} - \frac{EI_b}{cos(\theta)} \frac{d^2\theta}{ds^2} sin(\theta) \right) \frac{d\theta}{ds} + w_s cos(\theta) = 0$$

Dividing by $cos(\theta)$ and taking into account identity

$$sec(\theta) = \frac{1}{cos(\theta)}$$

we get

$$EI_b sec(\theta)\frac{d^3\theta}{ds^3} - T_h sec^2(\theta)\frac{d\theta}{ds} + EI_b sec(\theta)\frac{d^2\theta}{ds^2} tan(\theta)\frac{d\theta}{ds} + w_s = 0$$

Based on the trigonometric identity

$$\frac{d}{d\theta} sec(\theta) = sec(\theta)tan(\theta)$$

the above equation becomes

$$EI\frac{d}{ds}\left(sec(\theta)\frac{d^2\theta}{ds^2}\right) - T_h sec^2(\theta)\frac{d\theta}{ds} + w_s = 0 \qquad \mathbf{[3.6]}$$

This equation is also known as *the **nonlinear bending equation*** and is valid for both deep and shallow waters and small and large slopes. Taking into account the unknown suspended length of the pipeline before the pipe-laying process the problem becomes of fourth order.

For this problem no exact solutions are known and approximations must be considered either by numerical methods, or by equation simplification. Numerical approaches were studied for a beam with small deflections in (Wilhoit and Merwin, 1967), and a nonlinear method was studied by Bryndum et al. (1982). It should be mentioned that if the flexural rigidity vanishes, an exact analytical solution can be obtained for the problem, known as the natural catenary method which is already described in Chapter 3.1.3.

### 3.2.2 Governing Equations & Boundary Conditions

Equations 3.4 and 3.5 are the two governing differential equations that will be used for the solution of the pipelay problem. Specifically,

$$G.E.1: \; EI_b\frac{d^3\theta}{ds^3} - T\frac{d\theta}{ds} + w_s cos(\theta) = 0$$

$$G.E.2: \; \frac{dT}{ds} = w_s sin(\theta)$$

The boundary conditions are given as mentioned before at the touchdown point (s=0) and the stinger tip (s=L). At the touchdown point, the seabed is considered to be infinitely stiff (see Chapter 9.0 for the model considering seabed as a Winkler foundation) for therefore the bending moment M may be assigned to be zero. In addition the pipeline approaches the seabed in an horizontal configuration so angle θ is assigned to be zero also [4]. Based on that,

$$B.C.1 : \ \theta(0) = 0$$

$$B.C.2 : \ \left.\frac{d\theta}{ds}\right|_{s=0} = 0$$

The tension at the seabed is constant and equal to the bottom tension applied, so a third boundary condition can be applied as follows

$$B.C.3 : \ T(0) = T_h$$

The last boundary condition can be formulated using the angle $\theta_0$ at the other end of the suspended pipe (s=L), at the stinger tip,

$$B.C.4 : \ \theta(L\,) = \theta_0$$

The suspended length of the pipe L is an unknown parameter before the pipelay analysis. As it can be seen above, parameter L is included in the fourth boundary condition. Because solving the problem numerically with unknown boundary condition is difficult, the method of *variable substitution* will be used [1]. Thus,

$$s = \varepsilon \cdot L$$

where ε is a dimensionless variable between 0 (touchdown point) and 1 (stinger tip). Based on that, the governing equations become

$$G.E.1 : \ \frac{EI_b}{L^3}\frac{d^3\theta}{d\varepsilon^3} - \frac{T}{L}\frac{d\theta}{d\varepsilon} + w_s cos(\theta) = 0$$

$$G.E.2 : \ \frac{dT}{d\varepsilon} = w_s L sin(\theta)$$

and the fourth boundary condition

$$B.C.4 : \ \theta(1\,) = \theta_0$$

As the length of the pipeline is unknown, *an additional boundary condition* has to be added in the formulation of the problem. The fifth boundary condition is given by the axial tension at the stinger tip. Knowing the stinger configuration, the position of the stinger tip is known. Based on equation 2.1 the axial tension at the stinger tip is given by the relationship below

$$T(st) = T_h + w_s(D - y_{st})$$

where $y_{st}$ is the vertical distance between the stinger tip and the sea level. So the last boundary condition that is needed in order to solve the problem can be written as

$$B.C.5 : \ T(1\,) = T(st)$$

## 3.3 Installation Loads

The loads acting on a pipeline can be classified as static or dynamic. In the following sections of the thesis, the motion of the vessel as well as other dynamic loads due to environmental conditions (waves, currents, etc.) are not considered. Attention is limited to the static analysis of pipeline configuration taking into account the loads which are of main importance during pipelay such as tension forces, bending moments, hydrostatic pressure and contact forces on the stinger.

### 3.3.1 Installation Loads Identification

In order to identify the installation loads, the pipeline is divided in three different regions, the overbend, the sagbend and the laid pipe on the seabed.

#### 3.3.1.1 Overbend Region

At the overbend region the pipeline is supported by the stinger. The pipe is subjected to axial tension T. The magnitude of the axial tension acting on a cross section of the pipe depends on the applied force by the thrusters as the ship moves forward (this force is equal to the axial tension at the seabed, known as bottom tension), the vertical position of the cross section with respect to the seabed and the pipe unit submerged weight.

In addition to the axial force, the pipeline is subjected to contact forces $T_S$ at the points of contact with the roller boxes of the stinger and to external hydrostatic pressure in the part below the sea surface. Finally based on the stinger configuration, which depends on the project specifications (water depth, pipe characteristics, maximum allowable strains, etc.), a bending moment is applied along the stinger. Its magnitude depends on the flexural rigidity of the pipeline and the stinger radius-curvature.

#### 3.3.1.2 Sagbend Region

The part of the pipeline which is freely suspended in the water, from the lift-off point to the touchdown point, is subject to the axial tension (as described at the previous paragraph) and to external hydrostatic pressure. The bending moment becomes zero at the inflection point (see APPENDIX A for terminology), increases gradually at the opposite direction along the sagbend and decreases abruptly as it approaches the seabed becoming zero at the touchdown point.

The reverse bending at the lower part of the sagbend section in combination with possible plastic strains at the overbend is the main cause of rotation of the pipeline and it will be discussed in detail in next chapters.

#### 3.3.1.3 Seabed

Finally, after the touchdown point at the laid pipe acts a distributed normal force from the seabed which counteracts gravity forces.

A simple representation of the kind of static loads acting on the pipeline over the suspended length as well as the bending of the pipeline at the opposite direction can be seen in Figure 3-4 [5].

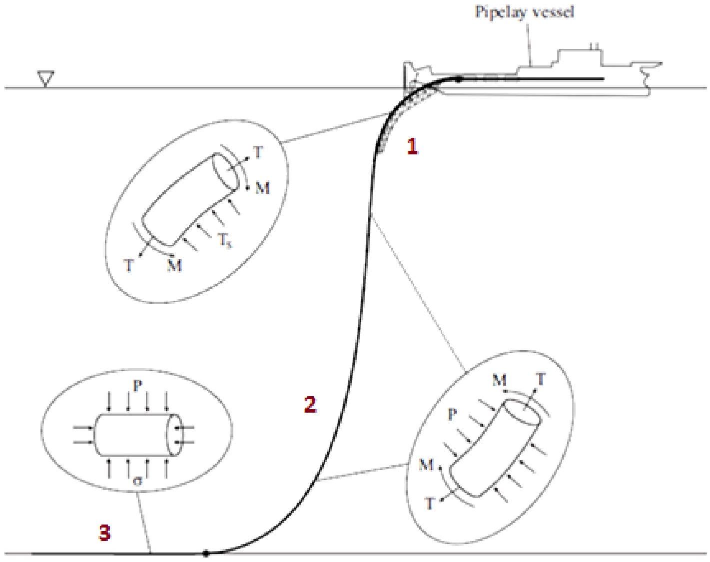


**Figure 3-4 Loads acting on different segments of pipe during S-lay installation**

### 3.3.2 Installation Loads Calculation

Having identified the loads which govern the pipeline installation, knowing the catenary shape of the pipeline, the axial force, bending moments and total strains along the suspended length can be determined.

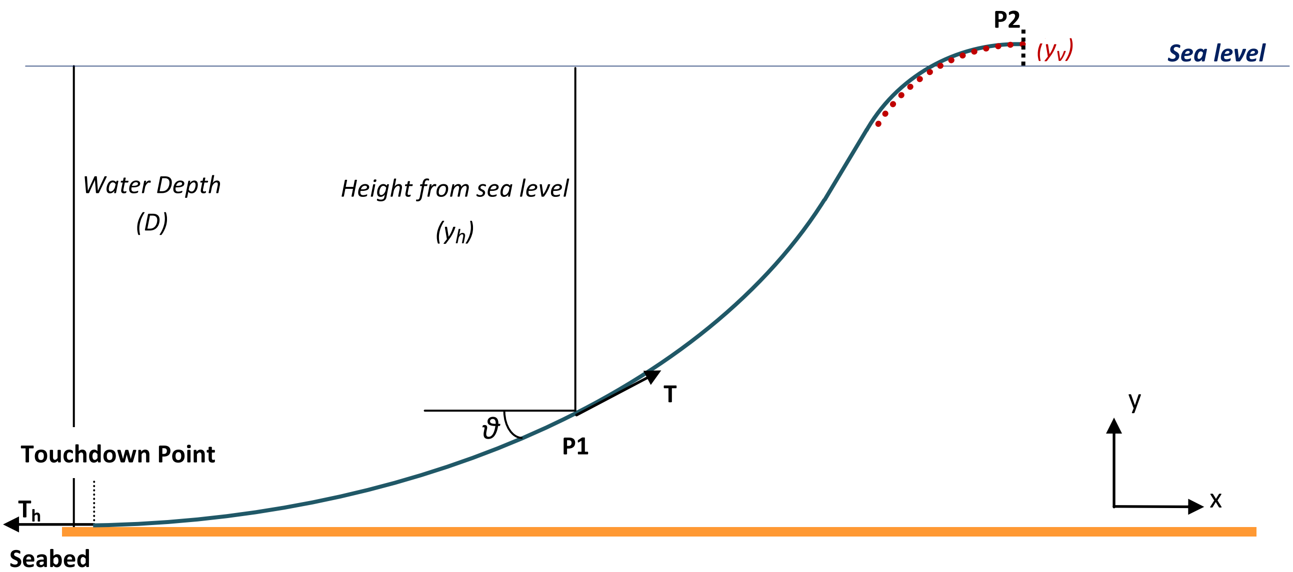


**Figure 3-5 S-lay method illustration**

Based on Figure 3-5, for an arbitrary point P1 between the sea level and the seabed *the **axial tension*** acting on the cross section of the pipeline is given by the following equation

$$T = T_h + w_s(D - y_h) \qquad [3.7]$$

where $T$ is the axial tension at P1, $T_h$ is the applied axial tension at the touchdown point - bottom tension -, D is the water depth, $y_h$ is the vertical distance [m] between point P1 and sea water level and $w_s$ is the unit submerged weight of the pipe. In case that the cross section of the pipe is above the sea level - point P2 -, the unit dry weight $w_d$ of the pipe has to be taken into account in order to calculate the axial tension. Based on the above, the top tension becomes

$$T = T_h + w_s D + w_d y_v \qquad [\mathbf{3.8}]$$

where $y_v$ is the vertical distance [m] between point P2 and sea water level.

It should be mentioned that equation 3.2 is used in order to calculate the top tension (axial force applied from the tensioners), excluding friction forces due to the contact of the pipe with the roller boxes.

*The **bending moment*** of the pipeline can be calculated at each point of the suspended length by the equation

$$M = E \cdot I_b \cdot \frac{d\theta}{ds} \qquad [\mathbf{3.9}]$$

where ds is an increment [m] of the pipeline along its length, θ [rad] is the angle between the pipeline and the horizontal and $I_b$ is the area moment of inertia.

The ***total strain*** of the suspended pipeline is a function of the bending, axial and hoop strain. According to that it can be written

$$\varepsilon_t = f(\varepsilon_b, \varepsilon_{ax}, \varepsilon_h)$$

where $\varepsilon_t$ is the total strain of the pipeline, as a result of the bending strain ($\varepsilon_b$),the axial strain ($\varepsilon_{ax}$) and the strain due to hoop stresses ($\varepsilon_h$). Specifically,

*The strain due to bending* can be calculated as follows [7],

$$\varepsilon_b = \frac{r}{R} = \frac{r}{\left(\frac{E \cdot I_b}{M}\right)} = \frac{M \cdot r}{E \cdot I_b}$$

where r is the pipeline radius [m] and R is the pipeline radius of curvature [m].
*The maximum strain due to the axial tension* can be calculated from the Hooke law adding a term which takes into account the depth of the pipeline section [14]. So,

$$\varepsilon_{ax} = \frac{\sigma}{E} - \frac{\pi \cdot D_o^2 \cdot \gamma \cdot h}{E \cdot A} \Rightarrow \varepsilon_{ax} = \frac{T}{E \cdot A} - \frac{\pi \cdot D_o^2 \cdot \gamma \cdot h}{E \cdot A}$$

where *A* is the cross section of the pipeline, $D_o$ the outside diameter of the pipe, $\gamma$ the specific weight of sea water and *h* the depth of the pipe section.

Finally the *hoop strain* can be calculated from the formula below [14]

$$\varepsilon_h = \frac{D_o \cdot \gamma \cdot h}{2 \cdot E \cdot t}$$

where *t* is the wall thickness of the pipeline .

Based on the above and having calculated at each position s of the suspended pipeline the bending, the axial and the hoop strain, the total strain can be calculated according to the ***Von Mises equivalent strain formula [14].***

$$\varepsilon_t\ (s) = \sqrt{[\varepsilon_b(s) + \varepsilon_{ax}(s)]^2 + \ \varepsilon_h^2(s) - [\varepsilon_b(s) + \varepsilon_{ax}(s)]\varepsilon_h(s)} \qquad [\mathbf{3.10}]$$

### 3.3.3 Numerical Solution

Having specified the governing equations and the appropriate number of boundary conditions the problem is solved using Matlab software. The problem can be specified as a *boundary value problem* [9],[11]. As it is hard to get the analytical solution of the mathematical model presented above, a fourth order accurate finite difference algorithm has been used to get the numerical solution. For this kind of boundary value problems a built in Matlab function is used, known as **bvp4c**. Function bvp4c is a finite difference code that implements the three-stage Lobatto IIIa formula [11].

The first step is to convert the governing differential equations to an equivalent system of first order ordinary differential equations [10], [11]. To do that we make the following substitutions,

$$z(1) = \theta\ , \qquad z(2) = \frac{d\theta}{d\varepsilon}, \qquad z(3) = \frac{d^2\theta}{d\varepsilon^2}, \qquad z(4) = T$$

The input (governing equations) that is given to the bvp4c function can be written as follows

$$\left[z(2)\ ;\ z(3)\ ;\ \frac{L^3}{EI_b}\left[\left(\frac{z(4)}{L}\right)z(2) - wcosz(1)\right]; w_s Lsinz(1)\right]$$

Respectively, taking into account that the boundaries of the problem are at the touchdown point (za) and at the stinger tip (zb), the set of boundary conditions that will be evaluated by the bvp4c function are written as follows

$$[za(1) = 0; za(2) = 0;\ za(4) = T_h;\ zb(1) = \theta_0\ ;\ zb(4) = T(st)]$$

After formulating the problem numerically, the problem is solved iteratively by the bvp4c solver until the suspended length of the pipeline satisfies the additional ($5^{th}$) boundary condition.

The output of the solution includes the angle θ (angle between pipeline and the horizontal along its suspended length), the first and second derivative of θ, the axial tension T along the length and the total suspended length of the pipe.

### 3.3.4 Pipelay Results Validation

The validity of the pipe-laying model is verified by means of a comparison with results obtained from the commercial finite element software OFFPIPE. A number of different cases studied with varying pipeline properties, stinger configuration and environmental conditions have been compared in order to check the validity of the model. For all the cases the following constants were used . It should be mentioned that OFFPIPE and Matlab use different mesh points and element length for the solution. The results from Matlab and OFFPIPE solution, which will be presented in this and in the next chapters, in order to be compared, were obtained after **applying linear interpolation** on the data points of Matlab solution to the data points of OFFPIPE solution. For all the cases presented for the pipe-lay model validation the following constant properties were used.

| | | |
|---|---|---|
| Sea water density | 1025 | $[kg/m^3]$ |
| Gravity acceleration | 9.81 | $[m/s^2]$ |
| Pipeline density | 7850 | $[kg/m^3]$ |
| Young`s Modulus | 207000 | $[MPa]$ |
| Concrete coating density | 3050 | $[kg/m^3]$ |

**Table 3-1 Constant properties used for cases**

The results from the cases studied are discussed in section 3.3.5.

#### 3.3.4.1 Case Study N°1

The data which were used for the case study N°1 are summarized in Table 3-1. A deep-water project (1826 meters) using vessel *Audacia* with a stinger length and radius of 100 meters. The specific characteristics of the pipeline installed and the coating properties can be seen at the table below.

| **Vessel** | | **Audacia** |
|---|---|---|
| Stinger Length | 110 | $[m]$ |
| Stinger Radius | 100 | $[m]$ |
| Water Depth | 1826 | $[m]$ |
| Pipeline Diameter | 20 | ["] |
| Pipeline Wall Thickness | 29.1 | $[mm]$ |
| Field Joint Length | 0.7 | $[m]$ |
| Pipe Joint Length | 12.2 | $[m]$ |
| Unit Submerged Weight | 1334.8 | $[N/m]$ |
| **Anti-Corrosion Coating** | | |
| Thickness | 0.6 | $[mm]$ |
| Density | 1160 | $[kg/m^3]$ |
| **Field Joint Infill Thickness** | | |
| Thickness | 0.635 | $[mm]$ |
| Density | 1153 | $[kg/m^3]$ |

**Table 3-2 Data used for case study N°1**

After the static pipelay analysis the pipeline configuration and bending moments distribution obtained from Matlab model and Offwin can be seen in Figure 3-6 and Figure 3-7 respectively. Comparisons between axial tension and sagbend strains can be seen in APPENDIX B

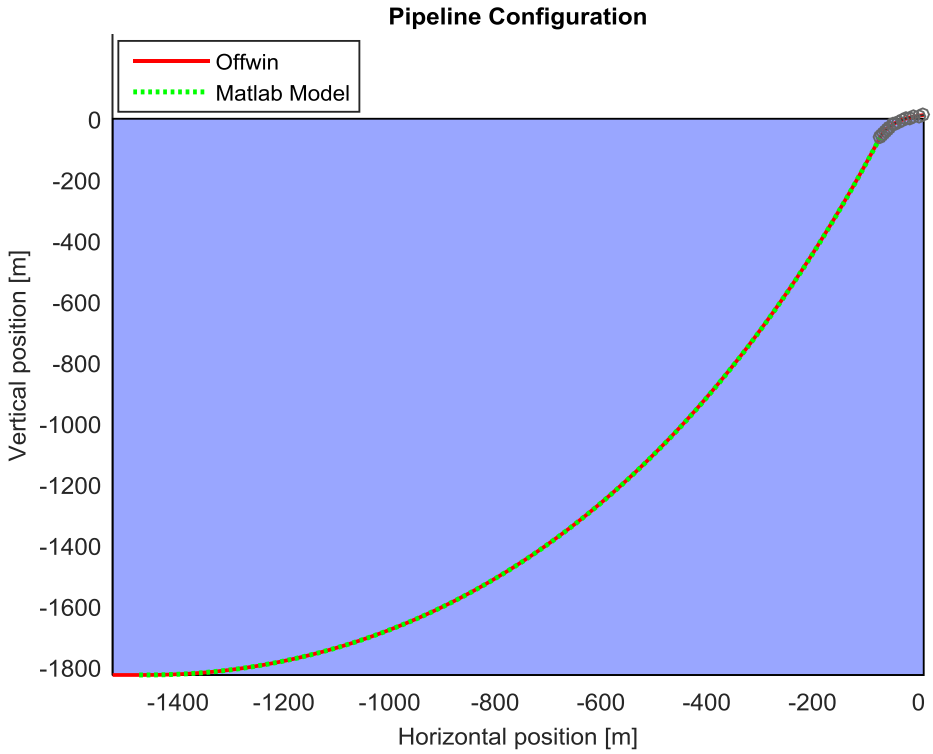


**Figure 3-6 Pipeline Configuration (Case Study N°1)**

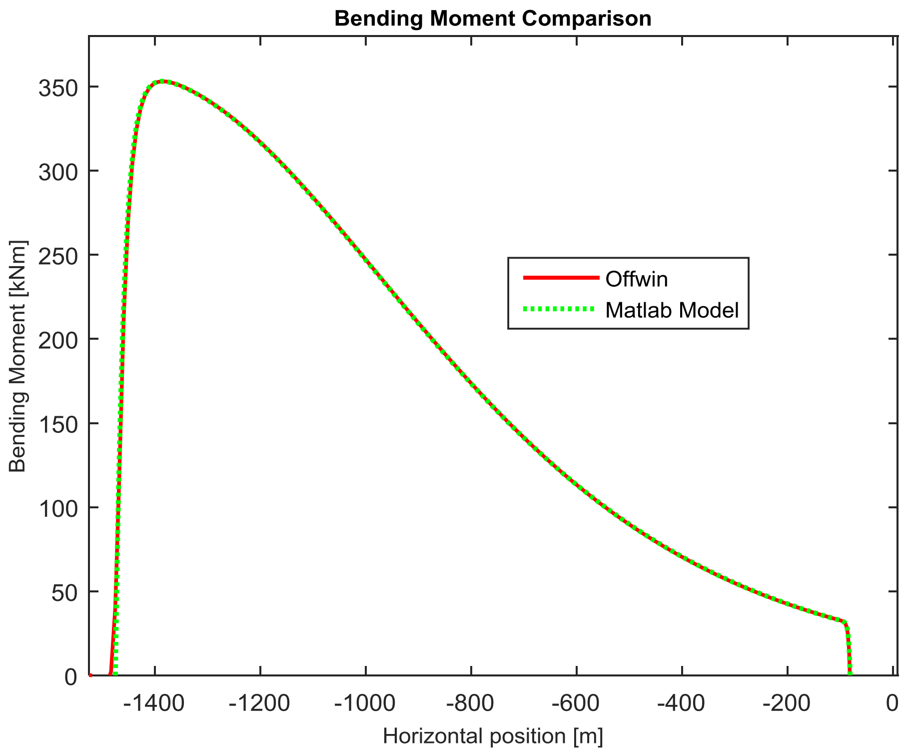


**Figure 3-7 Bending moment along the catenary (Case Study N°1)**

The most important quantities after the pipelay analysis are summarized in Table 3-3.

| Quantity | Unit | Offwin | Matlab Model | Absolute Error | Relative Error [%] |
|---|---|---|---|---|---|
| Suspended Length | $[m]$ | 2400.21 | 2400.17 | 0.04 | 0.0016 |
| Maximum Bending Moment | $[kNm]$ | 353.058 | 353.067 | 0.009 | 0.0028 |
| Maximum Sagbend Strain | [%] | 0.07940 | 0.07944 | $4*10^{-5}$ | 0.05 |
| Maximum Bending Strain | [%] | 0.03440 | 0.03439 | $1*10^{-5}$ | 0.03 |
| Maximum Tensile Strain | [%] | 0.03530 | 0.03530 | 0 | 0 |
| Top Tension (Tensioners) | $[kN]$ | 3454.75 | 3455.50 | 0.75 | 0.022 |

**Table 3-3 Comparison of basic quantities after pipelay analysis (Case Study N°1)**

### 3.3.4.2 Case Study N°2

The data which were used for the case study N°2 are summarized in Table 3-4. A shallow-water project (200 meters) using vessel *Lorelay* with a stinger length of 71 meters and radius of 150 meters is analyzed. The specific characteristics of the pipeline installed and the concrete coating properties can be seen at the table below.

| **Vessel** | | **Lorelay** |
|---|---|---|
| Stinger Length | 71 | $[m]$ |
| Stinger Radius | 150 | $[m]$ |
| Water Depth | 200 | $[m]$ |
| Pipeline Diameter | 10.75 | ["] |
| Pipeline Wall Thickness | 14.3 | $[mm]$ |
| Field Joint Length | 0.7 | $[m]$ |
| Pipe Joint Length | 12.2 | $[m]$ |
| Unit Submerged Weight | 472.88 | $[N/m]$ |
| **Concrete Coating** | | |
| Thickness | 10 | $[mm]$ |
| Density | 3050 | $[kg/m^3]$ |

**Table 3-4 Data used for case study N°2**

The most important quantities after the pipelay analysis are summarized in Table 3-5.

| Quantity | Unit | Offwin | Matlab Model | Absolute Error | Relative Error [%] |
|---|---|---|---|---|---|
| Suspended Length | $[m]$ | 411.14 | 408.27 | 2.87 | 0.7 |
| Maximum Bending Moment | $[kNm]$ | 48.9 | 48.91 | 0.009 | 0.02 |
| Maximum Sagbend Strain | [%] | 0.0416 | 0.04159 | $10^{-5}$ | 0.024 |
| Maximum Bending Strain | [%] | 0.0331 | 0.03306 | $4*10^{-5}$ | 0.12 |
| Maximum Tensile Strain | [%] | 0.0103 | 0.01025 | $5*10^{-5}$ | 0.48 |
| Top Tension (Tensioners) | $[kN]$ | 298.85 | 298.846 | 0.04 | 0.0013 |

**Table 3-5 Comparison of basic quantities after pipelay analysis (Case Study N°2)**

Pipeline configuration and bending moments distribution along the suspended length are shown in Figure 3-8 and Figure 3-9 respectively. Comparisons between axial tension and sagbend strains can be seen in APPENDIX B.

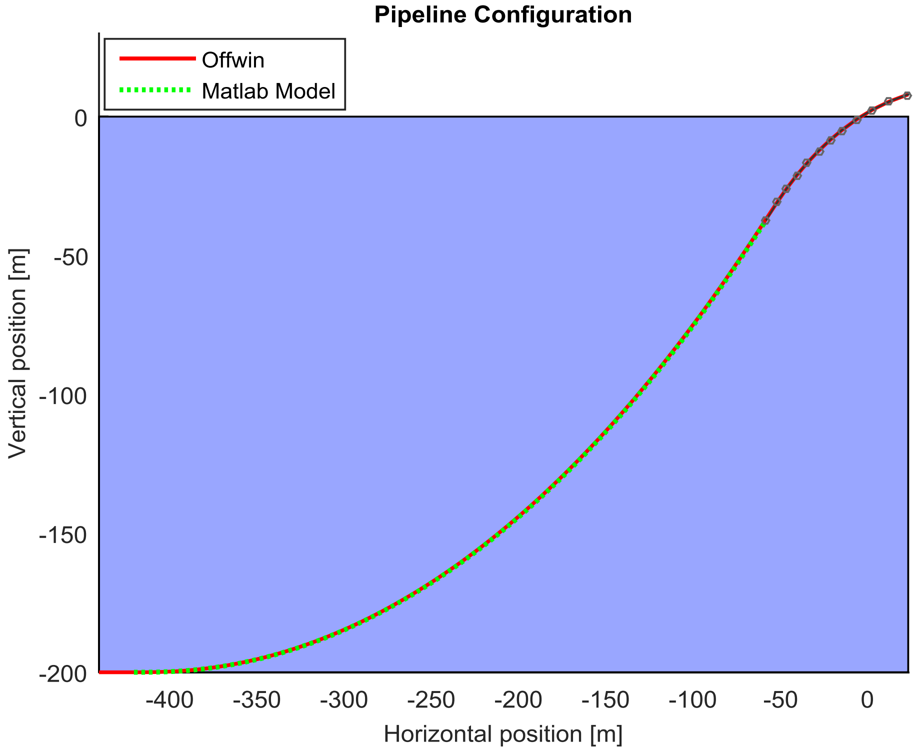


**Figure 3-8 Pipeline Configuration (Case Study N°2)**

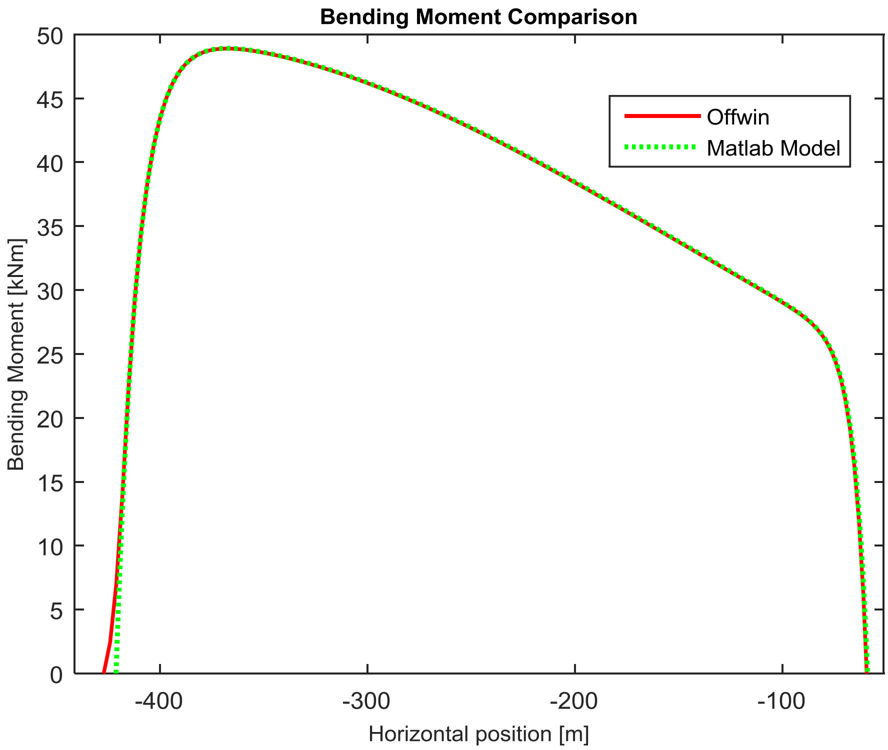


**Figure 3-9 Bending moment along the catenary (Case Study N°2)**

#### 3.3.4.3 Case Study N°3

The data which were used for the case study N°3 are summarized in Table 3-6. A mid-water project (600 meters) using vessel *Solitaire* with a stinger length of 140 meters and radius of 160 meters is analyzed. The specific characteristics of the pipeline installed and the concrete coating properties can be seen at the table below.

| Vessel | | Solitaire |
|---|---|---|
| Stinger Length | 140 | $[m]$ |
| Stinger Radius | 160 | $[m]$ |
| Water Depth | 600 | $[m]$ |
| Pipeline Diameter | 26 | $["]$ |
| Pipeline Wall Thickness | 25.4 | $[mm]$ |
| Field Joint Length | 0.7 | $[m]$ |
| Pipe Joint Length | 12.2 | $[m]$ |
| Unit Submerged Weight | 5966.9 | $[N/m]$ |
| **Concrete Coating** | | |
| Thickness | 120 | $[mm]$ |
| Density | 3050 | $[kg/m^3]$ |

**Table 3-6 Data used for case study N°3**

Pipeline configuration and bending moments distribution along the suspended length are shown in Figure 3-10 and Figure 3-11 respectively. Comparisons between axial tension and sagbend strains can be seen in APPENDIX B.

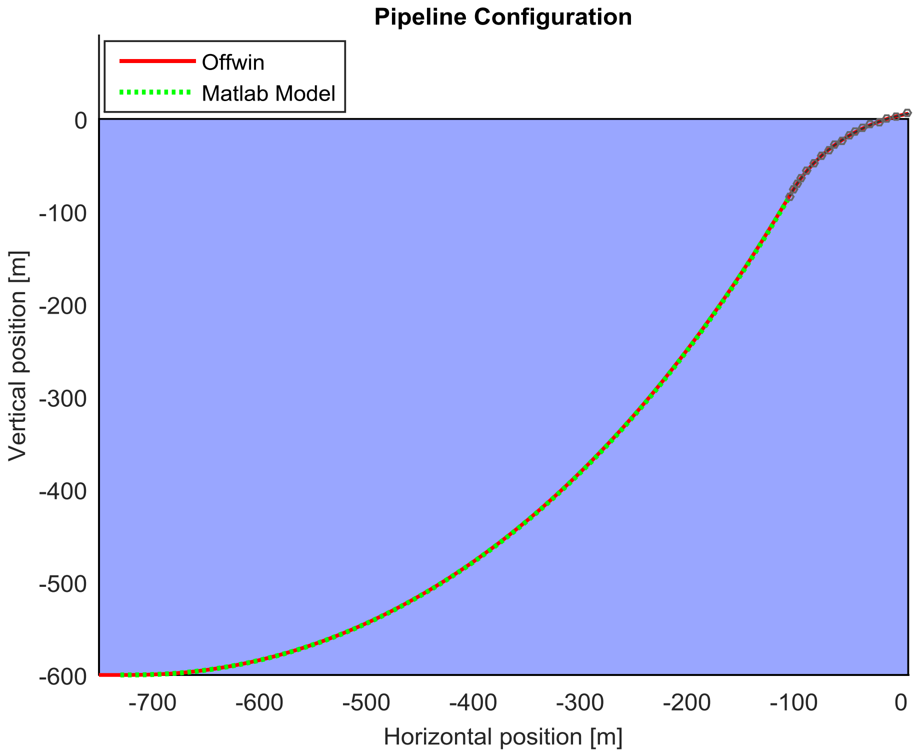


**Figure 3-10 Pipeline Configuration (Case Study N°3)**

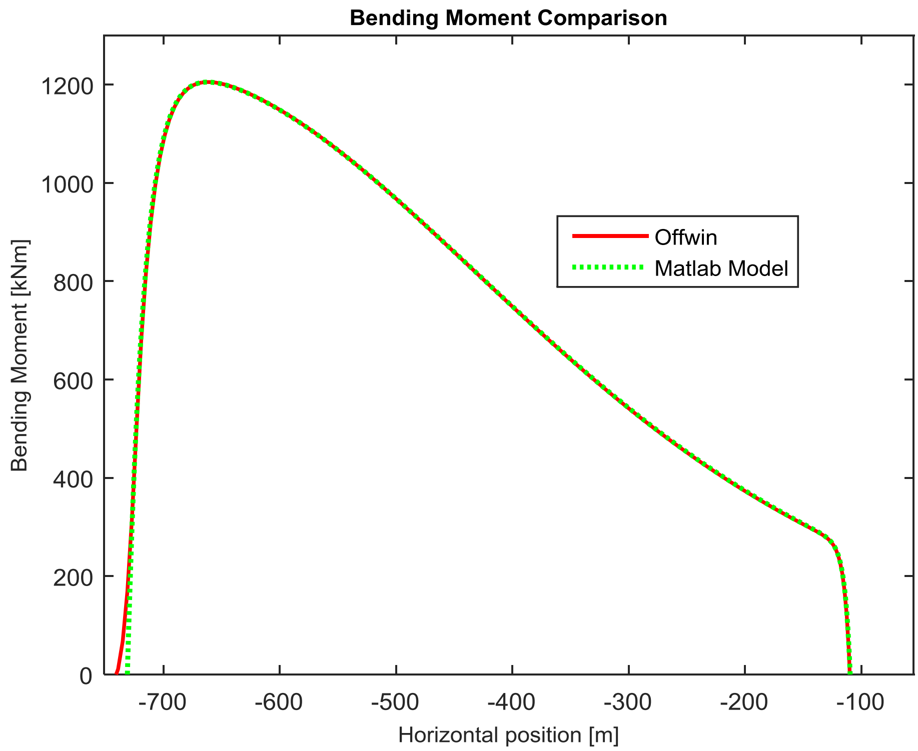


**Figure 3-11 Bending moment along the catenary (Case Study N°3)**

The most important quantities after the pipelay analysis are summarized in Table 3-7.

| Quantity | Unit | Offwin | Matlab Model | Absolute Error | Relative Error [%] |
|---|---|---|---|---|---|
| Suspended Length | $[m]$ | 857.05 | 856.087 | 0.963 | 0.11 |
| Maximum Bending Moment | $[kNm]$ | 1205.24 | 1205.04 | 0.2 | 0.016 |
| Maximum Sagbend Strain | $[\%]$ | 0.1042 | 0.10417 | $3*10^{-5}$ | 0.028 |
| Maximum Bending Strain | $[\%]$ | 0.0752 | 0.07514 | $6*10^{-5}$ | 0.08 |
| Maximum Tensile Strain | $[\%]$ | 0.0506 | 0.0509 | $3*10^{-5}$ | 0.09 |
| Top Tension (Tensioners) | $[kN]$ | 6257.31 | 6258.69 | 1.38 | 0.022 |

**Table 3-7 Comparison of basic quantities after pipelay analysis (Case Study N°3)**

#### 3.3.4.4 Case Study N°4

The data which were used for the case study N°4 are summarized in Table 3-8. A deep-water project (2000 meters) using vessel *Audacia* with a stinger length 71 meters and radius of 120 meters. The specific characteristics of the pipeline installed and the coating properties can be seen at the table below.

| **Vessel** | | **Lorelay** |
|---|---|---|
| Stinger Length | 71 | $[m]$ |
| Stinger Radius | 120 | $[m]$ |
| Water Depth | 2000 | $[m]$ |
| Pipeline Diameter | 8.625 | $["]$ |
| Pipeline Wall Thickness | 11.1 | $[mm]$ |
| Field Joint Length | 0.7 | $[m]$ |
| Pipe Joint Length | 12.2 | $[m]$ |
| Unit Submerged Weight | 180.38 | $[N/m]$ |
| **Anti-Corrosion Coating** | | |
| Thickness | 1 | $[mm]$ |
| Density | 1160 | $[kg/m^3]$ |

**Table 3-8 Data used for case study N°4**

After the static pipelay analysis the pipeline configuration and bending moments distribution obtained from Matlab model and Offwin can be seen in Figure 3-12 and Figure 3-13 respectively. Comparisons between axial tension and sagbend strains can be seen in APPENDIX B.

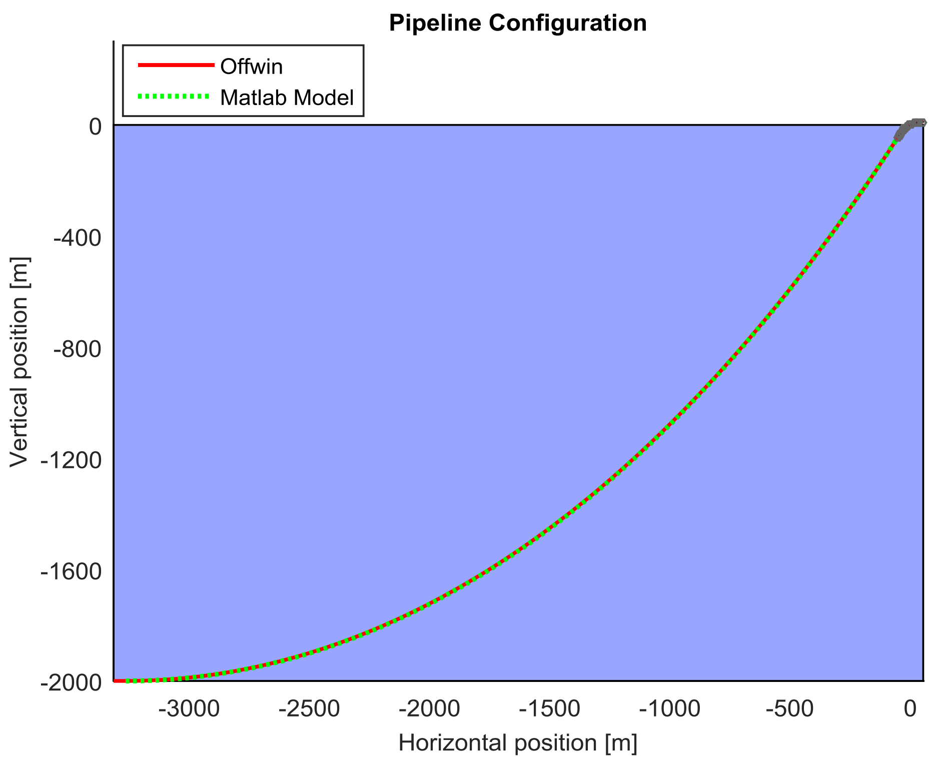


**Figure 3-12 Pipeline Configuration (Case Study N°4)**

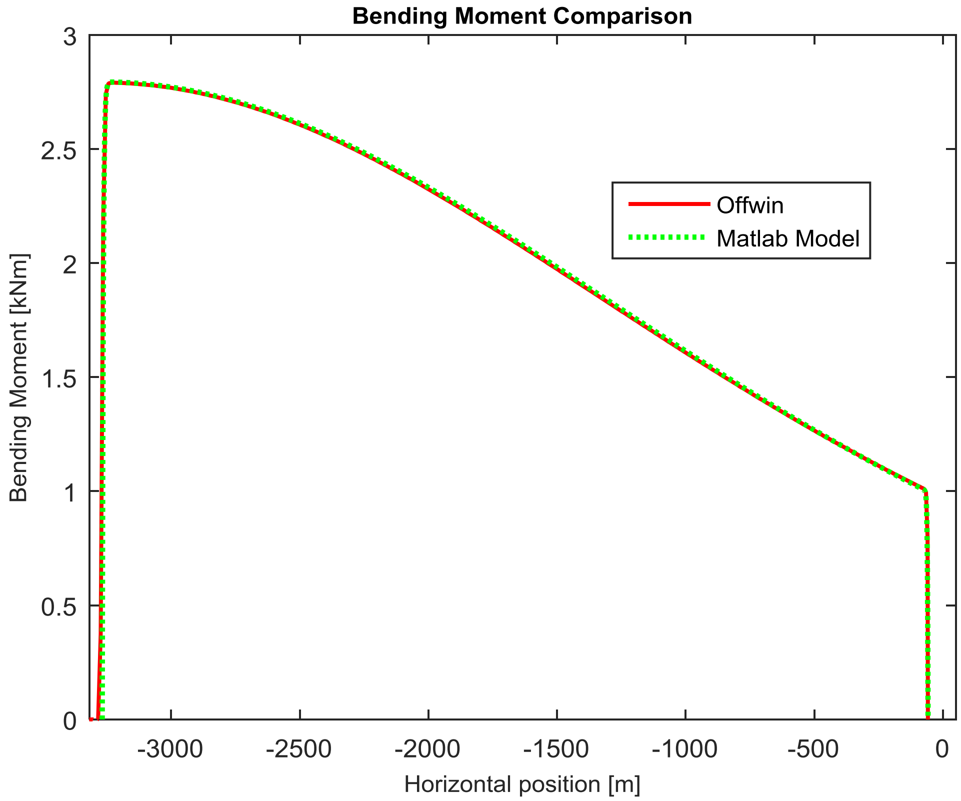


**Figure 3-13 Bending moment along the catenary (Case Study N°4)**

The most important quantities after the pipelay analysis are summarized in Table 3-9.

| Quantity | Unit | Offwin | Matlab Model | Absolute Error | Relative Error [%] |
|---|---|---|---|---|---|
| Suspended Length | $[m]$ | 3909.22 | 3906.02 | 3.2 | 0.08 |
| Maximum Bending Moment | $[kNm]$ | 2.791 | 2.794 | 0.003 | 0.09 |
| Maximum Sagbend Strain | [%] | 0.0905 | 0.09059 | $9*10^{-5}$ | 0.09 |
| Maximum Bending Strain | [%] | 0.00374 | 0.00375 | $1*10^{-5}$ | 0.2 |
| Maximum Tensile Strain | [%] | 0.0574 | 0.05744 | $4*10^{-5}$ | 0.07 |
| Top Tension (Tensioners) | $[kN]$ | 892.73 | 892.93 | 0.2 | 0.02 |
| TDP x-position (from stinger hinge) | $[m]$ | 3261.62 | 3258.02 | 3.6 | 0.11 |

**Table 3-9 Comparison of basic quantities after pipelay analysis (Case Study N°4)**

### 3.3.5 Pipelay Model Results Findings & Evaluation

Based on the results and on the comparisons which were made between Matlab model and the commercial finite element software Offwin the following conclusions can be made,

1. The Matlab model gives precise estimation of pipeline configuration at all the cases studied independently of the water depth, the stinger configuration and pipeline characteristics. The suspended length of the pipe at all the cases was determined accurately with the maximum relative error observed 0.7% for the case study with the shortest catenary length (Case Study N$^o$2 $- Ltot = 408\text{m}$) and the maximum absolute error 3.2m (Case Study N$^o$4 $- Ltot = 3906\text{m}$). The touchdown point position with respect to the stinger hinge at all the cases was estimated precisely with the maximum relative error observed around 0.11 % (Case Study N$^o$4).

2. At all the cases which were conducted the numerical solution gave accurate results for the bending moment along the suspended length of the pipeline. As it was observed from the comparisons, the maximum bending moment was estimated accurately with the maximum error being below 0.1% for all the cases. In addition its distribution along the catenary and the position of the maxima were determined precisely as it can be seen from the figures. The higher relative error at the touchdown point is converging to negligible errors almost from the 3$^{rd}$ or 4$^{th}$ point of our solution in all the cases studied. This error has small absolute value with respect to the maximum bending moment of each case study and is expected, as the seabed is not modelled in our solution (see Chapter 9.0 for the modelling of seabed as Winkler foundation).

3. The Matlab model gives accurate results for the calculation of the axial tension along the suspended length as it can be seen from the figures in APPENDIX B. For all the cases examined the average error was below 0.1% along the suspended length. In addition the top tension was calculated (tension provided by the tensioners) for all cases precisely with the maximum error observed 0.022%. The axial tension along the catenary depends on the bottom tension applied $T_h$, the unit submerged weight of the pipe $w_s$ and the vertical distance between a point $P_1$ and the sea level based on the following equation (see Figure 3-5)

$$T(P_1) = T_h + w_s \cdot [D - y_h(P_1)]$$

As the bottom tension (axial tension at the seabed - boundary condition), the water depth $D$ and the unit submerged weight are part of the input, these negligible errors can be explained by the slight difference at the determination of pipeline configuration along the catenary and as a consequence slight differences at the determination of the value of $y_h(P_1)$.

**4.** At all the cases, the Matlab model gave precise results for the bending, tensile and total sagbend strain along the suspended length of the pipeline. As it was observed from the comparisons, the maximum strain was estimated accurately with the maximum relative difference being below 0.2% for all the cases. It should be mentioned that the errors in strain comparisons are mainly due to the rounding of the values of Offwin at the 4$^{th}$ decimal, so they should not be taken into account. In addition their distribution along the catenary and the position of the maxima were determined accurately for all the cases as it can be seen from the figures in APPENDIX B. The highest error at the touchdown point can be explained as in the case of bending moments as a result of not modelling the seabed (it is considered to be infinitely stiff at the touchdown point, which is a rough assumption). That error does not affect the solution and the distribution of the strains along the catenary so for the purpose of the research is not considered as important and will not affect the rotation model of the pipeline.

Based on the above, it can be concluded that the pipelay model behaves with considerable accuracy for all the cases studied independently of the input parameters as the water depth, the stinger configuration, pipeline characteristics and their combinations. The relatively higher errors at the boundaries (touchdown point and stinger tip) can be explained by the fact that the boundary conditions are not identical. In the case of the touchdown point the soil is considered to be infinitely stiff while at the stinger tip area the overbend interface is simplified. The presence of these errors does affect the solution along the catenary for any of the cases studied. The pipeline configuration and its quantities (bending moment, axial tension, sagbend strain) along the suspended length are precisely represented with negligible errors, therefore the model can be developed further for the pipelay analysis of inline structure installation (see Chapter 4.0) and is fit for calculations of pipe rotation (see Chapter 5.0).

# 4.0 ILS INSTALLATION SEQUENTIAL MODEL

In this chapter the mathematical model of the pipelay problem will be described including different pipe sections and/or inline structures.

## 4.1 Different sections along catenary

In common pipelay operations, during installation, several pipe sections can be installed with different properties (cross section, wall thickness, bending stiffness etc.). In addition, inline structures are attached to the pipe for several purposes, depending on the project. Including different pipe sections and/or attached structural components along the suspended length of the pipe, the model has to be modified.

Having different sections along the catenary has as a consequence *abrupt changes in bending stiffness* and variation of the total *submerged weight* along the sagbend. These changes have to be taken into account in the mathematical modelling and governing equations. Additionally, *interface conditions have to be introduced* at the points of change in order to ensure the continuity and the structural integrity of the pipeline.

As mentioned in previous chapters, the pipe-laying problem is a boundary value problem, which is solved by a fourth order finite difference method using the bvp4c built -in solver of Matlab software. In order to solve the new problem, with different pipe sections and/or inline structures attached along the catenary the same numerical method is used with some modifications.

Here it should be mentioned, that the goal of the formulation of the new problem and its implementation is to solve *the pipe-laying problem and the rotational problem in a sequential* way. That means that the problem will not be solved directly with two different pipe sections of specific length along the catenary. The problem will be solved for one pipe section at the initial stage and then at each step a pipe joint of the relevant pipe section will be added to the whole catenary.

## 4.2 Mathematical formulation for different sections

To model the problem including several pipe sections, it is assumed that along the suspended length of the pipe there is a point where there is a transition from a *pipe element N$^o$ 1 to a pipe element N$^o$ 2.* Based on the geometrical and material characteristics, each pipe section has its own bending stiffness $E_1 I_{b1}, E_2 I_{b2}$ and submerged weight $w_{s1}, w_{s2}$ per unit length, respectively. Following the same procedure as in the case for one pipe element, the governing equations for the pipe can be found by considering the static forces on a short segment of the tensioned pipe at equilibrium, see Figure 4-1.

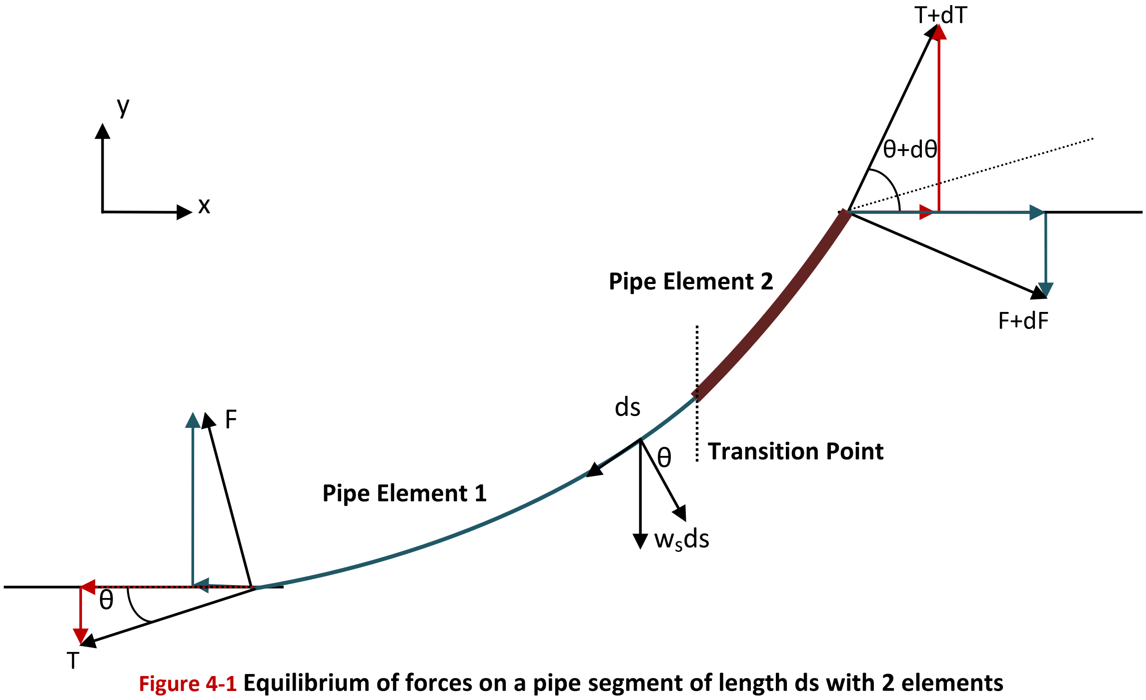

Figure 4-1 **Equilibrium of forces on a pipe segment of length ds with 2 elements**

As it can be seen from the Figure 4-1 at the pipe segment there is a point of transition between the two pipe elements. It should be reminded that, based on the static equilibrium, the governing equations of a pipe with uniform pipe characteristics along the suspended length can be described as follows

$$E \cdot I_b \frac{d^3\theta}{ds^3} - T \cdot \frac{d\theta}{ds} + w_s \cdot cos(\theta) = 0$$

$$\frac{dT}{ds} = w_s \cdot sin(\theta)$$

In case of different pipe sections as illustrated in the figure above the problem is described by a set of governing equations for each pipe element. Assuming that the point of transition is located at the position $\boldsymbol{s = P.o.T.}$ , where s is the distance along the pipe span, $s \in [0, L]$, the governing equations can be written in the following form

**For Pipe Element 1 :**

$$E_1 \cdot I_{b1} \frac{d^3\theta_1}{ds^3} - T \frac{d\theta_1}{ds} + w_{s1} \cdot cos(\theta_1) = 0$$

$$for\ s \leq P.o.T$$

$$\frac{dT}{ds} = w_{s1} \cdot sin(\theta_1)$$

**For Pipe Element 2 :**

$$E_2 \cdot I_{b2} \frac{d^3\theta_2}{ds^3} - T \frac{d\theta_2}{ds} + w_{s2} \cdot cos(\theta_2) = 0$$

$$for\ s > P.o.T$$

$$\frac{dT}{ds} = w_{s2} \cdot sin(\theta_2)$$

For each pipe section the same governing equations are used with the respective coefficients for each element. Since the cross-section experiences the abrupt change at $\mathrm{s} = \mathrm{P.o.T.}$ we have to formulate the interface conditions at this point in order to ensure the continuity and the structural integrity of the system [15]. The interface conditions can be summarized below

The angle just before and after the transition point shall be the same

$$\theta_1(P.o.T^+) = \theta_2(P.o.T^-)$$

The bending moment just before and after the transition point shall be the same

$$M(P.o.T^-) = M(P.o.T^+) \Rightarrow \ E_1 I_{b1} \frac{d\theta_1}{ds}\bigg|_{s=P.o.T^-} = E_2 I_{b2} \frac{d\theta_2}{ds}\bigg|_{s=P.o.T^+}$$

so

$$\theta_1'(P.o.T^+) = \frac{E_1 \cdot I_{b1}}{E_2 \cdot I_{b2}} \theta_2'(P.o.T^-)$$

Finally the shear force just before and after the transition point shall be the same

$$F(P.o.T^-) = F(P.o.T^+) \Rightarrow \frac{dM}{ds}\bigg|_{s=P.o.T^-} = \frac{dM}{ds}\bigg|_{s=P.o.T^+}$$

$$E_1 I_{b1} \frac{d^2\theta_1}{ds^2}\bigg|_{s=P.o.T^-} = E_2 \cdot I_{b2} \frac{d^2\theta_2}{ds^2}\bigg|_{s=P.o.T^+}$$

so the last interface condition becomes

$$\theta_1''(P.o.T^+) = \frac{E_1 I_{b1}}{E_2 I_{b2}} \theta_2''(P.o.T^-)$$

Pipelay installation operation is a continuous process. As the operation progresses, the pipe joints are gradually lowered towards the seabed as the vessel moves forward. In order to simulate the pipelay process in Matlab, a detailed explanation is given in Chapter 4.3.

### 4.3 Sequential Model Description

As a first step the common pipelay problem is solved given the water depth, the pipeline characteristics and stinger configuration. The pipelay analysis is done for one pipe element along the catenary and the solution gives the values of the angle θ, its 1st and 2nd derivative, the tension along the sagbend and the suspended length of the pipe. Having solved the pipelay problem, the characteristics of the new section have to be given. It can be a pipeline with different properties or an inline structure. In addition to the characteristics, the total length $L_{ad}$ of the new section has to be determined as an input.

In order to formulate each step of the pipe-laying process the code does not solve directly the new problem by setting the length of the new element $L_{ad}$. At each step a new joint of 12.2 or 24.4 (in case of double joint factory) meters of the new section is added to the catenary. The iteration method continues until the new section approaches the seabed. At each step of the iteration procedure the point of transition (P.o.T.) is determined along the suspended length and the problem is solved at once calling the *bvp4c* function and solving the governing equations

$$E_1 I_{b1} \frac{d^3\theta}{ds^3} - T\frac{d\theta}{ds} + w_{s1} cos(\theta_1) = 0 \quad and \quad \frac{dT}{ds} = w_{s1} sin(\theta_1) \quad for\ 0 \leq s \leq P.o.T$$

$$E_2 I_{b2} \frac{d^3\theta}{ds^3} - T\frac{d\theta}{ds} + w_{s2} cos(\theta_2) = 0 \quad and \quad \frac{dT}{ds} = w_{s2} sin(\theta_2) \ \ for\ P.o.T \leq s \leq L$$

In the equations above, s is the distance along the pipe span, the left boundary $(s = 0)$ is located at the touchdown point and the right boundary $(s = L)$ is located at the stinger tip. In addition, the interface conditions are formulated as described before at the transition point.

Based on the variable substitution we used in order to solve the common pipelay problem we have

$$s = \varepsilon \cdot L$$

where $\varepsilon \in [0,1]$ and L is the total suspended length of the pipe. For each iteration which corresponds to the addition of a pipe joint of the new section at the main line, the exact position of the transition point between the two different sections is estimated as follows

$$P.O.T. = 1 - \frac{i \cdot p.j.l.}{L}$$

where $\mathrm{i}$ is the index of iteration and $\mathrm{p.j.l.}$ is the length of the additional joint.

For i=0 (first iteration) the suspended length of the pipeline has only one pipe element and the point of transition is located at the stinger tip as it can be seen from the equation above $\mathrm{P.O.T.} = 1$. Adding more sections of the new pipe the transition point moves further away from the stinger tip (it can be better understood from the figures on the next pages). The procedure is continued until the additional element approaches the seabed where the transition point is located almost at the touchdown point and $\mathrm{P.O.T.} = 0$.

The next sequence of illustrations shows how the code works in practice.

- **Step N° 1**

The pipelay problem is solved with one pipe section along the catenary (Figure 4-2).

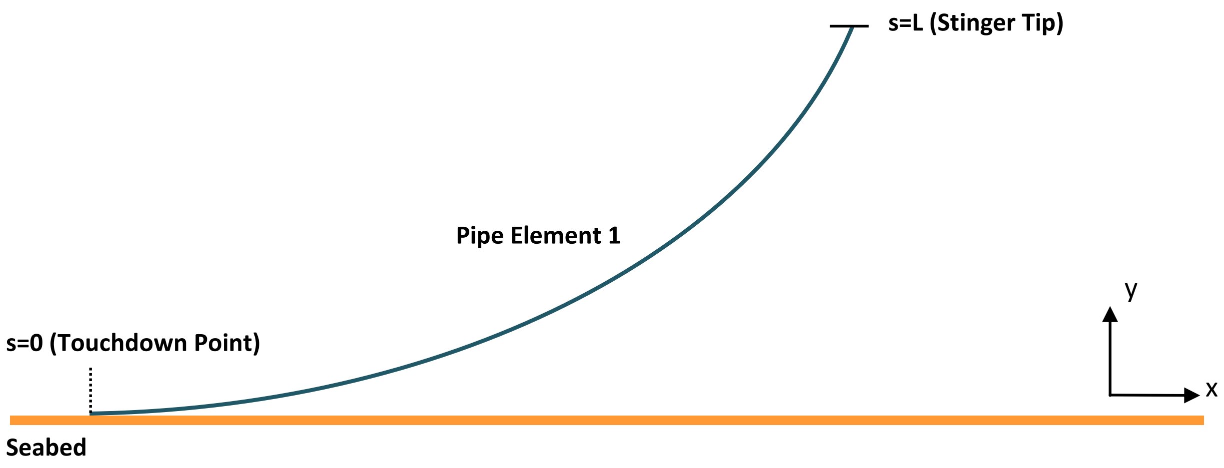


**Figure 4-2 Illustration of one pipe element along the catenary**

- **Step N° 2**

A joint of the new section is added at the location of  the stinger tip. The joint has a length of one 12.2 or 24.4 meters. The new situation is illustrated in Figure 4-3.

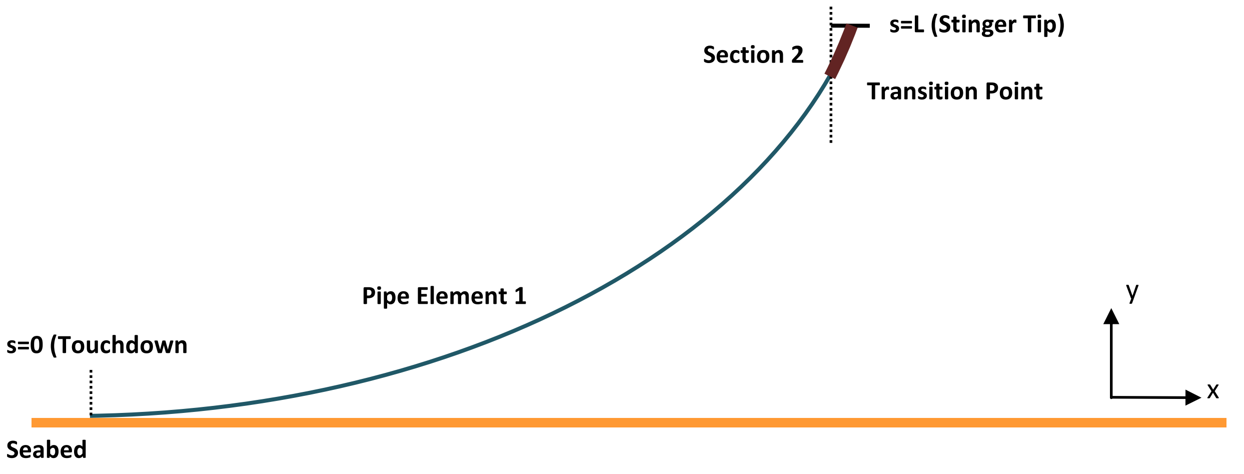


**Figure 4-3 Illustration of two pipe elements along the catenary (1 joint of Section 2)**

- **Step N°3**

A 2nd joint of the new section is added at the location of the stinger tip and the length of the additional section is gradually increasing. The new situation is illustrated in Figure 4-4.

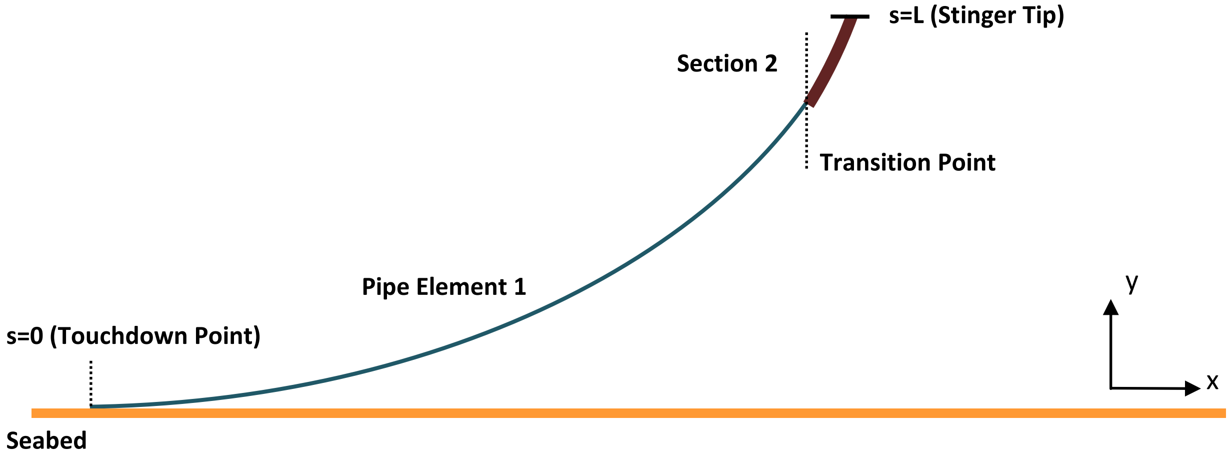


**Figure 4-4 Illustration of two pipe elements along the catenary (2 joints of Section 2)**

The new sagbend configuration includes two joints of the new element. The same procedure continues until the total length of the additional section reaches the seabed. Figure 4-5 shows the situation when the whole second element of length $L_{ad}$ is in the catenary.

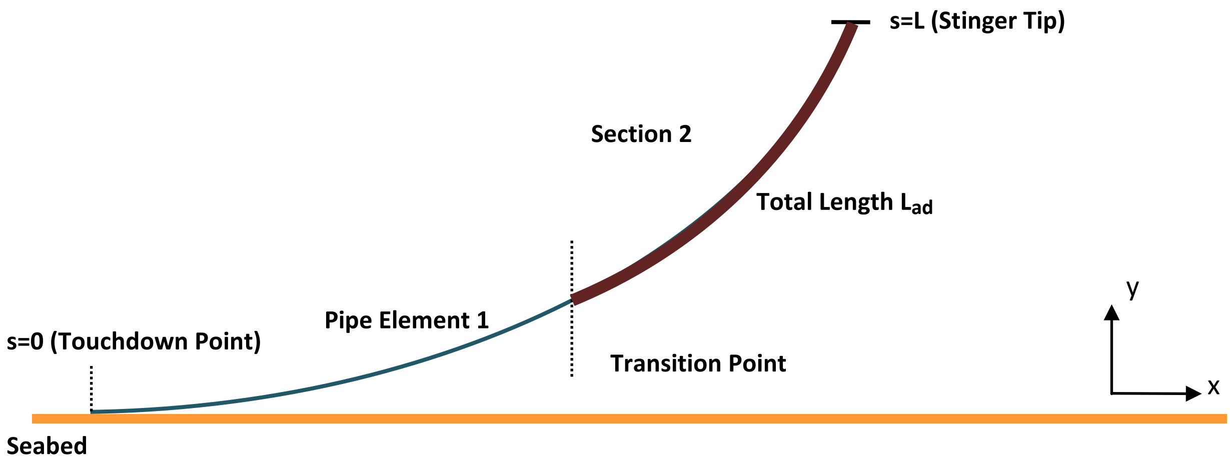


**Figure 4-5 Illustration of two pipe elements along the catenary (whole section 2 in the catenary)**

At each step-iteration of the pipelay process the characteristics of the sagbend configuration are calculated (angle θ, $\theta' \, and \; \theta''$) , the axial tension along the suspended length and the total length of the catenary. All the physical quantities as the bending moments, the sagbend strains and its contributions (bending, tensile and hoop strain) are determined and stored for each step.

Each time a new section of the new structure is added, the unit submerged weight of the whole catenary is increased or decreased based on the new pipe's section characteristics. During the first steps, because only a small number of joints are added, the contribution of the new pipe section to the submerged weight is small. However, gradually as the number of the elements of the new pipe section increases at the whole catenary, the submerged weight changes significantly. The change at the submerged weight has as an influence a change at the required tension applied in order to keep tip separation and sagbend strain within the acceptable limits.

In the case of installation of inline structures more elements are added at each side of the structure as transitions with the main pipeline, in order to ensure the structural integrity of the system. The reason for that is that the inline structures are much heavier and stiffer than the main pipe that is installed and there is need for a smooth transition to avoid failure of the main pipe due to buckling.

In that case the problem described above is solved with the same way, with the only difference that there are more transition points, depending on the total number of the different elements. Figure 4-6 shows a case where there are 4 different elements at the main line of the catenary. As it can be seen there are 4 transition points (indicated with numbers) which change position at each step.

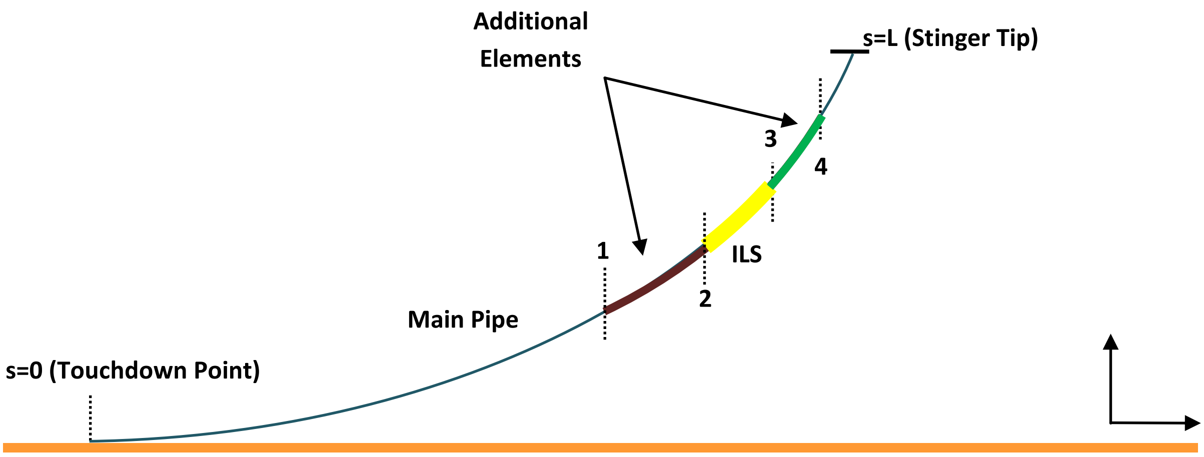


**Figure 4-6 Catenary with a main pipe, additional elements and ILS**

At each step the governing equations that are solved are written below.

$$E_i I_i \frac{d^3\theta}{ds^3} - T\frac{d\theta}{ds} + w_i cos(\theta) = 0 \quad \& \quad \frac{dT}{ds} = w_i sin(\theta)$$

where the values of the constants depend on the position of s.

For $0 < s \leq P.o.T1\ and\ \ P.o.T4 < s \leq L \quad \mathrm{E_i I_i} = \mathrm{E_2 I_{b2}}\ \&\ \mathrm{w_i} = \mathrm{w_{s2}}$

For $\mathrm{P.o.T1} < s \leq P.o.T2 \quad \mathrm{E_i I_i} = \mathrm{E_2 I_{b2}}\ \&\ \mathrm{w_i} = \mathrm{w_{s2}}$

For $\mathrm{P.o.T2} < s \leq P.o.T3 \quad \mathrm{E_i I_i} = \mathrm{E_{ILS} I_{ILS}}\ \&\ \mathrm{w_i} = \mathrm{w_{ILS}}$

For $\mathrm{P.o.T3} < s \leq P.o.T4 \quad \mathrm{E_i I_i} = \mathrm{E_3 I_{b3}}\ \&\ \mathrm{w_i} = \mathrm{w_{s3}}$

### 4.3.1 Determination of axial tension at stinger tip with varying submerged weight along the catenary

Because of the varying submerged weight along the catenary, the axial tension at each point of the suspended length of the pipeline, as well as at the stinger tip (the fifth boundary condition) has to be modified. Based on equation 3.2 the axial tension at each point of the catenary (below sea water level) can be calculated based on equation below

$$T = T_h + w_s D \qquad [\mathbf{5.1}]$$

In the case that along the catenary there are pipe sections with different submerged weight, as illustrated in Figure 4-7, the axial tension at each point along the catenary is estimated based on the vertical position of the point of transition $y_{P.o.T.}$ between the pipe sections and the vertical position at the point of interest (in case of stinger tip $H_{s.t.}$) . According to Figure 4-7 the axial tension at the stinger tip is given as follows

$$T(st) = T_h + \int_0^{y_{P.o.T.}} w_{s1}\, dy + \int_{y_{P.o.T.}}^{H_{s.t.} - y_{P.o.T.}} w_{s2}\, dy \Rightarrow$$

$$T(st) = T_h + w_{s1} \cdot (y_{P.o.T.}) + w_{s2} * (H_{s.t.} - y_{P.o.T.})$$

where $w_{s1}$ and $w_{s2}$ are the unit submerged weights ofpipe element 1 and 2 respectively.

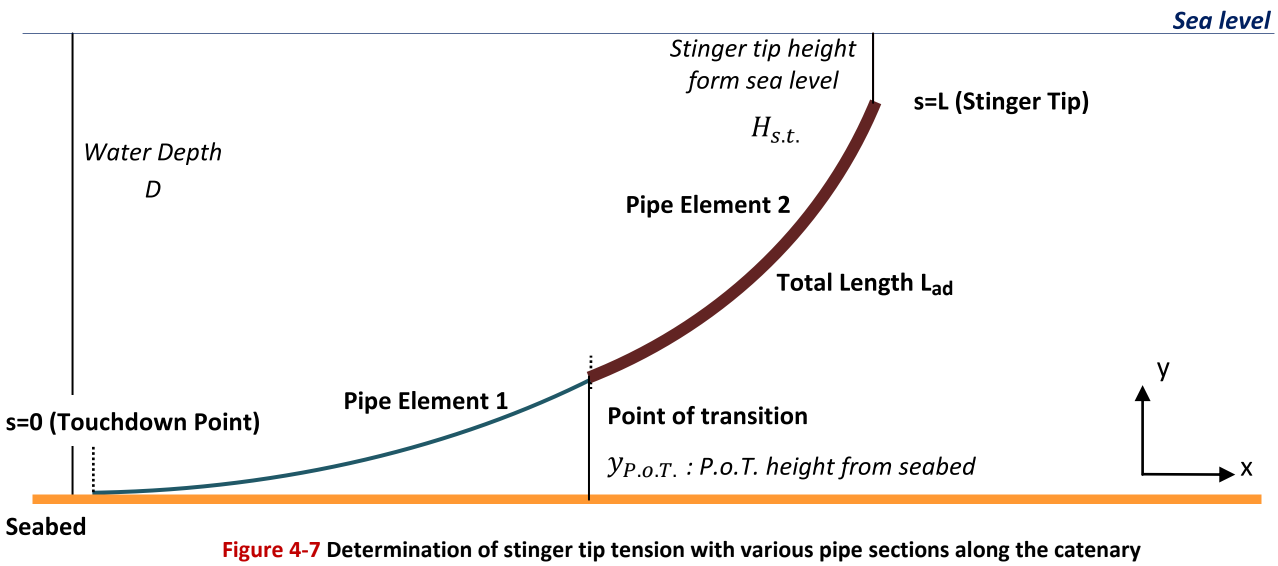


**Figure 4-7 Determination of stinger tip tension with various pipe sections along the catenary**

The principle of the determination of the axial tension remains the same for more pipe sections along the catenary. The equation for the determination of the axial tension at the stinger for N pipe sections along the catenary

$$T(st) = T_h + \int_0^{y_{P.o.T.1}} w_{s(1)}\, dy + \int_{y_{P.o.T.1}}^{y_{P.o.T.2}} w_{s2}\, dy + .. \int_{y_{P.o.T.i}}^{y_{P.o.T.i+1}} w_{s(i+1)}\, dy .. + \int_{y_{P.o.T.N}}^{H_{s.t.}} w_{s(N+1)}\, dy$$

## 5.0 PIPELINE ROTATION

### 5.1 Introduction to pipe rotation phenomenon

Subsea pipelines have the tendency to rotate during installation. This rotation can have multiple causes which are interfering with each other. Specifically, during S-lay installations, the pipe is exposed to plastic strains when it passes over the stinger exceeding a certain curvature. This residual curvature causes the pipeline to rotate along its suspended length. Additional causes which contribute to pipe rotation are possible tensioner misalignments (not considered in the model). Pipeline rotation is dependent on many factors such as water depth, pipeline characteristics (bending stiffness, submerged weight, etc.) and pipe tension. It is still unclear how these different contributions combine together.

When structures are installed in the pipeline it is necessary to determine the amount of rotation in the line, in order to ensure installation within acceptable limits. Because of the increasingly deep waters and the fact that the structures attached on the pipelines become heavier and more complex, there is a need to extend our knowledge on rotation problem. Due to the complexity of the phenomenon and its relative harmlessness during conventional installations, rotation has been – so far – mostly overlooked by the various actors of the Pipeline Engineering world.

In the literature, Bynum & Havik (1981) investigate the pipeline rotation phenomenon, employing an internal and external work balance approach. Damsleth et al. (1999) deals with the consequences of the plastic strain that can occur in the outer fibers of the pipe as it passes over the stinger during laying. Endal et al. (1995) deal with the behavior of offshore pipelines subjected to residual curvature during laying and approach the roll prediction in three different ways [16].

### 5.2 The effect of the residual curvature

During S-lay method, the pipe extends from the tensioners, bends over the stinger (overbend), and while sloping downward through the water (sagbend), bends gradually in the opposite direction onto the horizontal seabed. The tensioners provide the upper support for the pipe while the seabed provides the lower support, where residual tension is balanced by soil friction.

Pipe laying vessels have gradually adapted to the technical challenges of deep water projects by increasing their tension capacity and stinger length. The larger laying vessels have reached physical limitations, where further increase in their capacity would, in principle, be too costly for a low-price scenario. Taking advantage of the pipe strength capacity, curving the stinger more sharply to obtain steeper departure angles is a cost-effective alternative to the tension required to install the pipeline is lower.

Decreasing the stinger radius has as a consequence an increase of the total strains in the overbend region. In many cases, the deformations exceed the elastic limit of the pipe's material and the pipeline is exposed to plastic strains when it passes over the stinger. As a result it leaves the overbend with a residual curvature. As the pipe moves through the suspended section of the catenary (sagbend), it is bent in the reverse direction. If the pipe had been plastically deformed when passing over the stinger, the reverse bending occurs partially through bending and partially through rotating. The physical reason for this rotation is detailed and illustrated below

1. While passing over the stinger the pipe is exposed to plastic deformations.

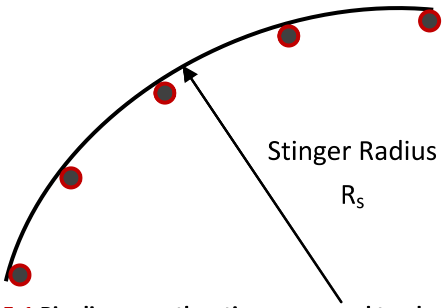


**Figure 5-1 Pipeline over the stinger exposed to plastic strains**

2. The pipe possess a residual curvature which is oriented as the overbend curvature.

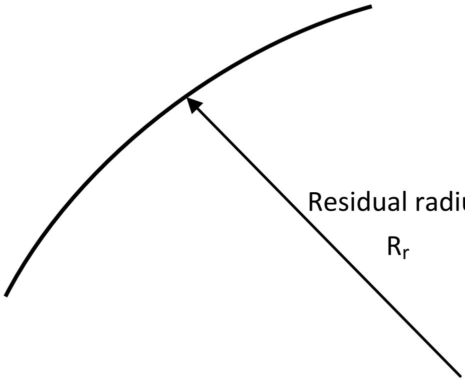


**Figure 5-2 Residual radius of pipe because after the overbend region**

3. While travelling through the sagbend , the pipe will be exposed to increasingly high bending moments, which act at the opposite direction of the residual curvature pipe. In order to facilitate the reversed bending in the sagbend area, the pipe may rotate to orientate its natural curvature favorably towards the direction of the sagbend curvature.

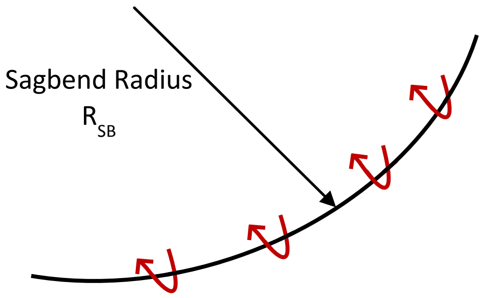


**Figure 5-3 Sagbend radius of pipe along the catenary**

In the following figures two "extreme" cases will be illustrated. At the first case the pipe is not rotated ($0^o$ degrees rotation) while at the second case the pipe is rotated $180^o$ degrees.

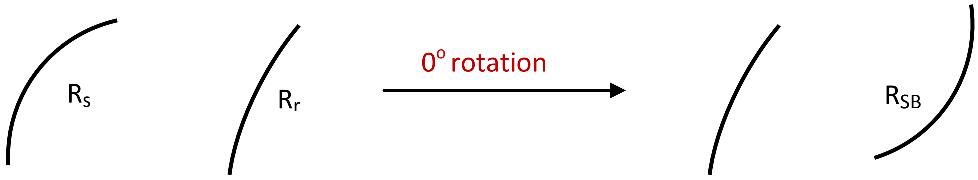


**Figure 5-4 Simplified illustration of a pipe section from overbend to sagbend with $0^o$ rotation**

In case of no rotation, the pipe in order to take the sagbend curvature has to overcome the residual curvature from the overbend. According to that, the total bending moment in the sagbend will be increased and estimated as follows

$$M = E \cdot I_b \cdot \left(\frac{1}{R_{SB}} + \frac{1}{R_r}\right)$$

In the case of $180^o$ rotation, the residual curvature from the overbend is reversed in the direction of the sagbend curvature. Based on that, the pipe is already in the preferable configuration and the total bending moment in the sagbend will be decreased

$$M = E \cdot I_b \cdot \left(\frac{1}{R_{SB}} - \frac{1}{R_r}\right)$$

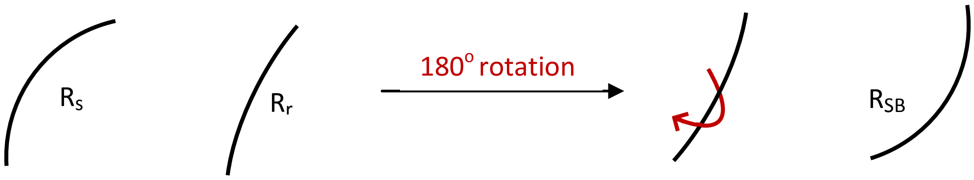


**Figure 5-5 Simplified illustration of a pipe section from overbend to sagbend with $180^o$ rotation**

The amount of pipe rotation depends on several parameters. The residual curvature is the "driving force" for the pipeline rotation. In general higher values of residual curvature lead to higher amount of rotation while if it lies below a certain threshold value, depending on the project, the rotation may not happen. In addition, the level of sagbend strains will determine the willingness of the suspended pipe to rotate in order to accommodate to the residual curvature. The suspended length of the pipe at sagbend is also important as it determines the torsional stiffness of the catenary, therefore allowing, or not, the pipe to rotate.

In the literature one paper deals with the rotation problem of a pipeline installed using the S-lay method, Geir Endal, Odd B. Ness and Richard Verley (1995) [16]. The paper deals with the pipe rotation problem employing a simplified energy approach, which is based on minimising the work conducted in the sagbend due to the reversed bending of the pipeline. The next chapter gives an insight about the method.

### 5.3 Endal's Approach

The underlying principle of Endal's calculation method is that along the catenary, which is not subjected to external forces, the pipeline will adopt the configuration for which its total mechanical energy is minimized. The approach complies with the following assumptions:

The pipeline rotation is assumed to occur between the inflection point and the touchdown point.

The pipeline is exposed to plastic strains over the stinger and as a result has a residual curvature $k_r$ due to bending at the overbend.

The sagbend pipe curvature $k(s)$ is assumed to be the sum of the following contributions

$$k(s) = k_0(s) + k_r cos\varphi(s) \qquad [\mathbf{5.1}]$$

where $k_0(s)$ is the nominal pipeline curvature function along the catenary $[m^{-1}]$, represented by a 2nd order polynomial and $\varphi(s)$ is the rotation angle function along the catenary represented by a 3rd order polynomial.

The boundary conditions used to find the coefficients of the rotation angle function are the following

- $\phi(0) = 0$ – Rotation angle at the inflection point is zero.
- $\phi'(0) = 0$ – Derivative of the rotation angle (torque) at the inflection point is zero.
- $\phi(L) = \varphi_0$ – Rotation angle at the touchdown point is $\phi_0$ (unknown).
- $\phi(L) = 0$ – Derivative of the rotation angle (torque) at the touchdown point is zero.

Applying the boundary conditions the rotation angle function is expressed as follows

$$\phi(s) = -2\varphi_0 \frac{s^3}{L^3} + 3\varphi_0 \frac{s^2}{L^2}$$

The term $k_r cos\varphi(x)$ is called "apparent residual curvature" and it expresses the projection of the residual curvature in the plane of the catenary, assuming pipe-laying as a 2D problem.

The total energy in the sagbend is assumed to consist of a rotation contribution $W_R$ and a bending contribution $W_B$ and is expressed by :

$$W_T = W_B + W_R$$

As mentioned in previous chapters the bending moment along the catenary is determined by the following expression

$$M = EI_b k(s)$$

Taking into account the residual curvature, based on equation 6.1, the total work due to bending along the suspended length is

$$W_B = EI_b \int_0^L (k_0(s) + k_r cos\varphi(s))^2 \, \mathrm{ds}$$

The work because of the rotation of the pipe along the catenary can be written as follows

$$W_R = GI_t \int_0^L \left(\frac{\mathrm{d}\phi}{\mathrm{d}s}\right)^2 \mathrm{d}s$$

where ϕ(s) is the rotation angle function along the catenary, G is the shear modulus of steel [Pa] and $I_t$ is the polar moment of inertia of the pipe in [$m^4$]. The minimization of the total Energy accounts for the fact that the pipeline will benefit from aligning its residual curvature towards the sagbend curvature. Since pipe rotation is driven by the reduction of internal forces along the catenary, Energy minimization is the most straightforward method to determine it.

An example of Endal's approach, with graphical representation is given below for the first case study (see Chapter 6.2.1.1).

The nominal curvature $k_0(s)$ distribution along the length, based on the 2nd order shape assumption is illustrated in Figure 5-6.

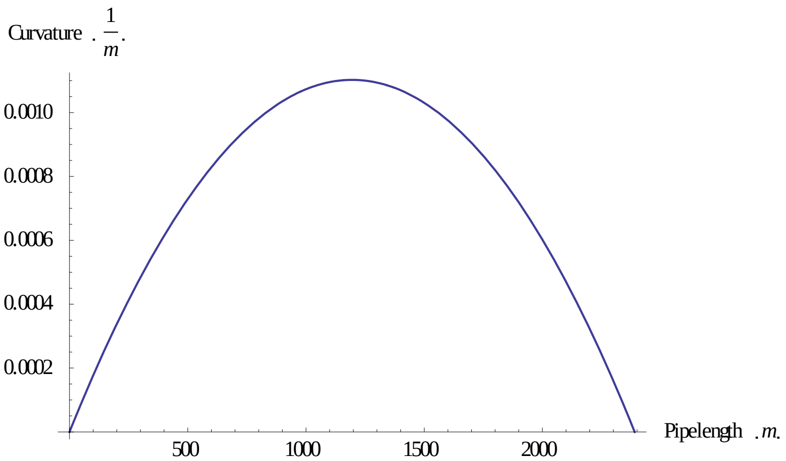


**Figure 5-6 Curvature along the catenary based on Endal's approach**

An illustration of the rotation angle profile along the catenary for different TDP rotation angles $\varphi_0$ is shown in Figure 5-7.

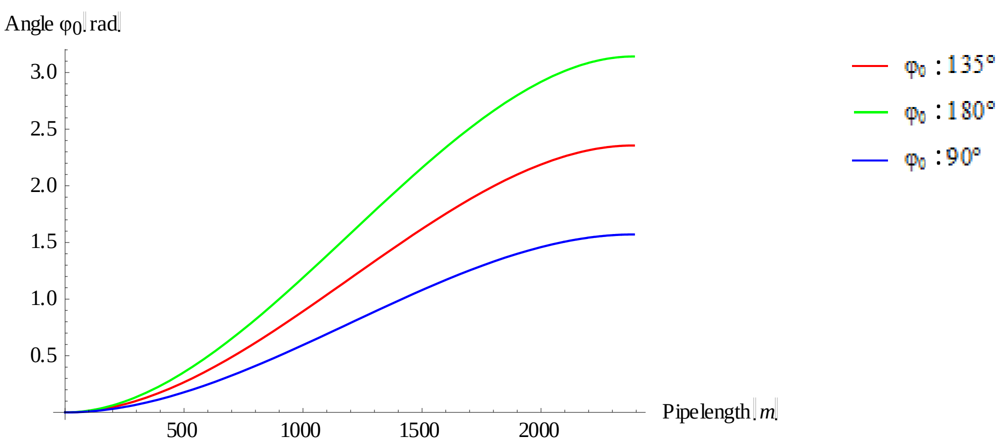


**Figure 5-7 Rotation angle profiles for different touchdown point angles $\varphi_0$**

Taking into account the residual curvature $k_r$ and the rotation profiles for the different TDP rotation angles (see Figure 5-7), the new curvature distribution along the catenary based on equation 6.1 is shown in Figure 5-8.

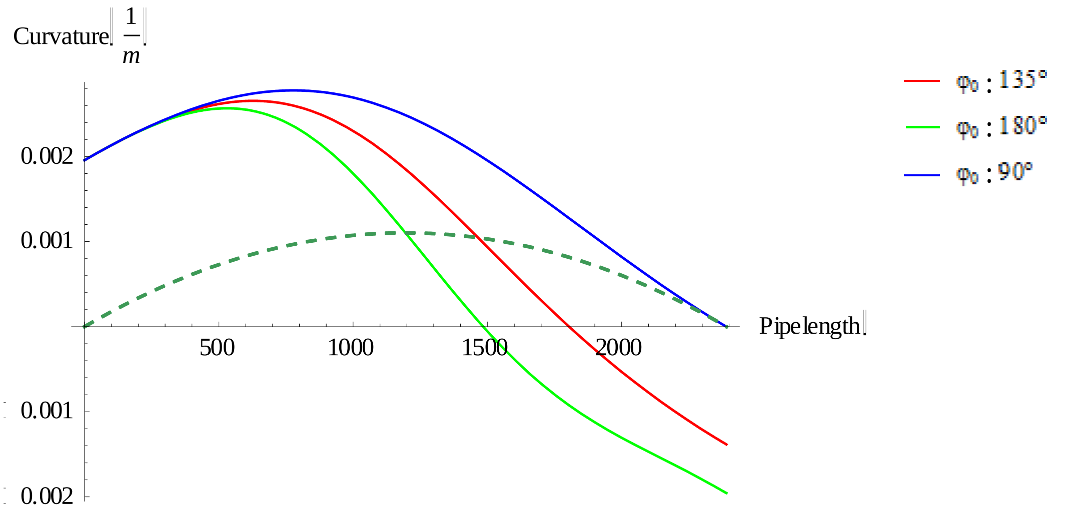


**Figure 5-8 Curvature profiles taking into account the residual curvature for various TDP angles $\varphi_0$**

Having all the needed information for the pipeline characteristics, bending, torsion and total energy can be determined based on the equations shown above, for various TDP angles $\varphi_0$. Figure 5-9 shows the a graphical representation of these calculations for the case study. As mentioned before the rotation angle $\varphi_0$ for which the total energy is minimized, is the actual rotation angle at the touchdown point $\varphi_{TDP}$ according to Endal's approach

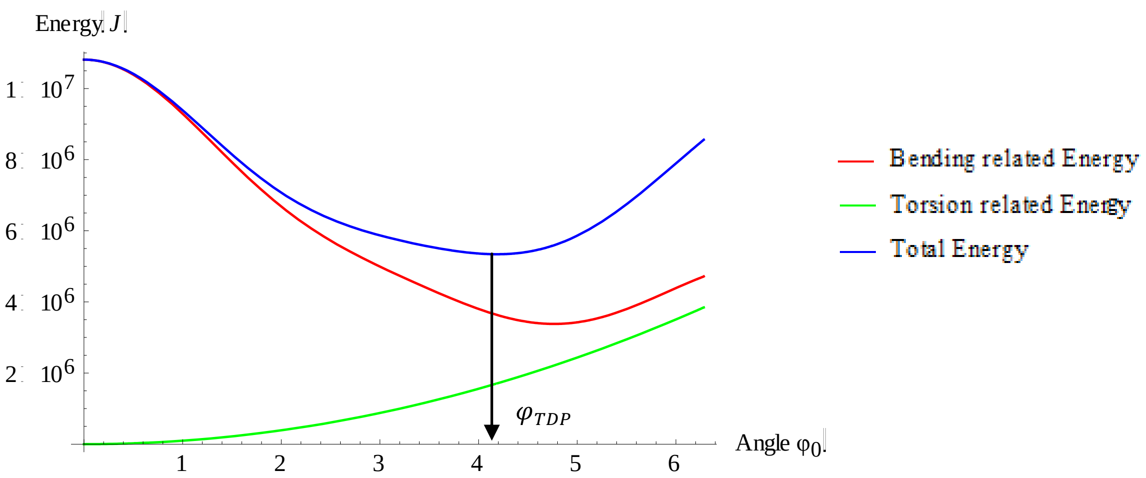


**Figure 5-9 Bending, Torsion and Total energy of the pipeline for various TDP rotation angles $\varphi_0$**

Although the main principle used by Endal's theory is correct, the assumptions made on both curvature and rotation profile function are not valid. Figure 5-10 shows the difference at the curvature shape along the catenary for the 4 cases which were conducted (see Chapter 3.3.4).

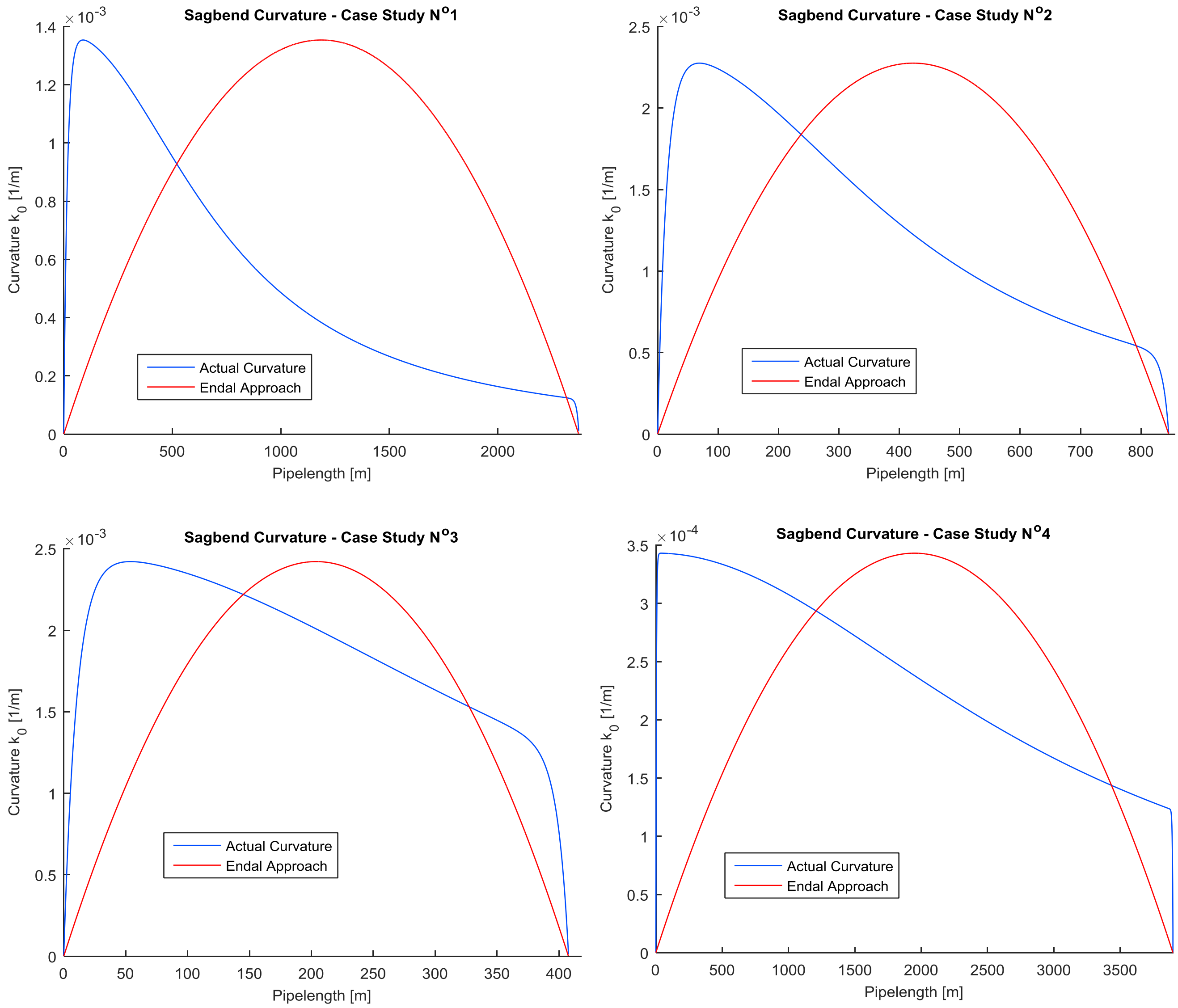


**Figure 5-10 Curvature obtained by pipelay analysis (Actual Curvature) and Endal's Approach**

As it can be seen for all the case studies there is significant difference between the curvature assumed by Endal's approach and the actual curvature. The simplified method proposed will not be further discussed here as it has been rendered obsolete by the use of modern numerical methods. In the next chapter the mathematical model and its implementation in Matlab will be described in detail.

## 6.0 PIPELINE ROTATION MATHEMATICAL MODEL

### 6.1 Pipeline Rotation Model Improvements

In order to determine the rotation profile, a numerical implementation of Lagrangian minimization is used. Unlike the original method described by Endal, the method used here does not require an assumption on the shape of the rotation function along the catenary. Instead, it relies on numerical minimization to find the arbitrary roll function that will induce the least amount of Energy to the pipe. Also, the curvature function $k_0(s)$ is not represented as a 2$^{nd}$ order polynomial, an assumption not valid (see Figure 5-10), as it is already determined by the pipelay analysis described in previous chapters. Finally, after the mathematical formulation which will be described in the next chapter, the boundary conditions needed for the rotation problem are two instead of four used at the Endal's approach.

### 6.2 Lagrangian Minimization

Based on the energy minimization principle, firstly the total strain energy in the pipe has to be defined. As mentioned in chapter 3.2.1 the pipeline is considered as a beam under the combined loading of tension, bending and torsion. Not considering in the model coupling between the different loads (coupling between bending and torsion will be discussed in later chapter) the strain energy along the suspended length of the pipe can be written

$$W_T = W_{ax} + W_B + W_R$$

Where $W_{Ax}$ is the work due to the axial tension and can be written

$$\mathrm{W_{ax}} = \frac{1}{2}\int_0^L EA[u'_{ax}(s)]^2 ds \qquad [\mathbf{6.1}]$$

and $u'_{ax}(s)$ is the axial displacement per unit length (axial strain) of pipe.

The total work due to bending can be written as

$$\mathrm{W_B} = \frac{1}{2}\int_0^L EI_b[k(s)]^2 ds \qquad [\mathbf{6.2}]$$

Where $k(s)$ is the curvature and depends on rotation function based on equation 6.1 .

The work due to torsion is expressed by

$$\mathrm{W_R} = \frac{1}{2}\int_0^L GI_t[\varphi'(s)]^2 ds \qquad [\mathbf{6.3}]$$

Where $\varphi'(s)$ is the rotation per unit length of pipe. The derivation of energy expression is shown in Based on the above the total work of a pipeline with suspended length L can be written

$$W_T = \frac{1}{2}\left[\int_0^L EA[u'_{ax}(s)]^2 ds \; + \int_0^L EI_b[k(s)]^2 ds + \int_0^L GI_t[\varphi'(s)]^2 ds\right]$$

Based on Lagrangian mechanics the rotation function ϕ(s) for which the total energy of the pipeline will be minimized, can be found from the following equation

$$\frac{\mathrm{d}}{\mathrm{ds}}\left(\frac{\partial\mathcal{L}}{\partial\phi'}\right) - \frac{\partial\mathcal{L}}{\partial\phi} = 0 \qquad [\mathbf{6.4}]$$

Where $\mathcal{L}$ is the total energy of pipe element of length ds, so

$$\mathcal{L} = \frac{1}{2}\left[EA\left[u_{ax}^{'}(s)\right]^2 + EI_b[k(s)]^2 + GI_t\left[\varphi^{'}(s)\right]^2\right]$$

Substituting the term $k(s)$ with

$$k(s) = k_0(s) + k_r cos\varphi(s)$$

The expression of $\mathcal{L}$ becomes

$$\mathcal{L} = \frac{1}{2}\left[EA\left[u_{ax}^{'}(s)\right]^2 + EI_b[k_0(s) + k_r cos\varphi(s)]^2 + GI_t\left[\varphi^{'}(s)\right]^2\right]$$

Expanding the second square we get

$$\mathcal{L} = \frac{1}{2}[EA[u'_{ax}(s)]^2 + EI_b\kappa_0^2(s) + 2EI_b\kappa_0(s)\kappa_r \cos\varphi(s) + EI_b\kappa_r^2 cos^2\varphi(s) + GI_t[\varphi'(s)]^2]$$

Taking into account that the axial strain $u'_{ax}(s)$ is independent of the rotation angle $\varphi(s)$ and based on equation 7.4 and the expression above becomes

$$\frac{\partial\mathcal{L}}{\partial\phi} = \frac{1}{2}[-2EI_b\kappa_0(s)\kappa_r \sin\varphi(s) - 2EI_b\kappa_r^2 cos\varphi(s)sin\varphi(s)]$$

and

$$\frac{\mathrm{d}}{\mathrm{ds}}\left(\frac{\partial\mathcal{L}}{\partial\phi'}\right) = \frac{\mathrm{d}}{\mathrm{ds}}\frac{1}{2}\big(2GI_t\varphi'(s)\big) = \frac{1}{2}[2GI_t\varphi''(s)]$$

So the energy minimization equation [7.4] can be written

$$\frac{1}{2}[2GI_t\varphi''(s)] - \frac{1}{2}[-2EI_b\kappa_0(s)\kappa_r \sin\varphi(s) - 2EI_b\kappa_r^2 cos\varphi(s)sin\varphi(s)] = 0$$

Based on the expression above the differential equation that describes the rotation profile function is

$$\varphi''(s) + \frac{EI_b}{GI_t}\kappa_0(s)\kappa_r \sin\varphi(s) + \frac{EI_b}{GI_t}\kappa_r^2 cos\varphi(s) sin\varphi(s) = 0, \;\; \mathrm{s} \in [0, \mathrm{L}] \qquad [\mathbf{6.5}]$$

It should be mentioned that at the equation above $\kappa_0(s)$ is the sagbend curvature function along the catenary which is already determined by the pipe-lay problem described in previous chapters. The residual curvature $\kappa_r$ is based on pipe properties, the maximum bending strains and associated tension.

The differential equation is of second order so there is need of two boundary conditions. These boundary conditions can be imposed to the rotation angle itself, or its derivative, which is proportional to the torque. For Pipelay operations, the most natural boundary conditions to start with are:

$$(\mathbf{1})\ \phi(0) = 0 \qquad\qquad (\mathbf{2})\ \left.\frac{d\phi}{ds}\right|_{s=L} = 0$$

The *first boundary* condition imposes that the rotation at the origin (stinger tip) is zero. Assuming that the rotation starts at the point where the reverse bending begins (inflection point).

The *second boundary* condition expresses the fact that, during a steady-state pipe-laying process (uniform pipe properties, constant tension and constant water depth), the rotation at touchdown point will not change. The orientation of the laid pipe is constant near touchdown point, therefore the derivative of the roll profile is zero.

The differential equation described in equation 6.5 and the set of boundary conditions are solved using Matlab boundary value solver bvp4c. The boundary value problem must first be rewritten in a state space system using $\mathrm{y}_1 = \phi(\mathrm{s})$ and $\mathrm{y}_2 = \phi'(\mathrm{s})$ as shown below

$$Matlab\ Input \left\{ \begin{array}{c} y_1' = y_2 \\ y_2' = M \cdot sin(y_1) + N \cdot cos(y_1)\, sin(y_1), \qquad s \in [0, L] \\ M = -\dfrac{EI_b}{GI_t}\kappa_0(s)\kappa_r \\ N = -\dfrac{EI_b}{GI_t}\kappa_r^2 \\ y_1(0) = 0 \\ y_2(L) = 0 \end{array} \right\}$$

For the all the cases which were presented in Chapter 3.3.4, the rotation angle profile was estimated along the catenary. For each case study the residual radius was obtained from BendPipe based on the maximum bending strain at the overbend and the corresponding axial tension. For each case the effect of the residual radius/curvature is shown at the rotation profile

#### 6.2.1.1 Case study N°1

| Quantity | Value | Unit |
|---|---|---|
| Maximum Overbend Strain | 0.28 | $[\%]$ |
| Residual Radius | 511.1 | $[m]$ |
| Touchdown Point Rotation Angle | 118.099 | $[Deg]$ |

**Table 6-1 Rotation profile data (Case Study N°1)**

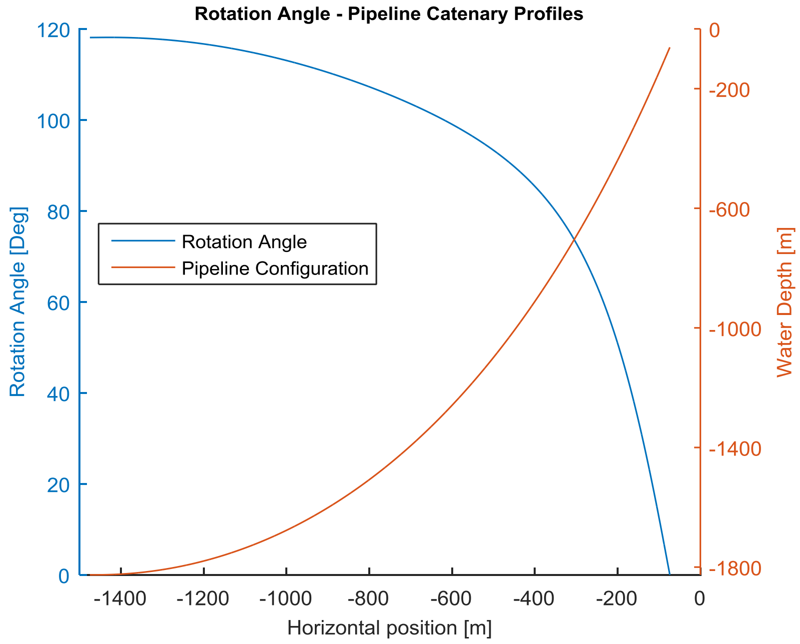


**Figure 6-1 Rotation Angle profile along the catenary (Case N°1)**

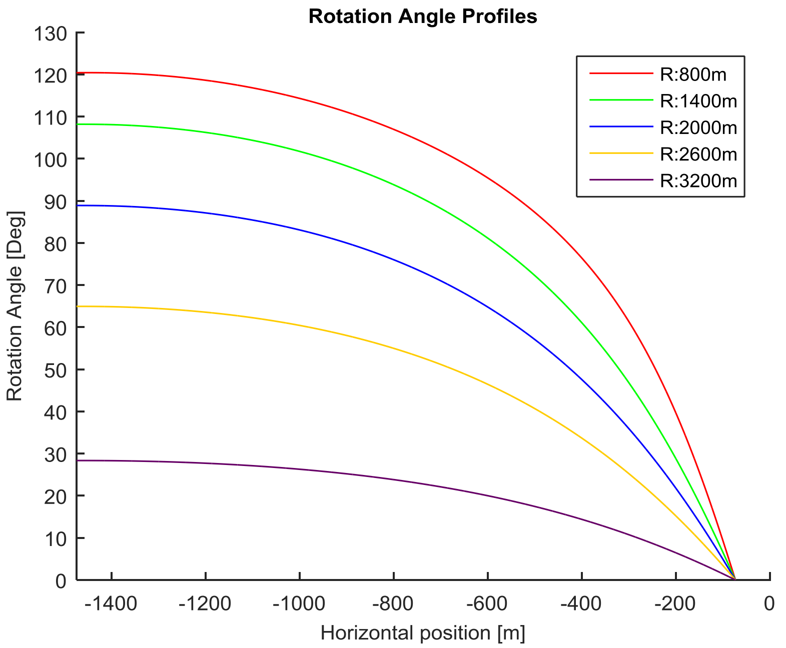


**Figure 6-2 Rotation Angle profiles for different residual curvature (Case N°1)**

### 6.2.1.2 Case study N°2

| Quantity | Value | Unit |
|---|---|---|
| Maximum Overbend Strain | 0.276 | $[\%]$ |
| Residual Radius | 360.6 | $[m]$ |
| Touchdown Point Rotation Angle | 40.578 | $[Deg]$ |

**Table 6-2 Rotation profile data (Case Study N°1)**

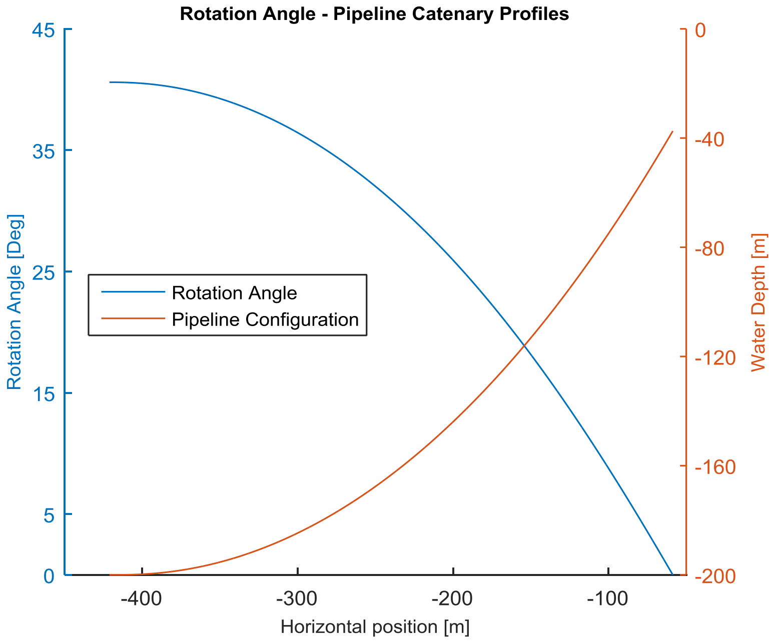


**Figure 6-3 Rotation Angle profile along the catenary (Case Study N°1)**

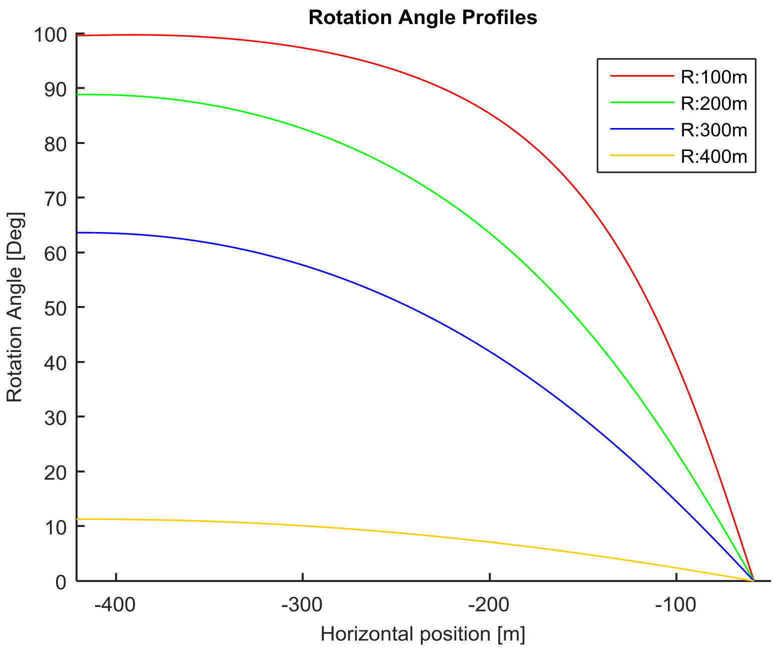


**Figure 6-4 Rotation Angle profiles for different residual curvature (Case N°2)**

#### 6.2.1.3 Case study N°3

| Quantity | Value | Unit |
|---|---|---|
| Maximum Overbend Strain | 0.2356 | $[\%]$ |
| Residual Radius | 791 | $[m]$ |
| Touchdown Point Rotation Angle | 63.702 | $[Deg]$ |

**Table 6-3 Rotation profile data (Case Study N°3)**

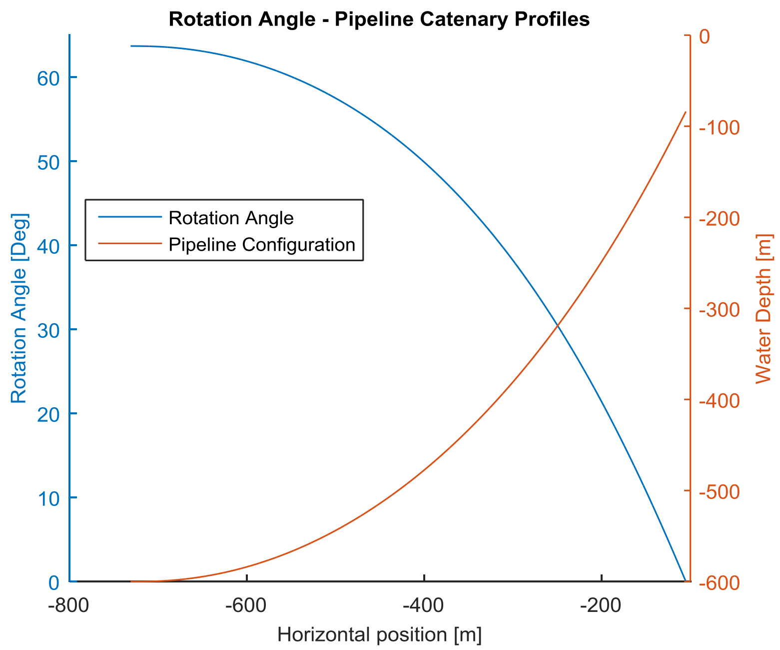


**Figure 6-5 Rotation Angle profile along the catenary (Case Study N°3)**

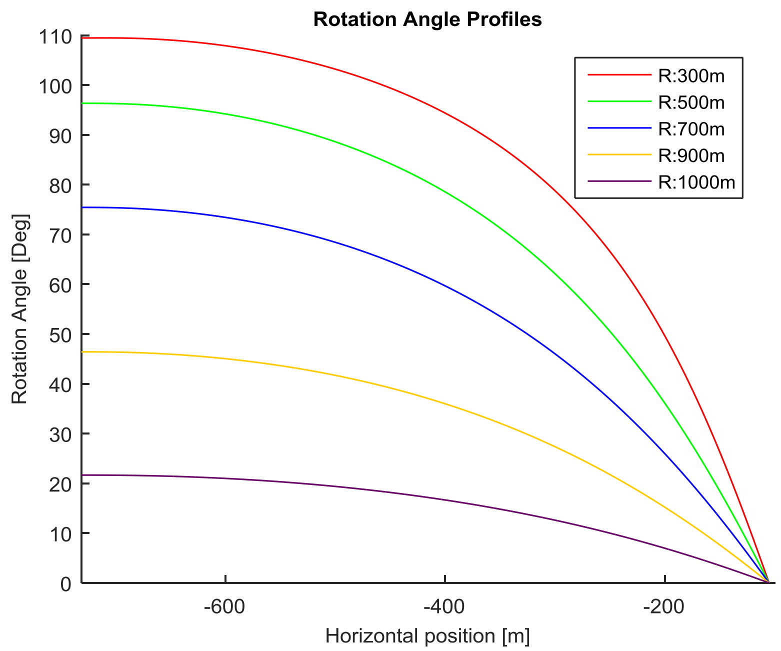


**Figure 6-6 Rotation Angle profiles for different residual curvature (Case N°3)**

#### 6.2.1.4 Case Study N°4

| Quantity | Value | Unit |
|---|---|---|
| Maximum Overbend Strain | 0.15 | $[\%]$ |
| Residual Radius | 2262 | $[m]$ |
| Touchdown Point Rotation Angle | 88.735 | $[Deg]$ |

**Table 6-4 Rotation profile data (Case Study N°1)**

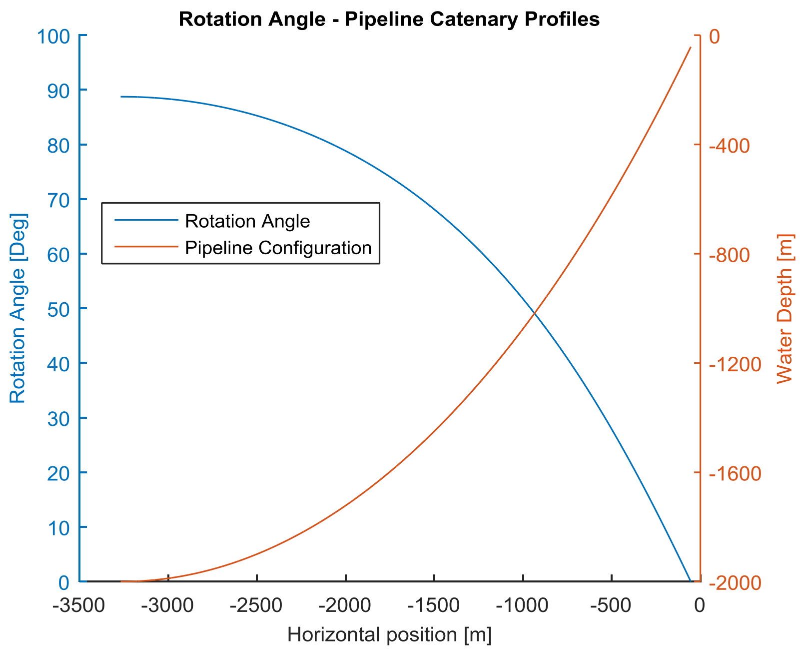


**Figure 6-7 Rotation Angle profile along the catenary (Case Study N°4)**

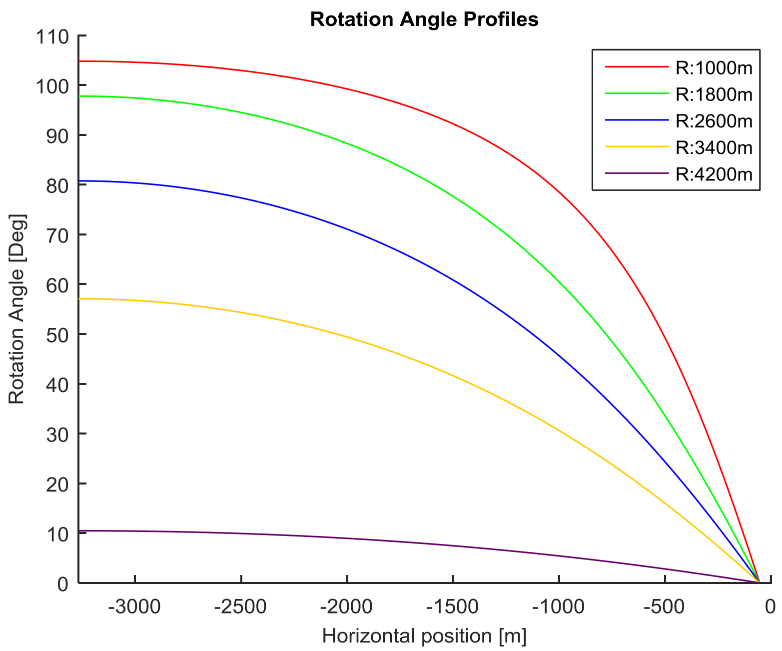


**Figure 6-8 Rotation Angle profiles for different residual curvature (Case N°4)**

As it can be seen from the figures above the rotation profile along the catenary has the same shape for all the cases studied. Depending on the residual radius, the characteristics of the pipe and the stinger configuration touchdown point rotation angle differs. In order to have a better understanding of the relationship between the TDP rotation angle is found for a large range of values of the residual radius as shown in Figure 6-9.

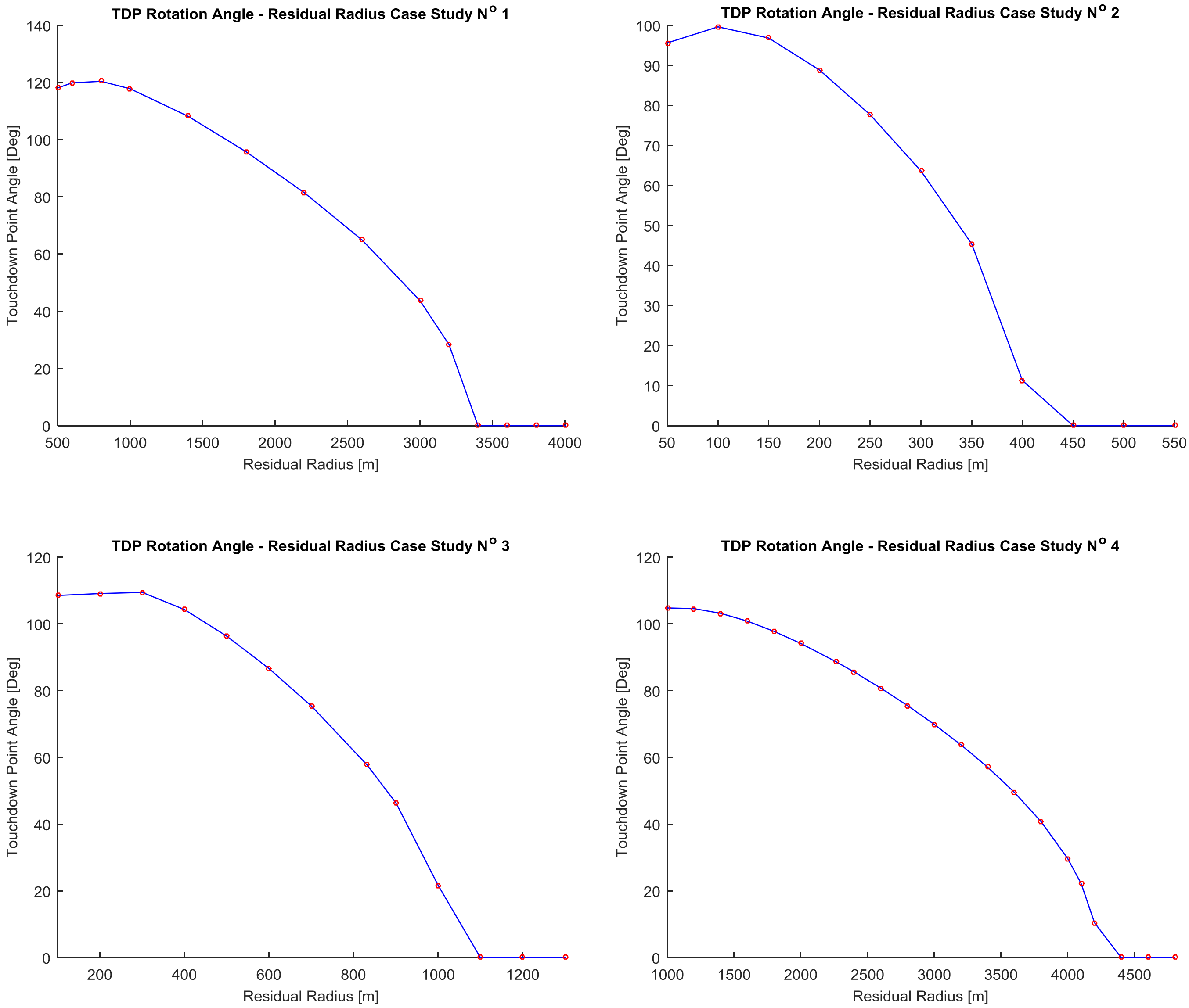


**Figure 6-9 Relation between residual radius and touchdown point angle**

Based on Figure 6-9 it is noticed that for all the case studies the reduction of the residual radius - increase of the residual curvature - has as a result the increase of the touchdown point rotation angle. However, for extreme low values of residual radius it can be seen that the touchdown point rotation angle decreases. In addition, it should be mentioned that for all the cases there is a threshold value of residual radius for which the pipeline does not rotate along the catenary and thus the TDP angle equals to zero. If the residual radius exceed that threshold value there is a steep increase of the touchdown angle.

## 6.3 Inline Structure Rotation Model

Although rotation is harmless for the pipeline itself, when an inline structure is attached to the pipe, it usually needs to be installed within certain verticality tolerance to allow for future connections or ROV access. Examples of inline structure are shown in Figure 6-10 and Figure 6-11.

**Figure 6-10 Inline Structure being transported**

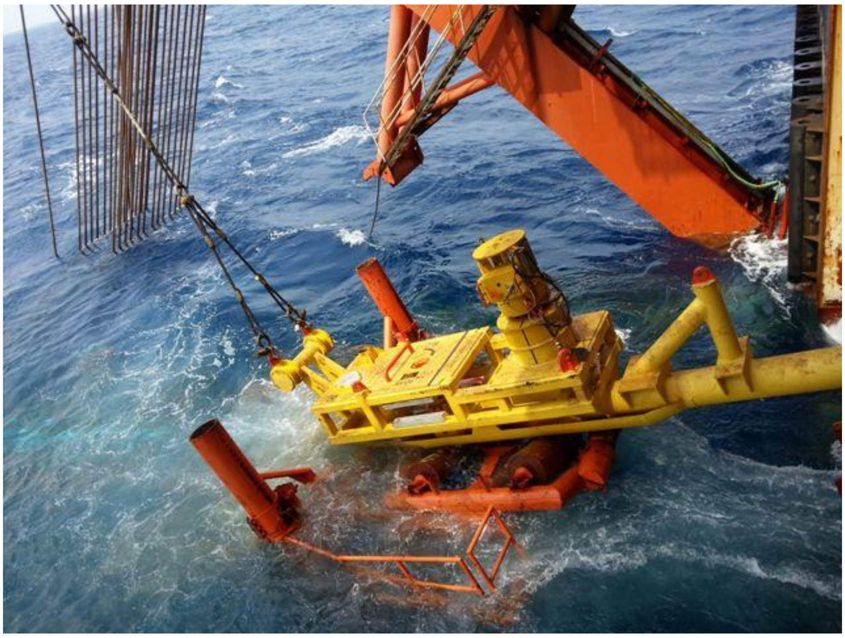

**Figure 6-11 Inline Structure during installation**

The determination of ILS rotation during its installation is performed based on Lagrangian minimization principle, as described in Chapter 6.2. The minimization method considers two separate pipe catenaries. The first part of the catenary starts at the stinger tip, ending at the inline structure, also called "pre ILS" catenary. The second part of the catenary starts at the position of the inline structure and ends at the touchdown point, known as "post ILS" catenary.

A simplified illustration of the ILS along the catenary and the two parts is shown in Figure 6-12.

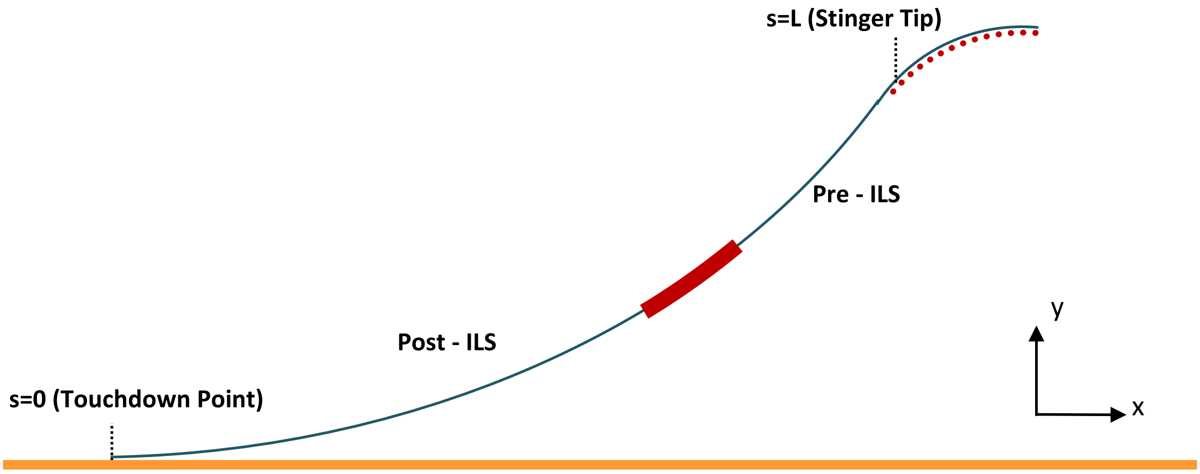


**Figure 6-12 Illustration of ILS along the catenary with pre and post catenary parts determination**

As it can be seen from Figure 6-10 and Figure 6-11 inline structures are much heavier than the pipeline. In addition, their center of gravity is above the centerline of the pipe. Because of these facts, the presence of an ILS in the catenary can result to a destabilizing torque (or overturning moment) and as a consequence to rotation instability.

Taking into account that the most relevant properties for rotation estimation is the total submerged weight as well as the location of the center of gravity with respect to the pipe centerline, the overturning moment induced by the ILS is calculated with the following formula

$$T_{ILS} = w_{ILS} \cdot h_{CoG} \cdot cos(\theta) \cdot sin(\phi_{ILS}) \qquad [\mathbf{6.6}]$$

Where

- $T_{ILS}$ is the overturning moment in [Nm]
- $w_{ILS}$ is the total submerged weight in [N] of the inline structure
- $h_{CoG}$ is the distance in [m] between the centre of gravity of the inline structure and the pipe centreline.
- $\vartheta$ is the horizontal angle of the pipe at the ILS location,
- $\phi_{ILS}$ is the rotation angle at the ILS

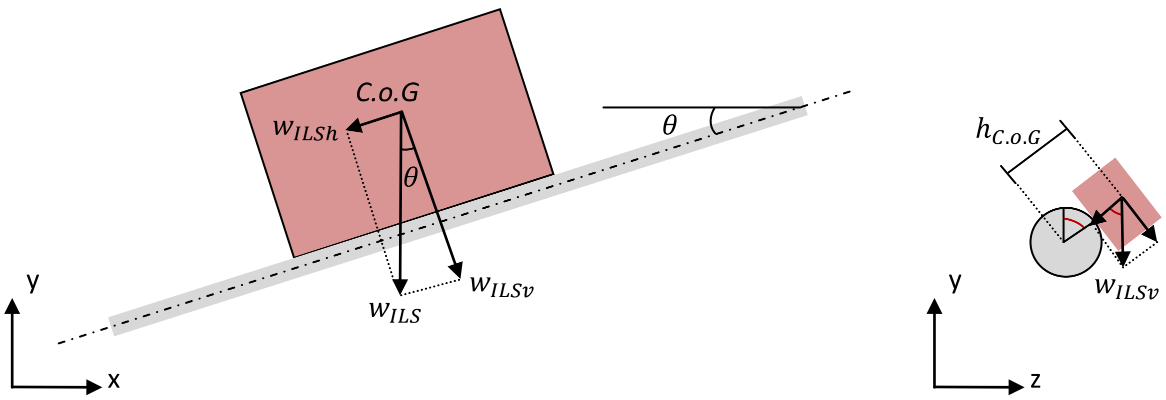


**Figure 6-13 Simplified illustration of an ILS attached in the main pipeline in x-y and y-z plane**

As mentioned above, whenever an inline structure is installed, mitigation measures are determined in order to reduce the amount of rotation. The mitigation is generally done by one or more buoyancy modules which act on the pipe catenary through a yoke.

Including a buoyancy module in the catenary is shown in Figure 6-14

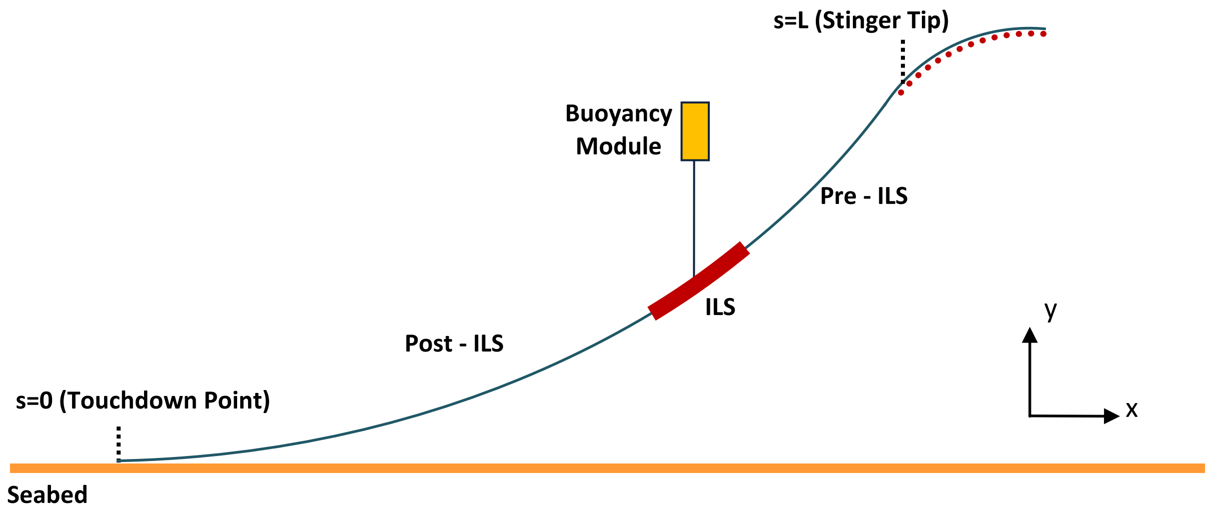


**Figure 6-14 ILS along the catenary with buoyancy module**

In most of the cases effect of the buoyancy module depends on the pipeline configuration and its angle $\theta$ with the horizontal. When the pipe is nearly the vertical configuration ($\theta = 90°$) the lever arm between the effective buoyancy force and the axis of rotation is very small, having as a consequence a limited effect of the buoyancy in the reduction of the rotation angle of the ILS. On the other hand, when ILS is nearly the horizontal configuration (i.e. when it approaches the seabed) the effect of the buoyancy module increases, reducing considerably the rotation angle of the ILS.

An illustration of the ILS and the unrestrained buoyancy module configuration in different positions along the catenary can be seen in Figure 6-15.

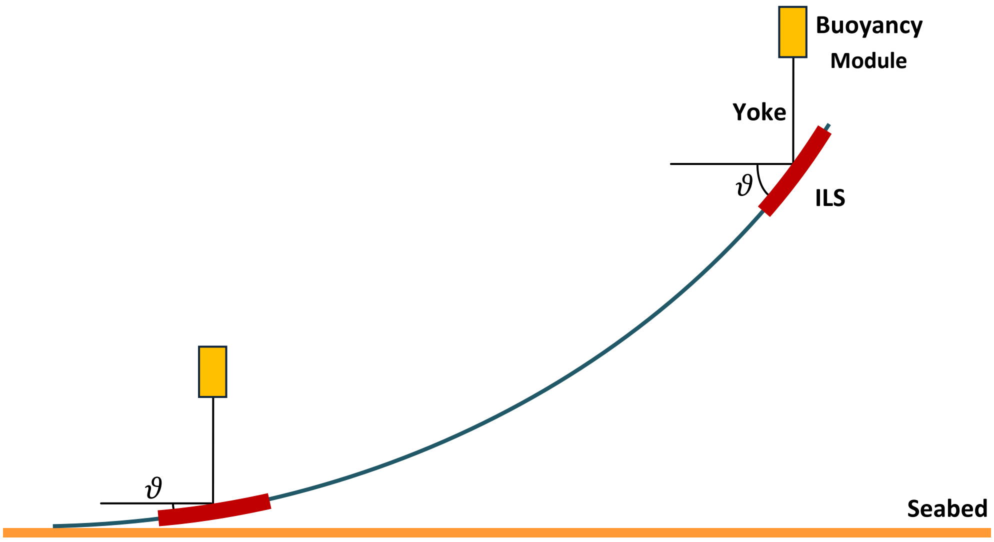


**Figure 6-15 ILS and unrestrained buoyancy module in different positions along the catenary**

When a higher efficiency of the buoyancy module is required, restrained buoyancy configuration is used, where the effect of the buoyancy module does not depend on the pipeline configuration and its angle $\theta$ with the horizontal. An illustration of the ILS and the restrained and unrestrained buoyancy module configuration can be seen in Figure 6-16.

Figure 6-16 shows the unrestrained and restrained buoyancy arrangement configuration under a rotation angle of ILS $\varphi_{ILS}$ in the x-y and the y-z plane respectively. Buoyancy arrangements in x-y plane

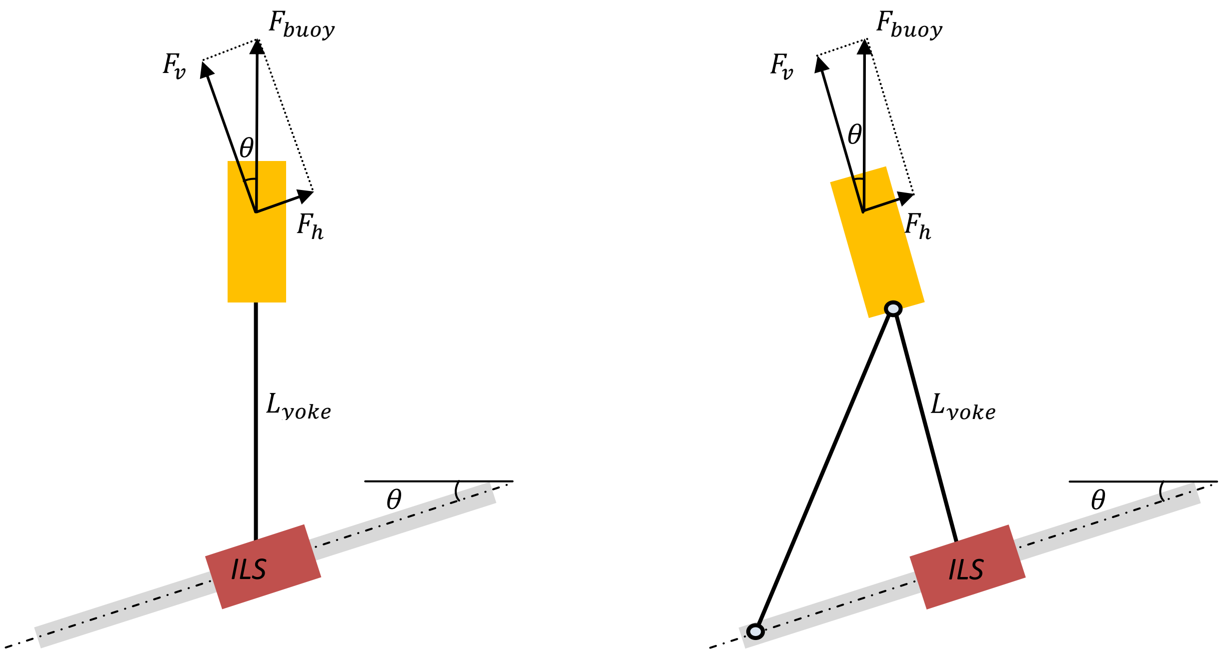


**Figure 6-16 Sketch of unrestrained and restrained buoyancy arrangement (x-y plane)**

In the case of the *unrestrained buoyancy module* arrangement the lever arm depends on the angle between the yoke and the pipeline. As it can be seen from Figure 6-16 this angle is equal to $\frac{\pi}{2} - \theta$. The lever arm can is determined based on the equation

$$L = L_{yoke} \cdot sin\left(\frac{\pi}{2} - \theta\right) = L_{yoke} \cdot cos(\theta)$$

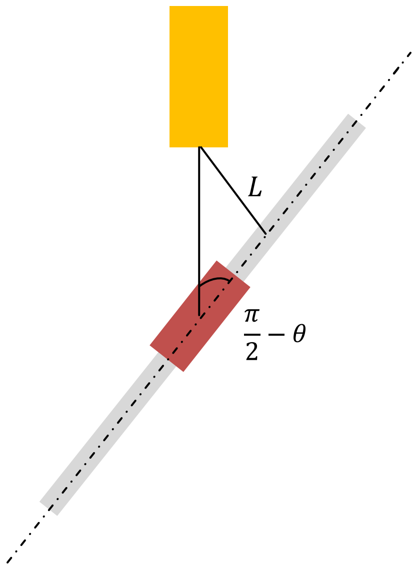


**Figure 6-17 Unrestrained buoy simplified illustration**

For the restrained buoy arrangement the lever arm is constant and equals to the yoke length. As it can be seen from Figure 6-18 which shows the buoyancy arrangement under a rotation angle of ILS $\varphi_{ILS}$ in the y-z plane.

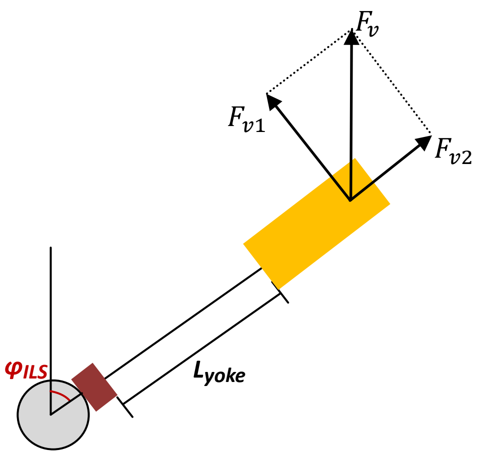


**Figure 6-18 Sketch of restrained buoyancy arrangement (y –z plane)**

Both for the unrestrained and for the restrained buoyancy configuration, force $F_{v1}$ causes the counteracting torque

$$T_{buoy} = F_{v1} \cdot L$$

Force can be determined as follows

$$F_{v1} = F_v * sin(\phi_{ILS}) = F_{buoy} \cdot cos(\vartheta) \cdot sin(\phi_{ILS})$$

The lever arm for the unrestrained buoy equals to $L = L_{yoke} \cdot cos(\theta)$

so the counteracting torque is calculated based on the following equation

$$T_{buoy(un)} = F_{buoy} \cdot cos^2(\vartheta) \cdot sin(\phi_{ILS}) \cdot L_{yoke} \qquad [\mathbf{6.7}]$$

while for the restrained buoy the lever arm equals to $L = L_{yoke}$

so the counteracting torque is determined by

$$T_{buoy(r)} = F_{buoy} \cdot cos(\vartheta) \cdot sin(\phi_{ILS}) \cdot L_{yoke} \qquad [\mathbf{6.8}]$$

Where

- $T_{buoy}$ is the counteracting torques in [Nm]
- $F_{buoy}$ is the net buoyancy force (uplift) in [N]
- $L_{yoke}$ is the length of the yoke of the buoy (see Figure 6-18) in [m]
- $\vartheta$ is the horizontal angle of the pipe at the ILS location,
- $\phi_{ILS}$ is the rotation angle at the ILS

### 6.4 In-Line Structure Equilibrium

Based on the above, ILS is subject to

1. Overturning moment due to its weight and location of centre of gravity
2. Counteracting moment due to the buoyancy forces
3. Internal torque from the pipeline

The equilibrium of torques around the pipeline axis at the ILS can be expressed by the following equation

$$T_{buoy}(\phi_{ILS}) - T_{ILS}(\phi_{ILS}) - T_{pipe}(\phi_{ILS}) = 0 \qquad [\mathbf{6.9}]$$

As it can be seen from equations 7.6, 7.7 and 7.8, $T_{ILS}$ and $T_{buoy}$ are both dependent on the rotation angle at the position of the inline structure. The internal torque of the pipe, $T_{pipe}$ depends on the pipeline rotation profile for a given ILS angle and therefore doesn't have a simple analytical expression. In order to determine the equilibrium state, the catenary is split in two parts (catenary before and after ILS) and is solved using energy minimization principle for different ILS rotation angles $\phi_{ILS}$. The angle $\phi_{ILS}$for which the internal torque of the pipe equals to the combined torque induced from the buoyancy module and the ILS (see eq. 7.9) gives the equilibrium state of the catenary.

Figure 6-19 shows the two parts of the catenary and a simplified illustration of the pipe torque at the stinger tip, the touchdown point and the two sides of the inline structure. It should be mentioned that the torques T1 and T2 illustrated are calculated by the equations

$$T_1 = G \cdot I_t \cdot \phi_1'\left(\phi_{ILS}(i)\right) \quad @\, x = x_{ILS}$$

and

$$T_2 = G \cdot I_t \cdot \phi_2'\left(\phi_{ILS}(i)\right) \quad @\, x = x_{ILS}$$

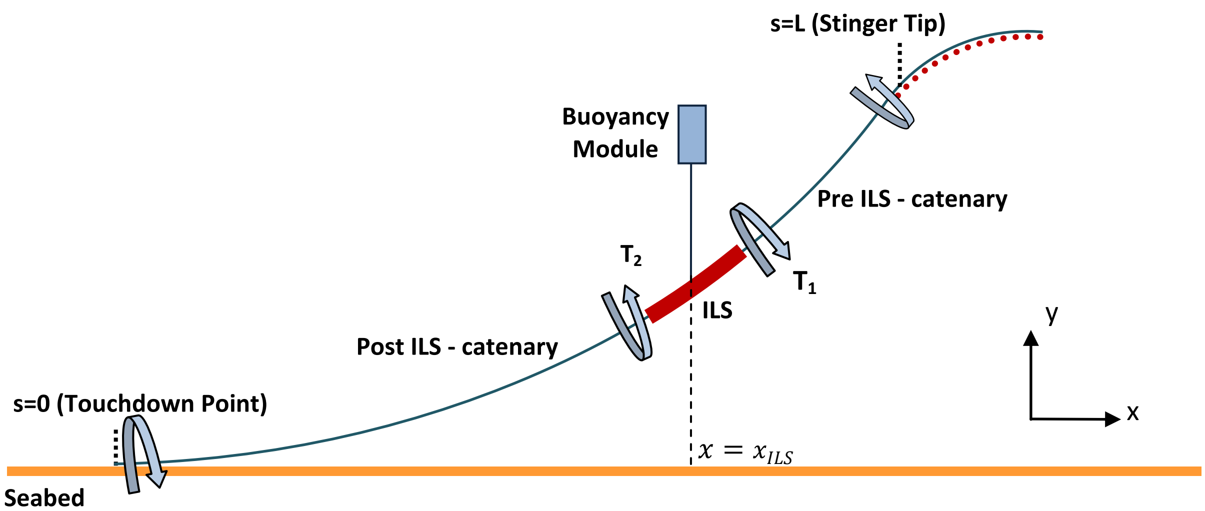


**Figure 6-19 Illustration of ILS along the catenary with internal torques**

The procedure discussed above, is described in detail in the following steps including graphical representation of a case with a 20" pipe, in 2237 meters water depth with a total suspended length of 3020 meters . Two cases will be illustrated. At the 1st case an inline structure and a buoyancy module of 200 kN are positioned at a distance of 1400 meters along the catenary from the stinger tip and at the 2nd case they are located 2400 meters from the stinger tip. Thus,

1. Apply Lagrangian minimization principle in order to find the rotation profile with no ILS along the catenary. Based on the solution, the angle at touchdown point $\phi_{TDP}$ is known.

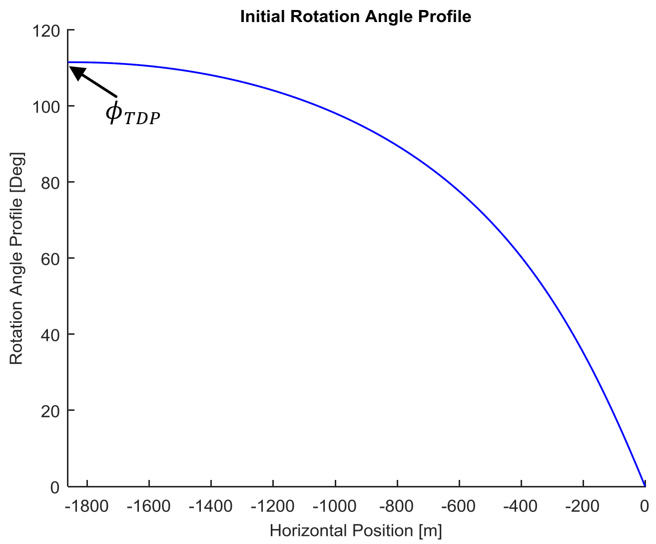


**Figure 6-20 Rotation Profile along the catenary without ILS**

2. Determination of the inline structure location $x_{ILS}$ along the catenary .

3. Split the rotation problem into two parts.

   a) The first part describes the rotation profile between the origin of the catenary (stinger tip) and the ILS position ($x_{ILS}$). See Figure 6-14, “pre-ILS” catenary part.

   b) The second part describes the rotation profile between the ILS position ($x_{ILS}$)and the touchdown point. See Figure 6-14, “post-ILS” catenary part.

4. Apply Lagrangian minimization principle in order to solve the rotation problem for each catenary part for a range of ILS rotation angles, $\phi_{ILS}$.

   The buoyancy modules have as an effect the reduction of rotation angle at the position of the ILS. Based on that, the range for which the problem will be solved is

$$\phi_{ILS}(i) \in [0, \varphi(\mathrm{x}_{\mathrm{ILS}})]$$

   Where $\varphi(\mathrm{x}_{\mathrm{ILS}})$ (upper bound of the range) is the angle at the ILS location obtained by problem at step 1. The boundary conditions for each problem are at

   a) “Pre-ILS” catenary : $(\mathbf{1})\ \phi_1(0) = 0$ $\quad(\mathbf{2})\ \phi_1(x_{ILS}) = \phi_{ILS}(i)$
   b) “Post-ILS” catenary : $(\mathbf{1})\ \phi_2(x_{ILS}) = \phi_{ILS}(i)$ $\quad(\mathbf{2})\phi_2(L) = \phi_{TDP}$

Figure 6-21 Shows the rotation profiles for different ILS rotation angles $\phi_{ILS}$ at $x_{ILS}$ .

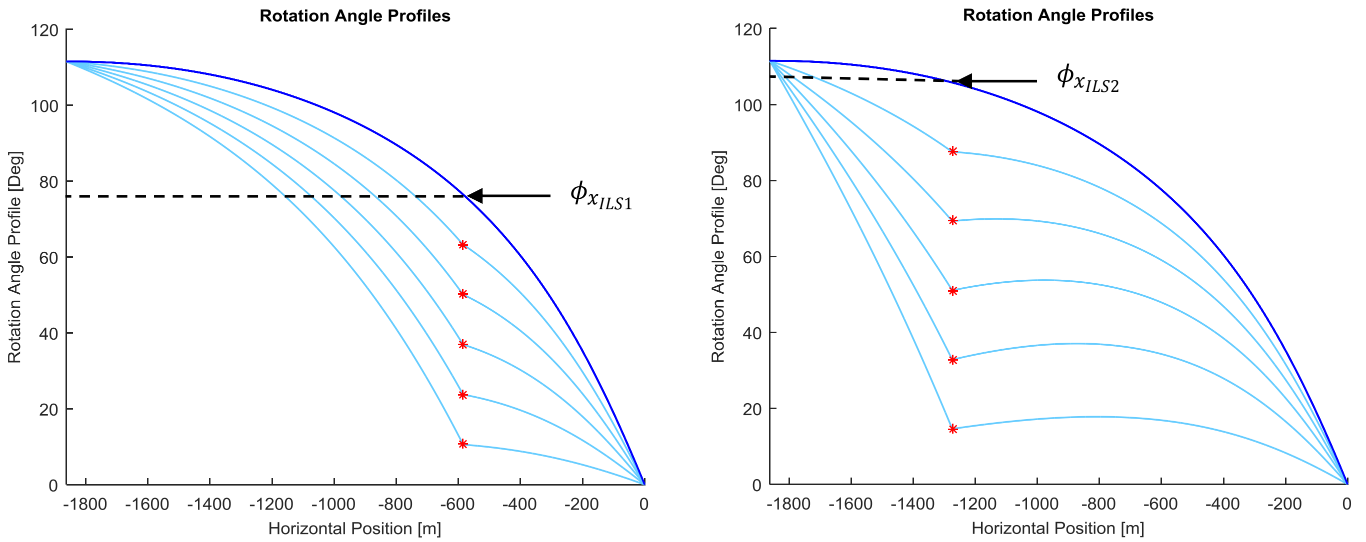


**Figure 6-21 Rotation profiles for different ILS rotation angles between 0 and $\varphi(\mathbf{x}_{\mathbf{ILS}})$**

5. For each angle $\phi_{ILS}(i)$ that the two problem are solved, the internal torque of the pipeline at the ILS position is calculated based on the equation

$$T_{pipe}(x_{ILS}, \phi_{ILS}(i)) = G \cdot I_t \cdot \left[\phi_2'\left(x_{ILS}, \phi_{ILS}(i)\right) - \phi_1'\left(x_{ILS}, \phi_{ILS}(i)\right)\right]$$

6. Having found the internal torque of the pipeline at the ILS position the equilibrium can be determined according to equation 7.9. If the total torque induced by the ILS and the buoyancy module(s) is equal to the internal toque of the pipeline then Equilibrium position have been found and the equilibrium angle is called $\phi_{ILS,eq}$.

$$Equilibrium\ state : T_{yoke}\left(\phi_{ILS,eq}\right) - T_{ILS}\left(\phi_{ILS,eq}\right) = T_{pipe}\left(\phi_{ILS,eq}\right)$$

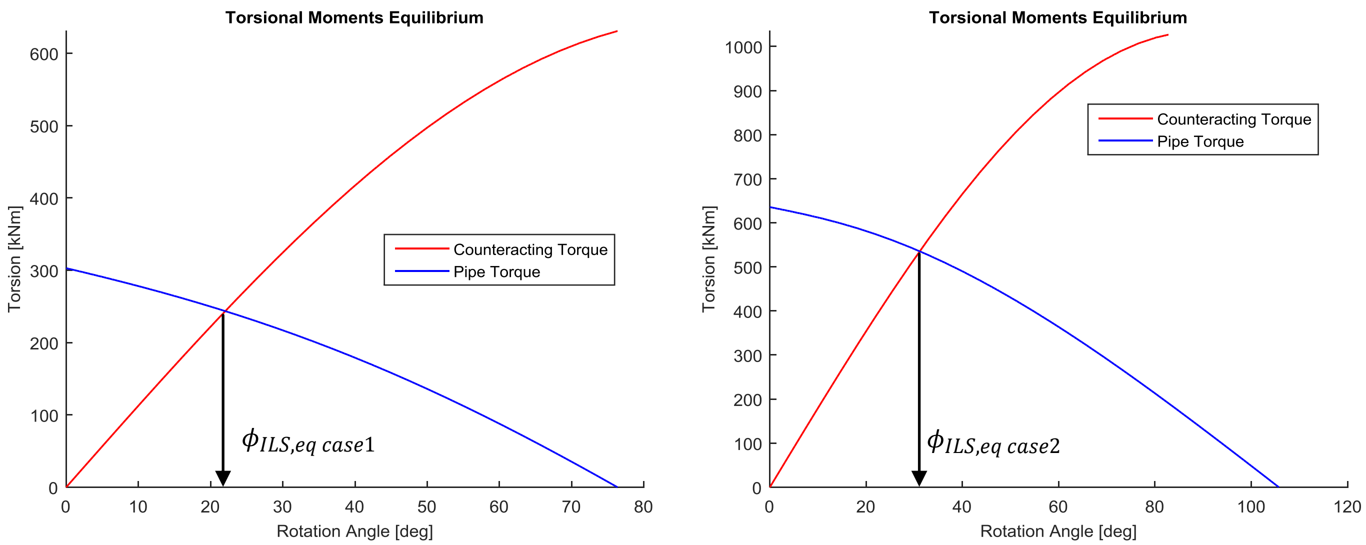


**Figure 6-22 Torsional moments equilibrium**

Having found the inline structure equilibrium angle based on the torsional moments the final rotation profiles can be seen in .

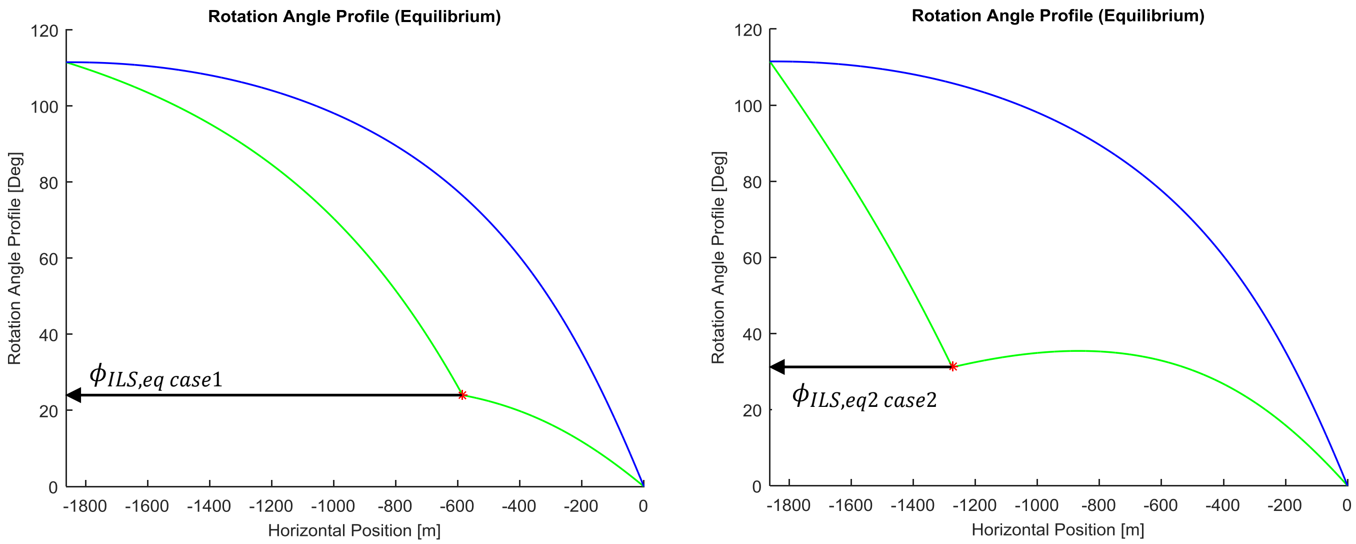


**Figure 6-23 Rotation profiles for ILS equilibrium rotation angle**

It should be noticed that this is not the final equilibrium of the inline structure as the pipe-seabed interaction is not taken yet into account. Chapter 6.5 describes the procedure followed to determine the equilibrium state, taking into account the soil friction without taking into account the torque in the laid pipe. Further in Chapter 6.6, the sequential model is described and how the problem is solved taking into account the torque in the laid pipe during installation operation.

## 6.5 Pipe-Soil Interaction

At this chapter the interaction between the soil and the laid pipeline will be discussed. The chapter is divided in two parts. At the first part is described the procedure to find the ILS equilibrium when the inline structure is put in an arbitrary position along the catenary (as described at the section before). In that case the existing torque in the laid pipeline is not taken into account in order to find the equilibrium. The second part of the chapter describes the procedure followed at the sequential model, which is the final model of the research. At the sequential model as described in Chapter 4.0 the inline structure is located at the stinger tip at the first step and then it moves gradually to the touchdown point. For each step the existing torque in the laid pipe from the previous step is taken into account.

### 6.5.1 Initial Step

Because of the influence of the ILS, there is an amount of torque at the touchdown point as it can be seen from. Because of this torque, the pipeline will slip for a certain length $(L_{slip})$, and the touchdown point equilibrium angle will be reduced by an angle $\Delta\varphi_{eq}$,depending on the pipeline-soil interaction and the seabed properties (soil friction). Assuming that the soil friction is uniformly distributed along the seabed, the torque which will be resisting the rotation of the laid pipe will be linearly distributed from the touchdown point until the end of slip. Thus, let

- $T_{soil}$ be the linear torque ($in\ [N \cdot m/m]$) resisting pipe rotation and,
- $L_{slip}$ be the length of pipe ($in\ [m]$) that will slip under the influence of torque from touchdown point $T_{TDP}$

In case of a pipeline laid with a constant rotation angle (i.e. torque free) on seabed, the torque in the laid pipe is linearly decreasing from $T_{TDP}$ to zero over the distance $L_{slip}$, due to the uniformly distributed soil friction. Thus,

$$T_{laid}(x) = a \cdot x + b$$

The torque equilibrium of the pipeline at the seabed gives

$$T_{TDP} - \int_{L_{slip}} T_{soil} dx = 0 \Rightarrow T_{soil} = \frac{T_{TDP}}{L_{slip}}$$

In order to find the coefficients $a$ and $b$ the boundary conditions will be used. At the touchdown point (x=0), the torque is equal to the torque obtained by the pipeline rotation problem $T_{TDP}$ and at $x = L_{slip}$ , the torque is zero, $T_{laid}(L_{slip}) = 0$, thus

$$a = -\frac{T_{TDP}}{L_{slip}} = -T_{soil}$$

According to the above the torque along the laid pipeline can be expressed

$$T_{laid}(x) = T_{TDP} - T_{soil} \cdot x$$

with x being the distance from touchdown point along the laid pipe. Based on the equation

$$T_{laid}(x) = G \cdot I_t \cdot \frac{d\varphi}{dx}$$

The rotation profile on the seabed can be written

$$\varphi(x) = \int_0^x \frac{T_{laid}(x)}{G \cdot I_t} dx = \frac{1}{G \cdot I_t} \int_0^x (T_{TDP} - T_{soil} \cdot x) dx = \frac{1}{G \cdot I_t} \int_0^x T_{soil} \cdot (L_{slip} - x) dx$$

Integrating the equation above

$$\varphi(x) = \frac{T_{soil}}{G \cdot I_t} \left(L_{slip} - \frac{x}{2}\right) \cdot x \qquad [\mathbf{6.10}]$$

The absolute difference between the rotation angle at the touchdown point and the rotation angle and the end of slip length is

$$\Delta\varphi = \frac{T_{soil}}{G \cdot I_t}\left(L_{slip} - \frac{L_{slip}}{2}\right) \cdot L_{slip} \Rightarrow \Delta\varphi = \frac{T_{soil} \cdot L_{slip}^2}{2 \cdot G \cdot I_t}$$

According to that the length of slipping pipe can be calculated for any value of rotation angle at touchdown point

$$L_{slip} = \sqrt{\frac{2 \cdot G \cdot I_t \cdot \Delta\varphi}{T_{soil}}} \qquad [\mathbf{6.11}]$$

A simplified illustration of the pipeline on the seabed with the rotation and torque profile along the laid pipeline is given in Figure 6-24. The extend of slip caused by the pipe torque at touchdown point is determined by compatibility conditions at TDP. Both rotation and torque profile shall be continuous around touchdown point.

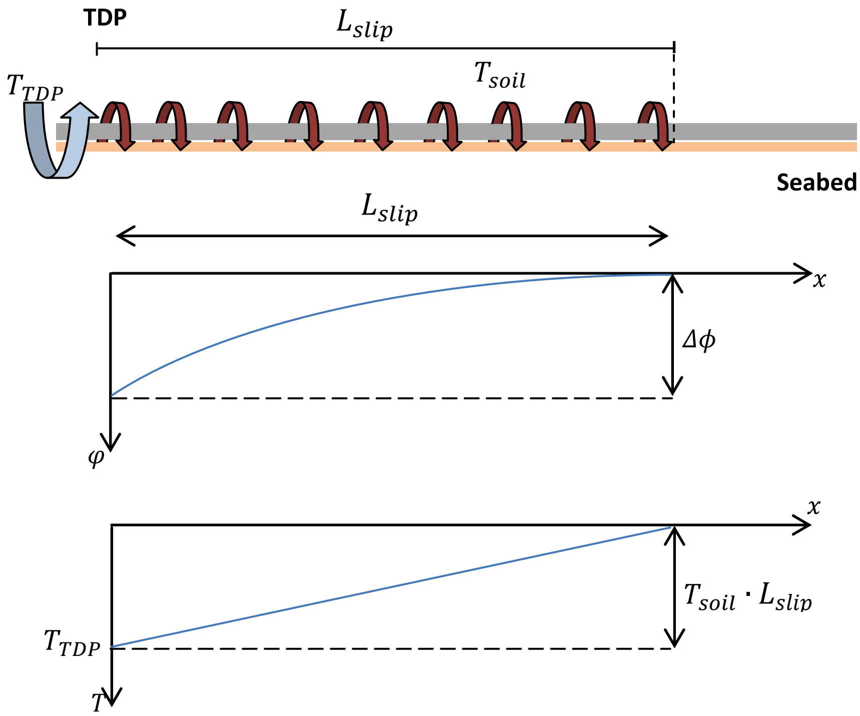


**Figure 6-24 Pipeline state on seabed with corresponding rotation and torque profile at the seabed**

The rotation profile along the seabed taking into account the rotation angle at the touchdown point $\phi_{TDP}$ , can be found as follows

$$\varphi_{soil}(x) = (\varphi_{TDP} - \Delta\varphi) + \frac{T_{soil}}{G \cdot I_t}\left(L_{slip} - \frac{x}{2}\right) \cdot x$$

With $\varphi_{TDP}$ being the rotation angle of the pipeline at the touchdown point before slipping.

In order to find the rotation angle and the torque at the touchdown point for which these conditions are satisfied the procedure below is followed.

1. Calculate the "post-ILS" catenary rotation profile for different values of $\delta\varphi$ with boundary conditions

$$(\mathbf{1})\ \phi_2(x_{ILS}) = \phi_{ILS,eq} \qquad (\mathbf{2})\ \phi_2(L) = \phi_{TDP} - \delta\varphi$$

Where $\phi_{ILS,eq}$ is the equilibrium rotation angle of the inline structure (see Chapter 6.4.)

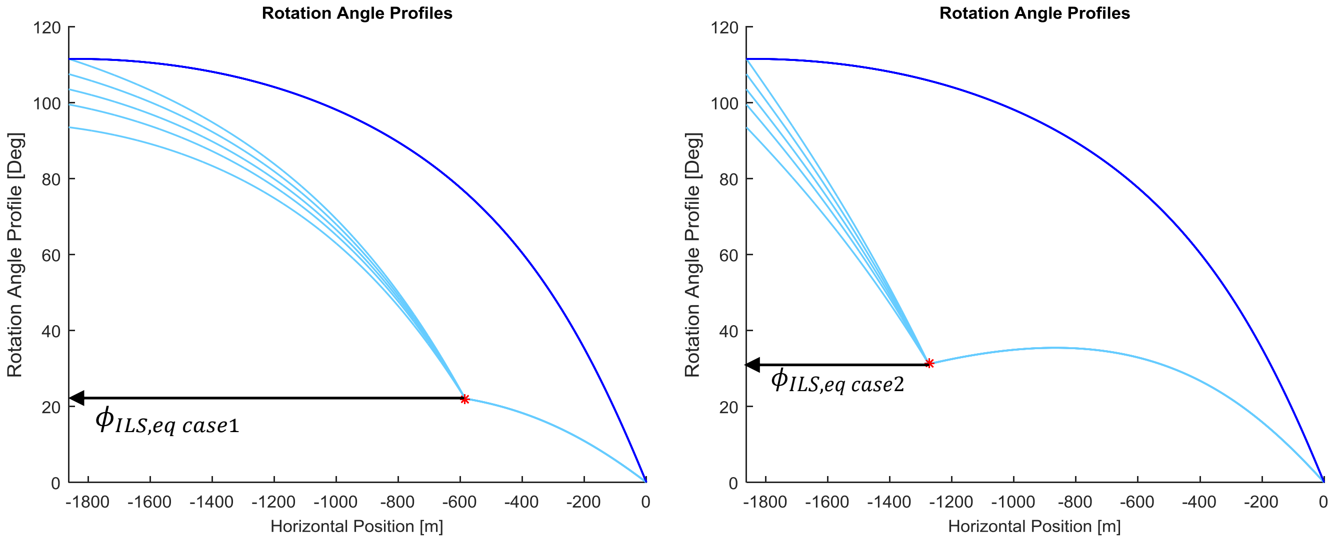


**Figure 6-25 Rotation profiles for different values of $\delta\varphi$**

2. Obtain the torque at the touchdown point based on equation for each $\phi_2(L)$

$$T_{TDP} = G \cdot I_t \cdot \phi_2'(\phi_{ILS,eq}, \phi_{TDP} - \delta\varphi)$$

3. Determine the theoretical soil torque at the touchdown point based on the rotation profile of the seabed .

$$T_s(x_{TDP}) = G \cdot I_t \cdot \left.\frac{d\varphi_{soil}(x)}{dx}\right|_{x=0}$$

By simple algebraic operations

$$T_s(x_{TDP}) = T_{soil} \cdot L_{slip} \overset{[7.12]}{\Longrightarrow} T_s(x_{TDP}) = T_{soil} \cdot \sqrt{\frac{2 \cdot G \cdot I_t \cdot \Delta\varphi}{T_{soil}}}$$

Thus

$$T_s(x_{TDP}) = \sqrt{2 \cdot T_{soil} \cdot G \cdot I_t \cdot \delta\varphi}$$

The expected rotation angle at the touchdown point is found for the angle $\Delta\varphi_{eq}$ for which the pipeline torque at TDP (obtained from step 2) equals the theoretical soil torque at TDP (obtained from step 3).

The angle at the touchdown point is

$$\phi_{TDP,eq} = \phi_{TDP} - \Delta\varphi_{eq} \qquad [\mathbf{6.12}]$$

The theoretical value of the torque can be expressed as

$$T_{TDP,eq} = \sqrt{2 \cdot T_{soil} \cdot G \cdot I_t \cdot \Delta\varphi_{eq}} \qquad [\mathbf{6.13}]$$

Or

$$T_{TDP,eq} = G \cdot I_t \cdot \phi_2' \left(\phi_2(x_{ILS}) = \phi_{ILS,eq}, \ \phi_2(L) = \phi_{TDP} - \Delta\varphi_{eq}\right)$$

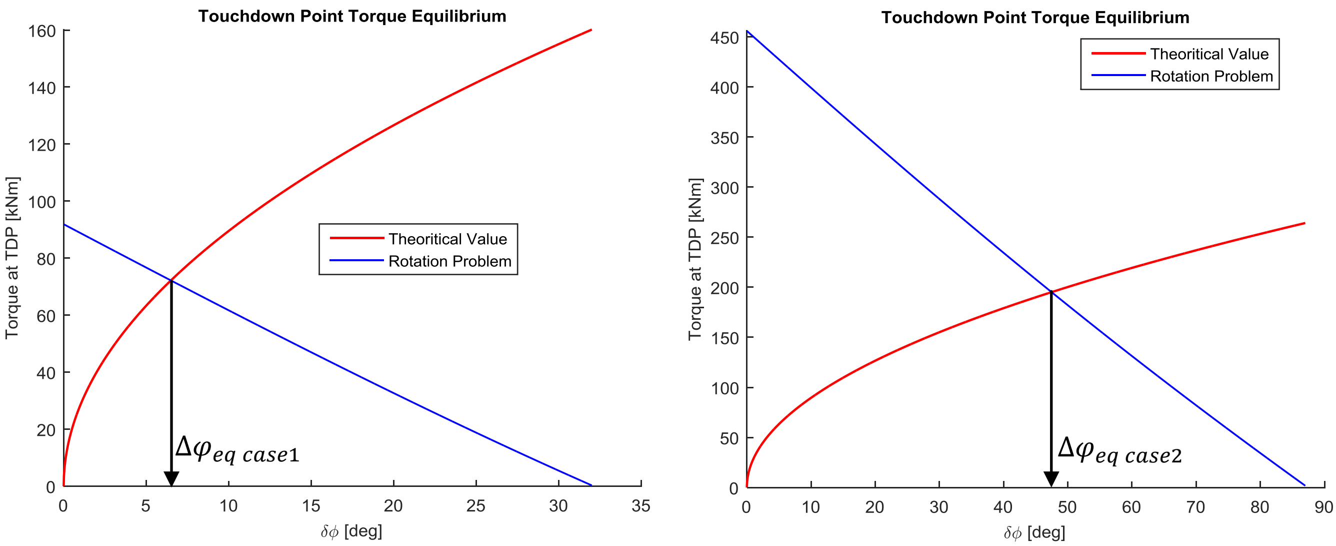


**Figure 6-26 Touchdown point Torque Equilibrium**

Having found the equilibrium state, taking into account the soil friction, the inline structure equilibrium angle is found again (iteration process) based on the procedure described in Chapter 6.3 using as boundary conditions for the "Post-ILS" catenary either the equilibrium angle at the TDP (**Eq. 6.12**) or the equilibrium torque at TDP (**Eq. 6.13**) obtained taking into account the soil friction.

$$(\mathbf{1})\ \phi_2(x_{ILS}) = \phi_{ILS}(i) \qquad (\mathbf{2})\ \phi_2(L) = \phi_{TDP,eq}$$

**or**

$$(\mathbf{1})\ \phi_2(x_{ILS}) = \phi_{ILS}(i) \qquad (\mathbf{2})\ T_{TDP}(L) = T_{TDP,eq}$$

The reason two different boundary conditions were used at the touchdown point was to validate that the method used and the solution converges to the same equilibrium state independently of the boundary conditions which are used.

Flowchart shown in Figure 6-27 shows the iteration process described in Chapters 6.4 and 6.5 in order to find the ILS static equilibrium state. The flowchart shows the method used and the iteration process in order to determine the final ILS equilibrium angle, touchdown point and the final slip length.

The flowchart for the calculation of the ILS equilibrium can be seen in Figure 6-27.

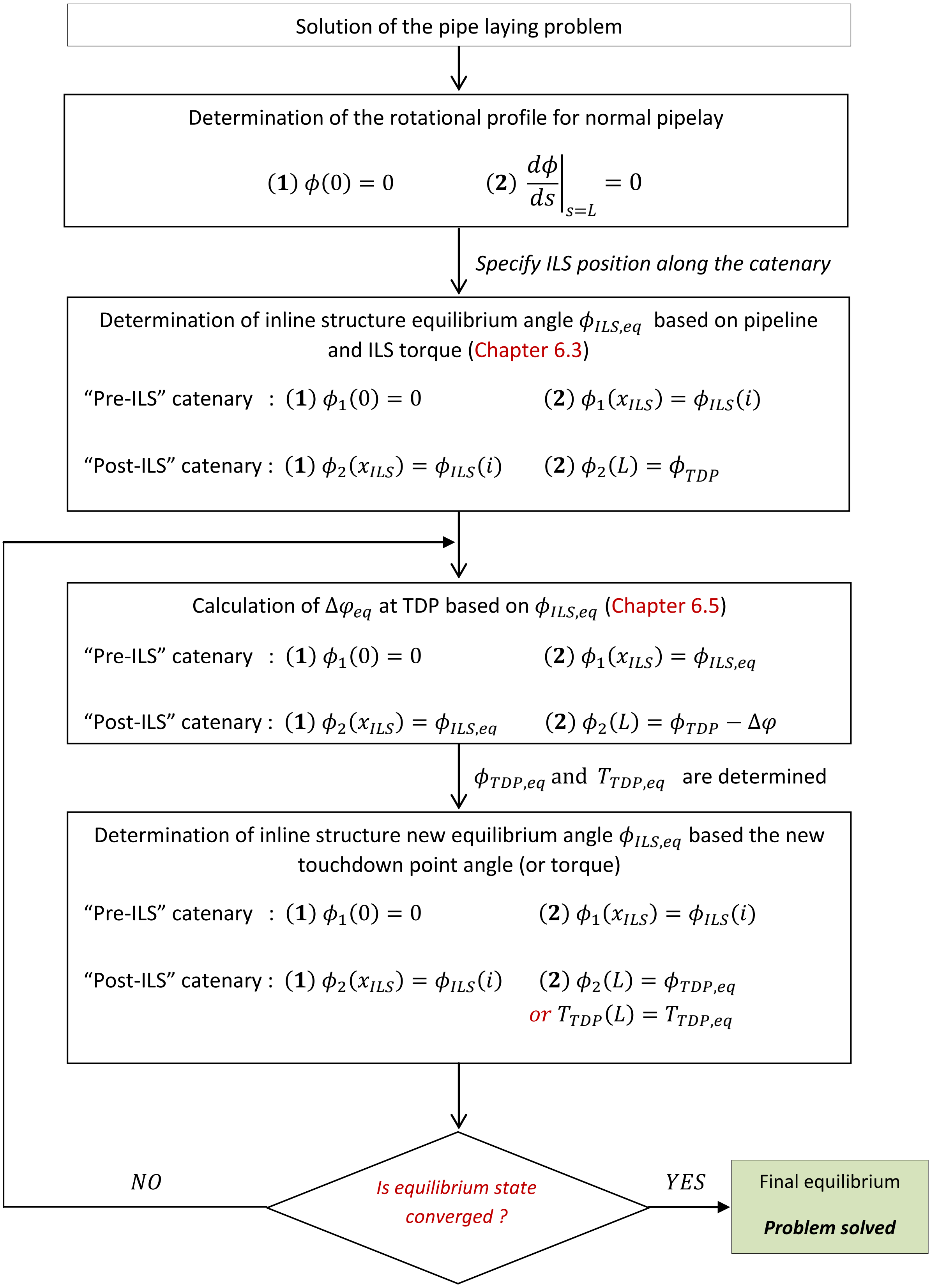


**Figure 6-27 Procedure for ILS static equilibrium state in case of no existing torque in the laid pipe**

The rotation profiles of the converged equilibrium state for case N°1 (ILS 1400 meters from the stinger tip) and N°2 (ILS 2400 meters from the stinger tip) are shown in below.

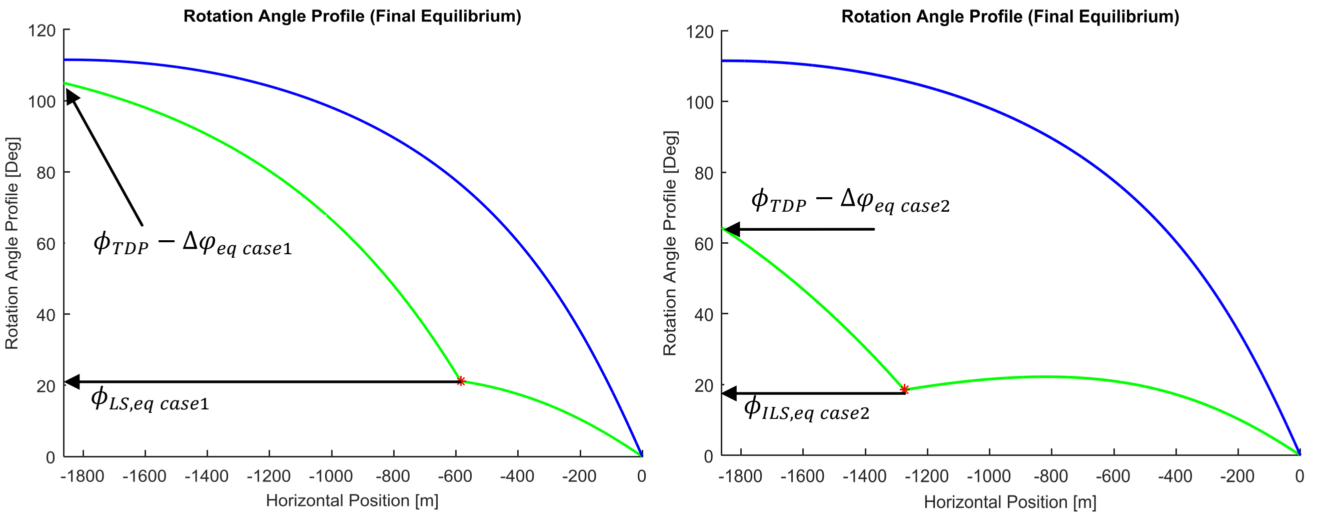


**Figure 6-28 Rotation Profile of the converged equilibrium state**

Following figures show the convergence of the convergence of the ILS and TDP rotation angle for the case where ILS is 1400m from stinger tip. Although the two boundary conditions give different results at the first iteration, they converge to the same equilibrium state after the third iteration.

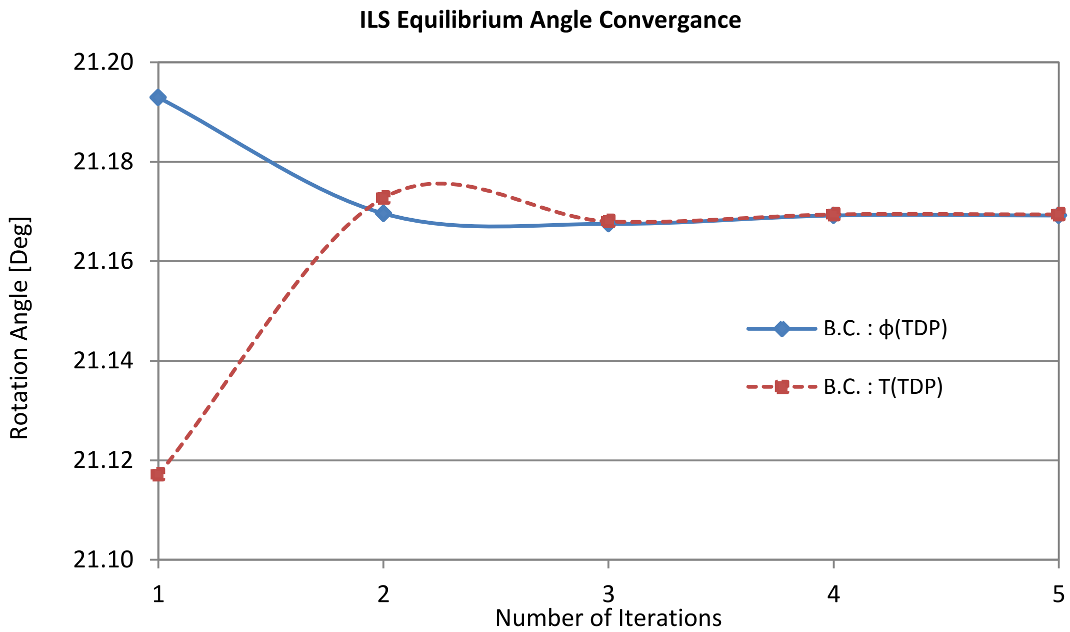


**Figure 6-29 ILS Equilibrium Convergence – ILS 1400m from stinger tip**

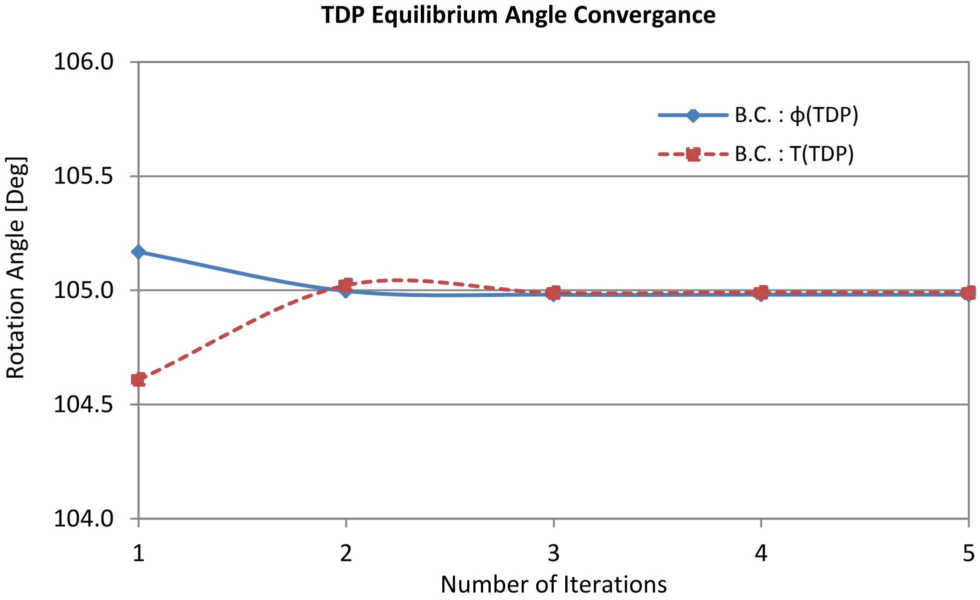


**Figure 6-30** **TDP Equilibrium Angle Convergence – ILS 1400m from stinger tip**

**Figure 6-31** and **Figure 6-32** show the convergence of the ILS and TDP rotation angle for the case where ILS is 2400m from stinger tip. Although the two boundary conditions give different results at the first iteration as in the previous case, it can be seen they converge to the same equilibrium state after the fourth iteration.

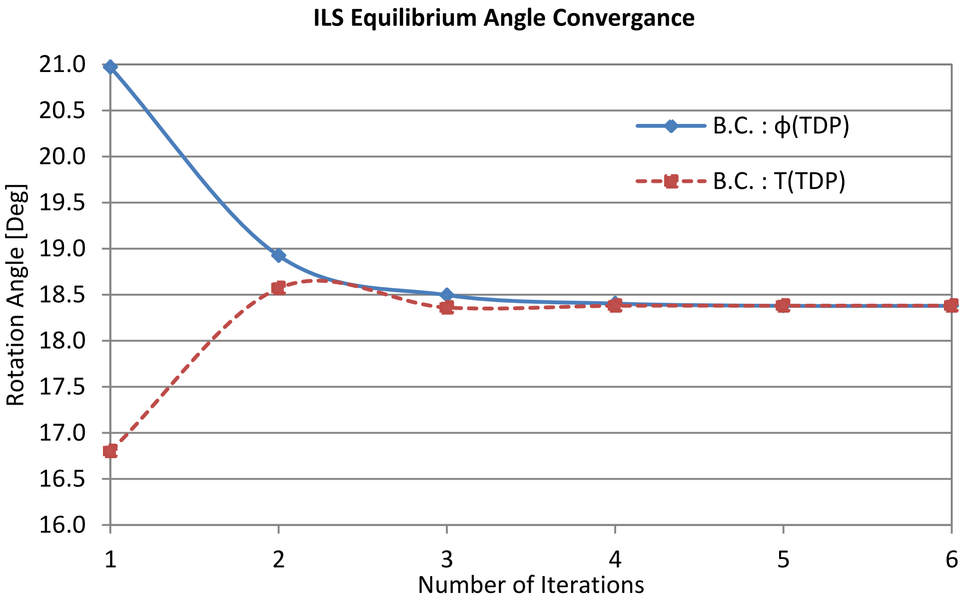


**Figure 6-31** **ILS Equilibrium Angle Convergence – ILS 2400m from stinger tip**

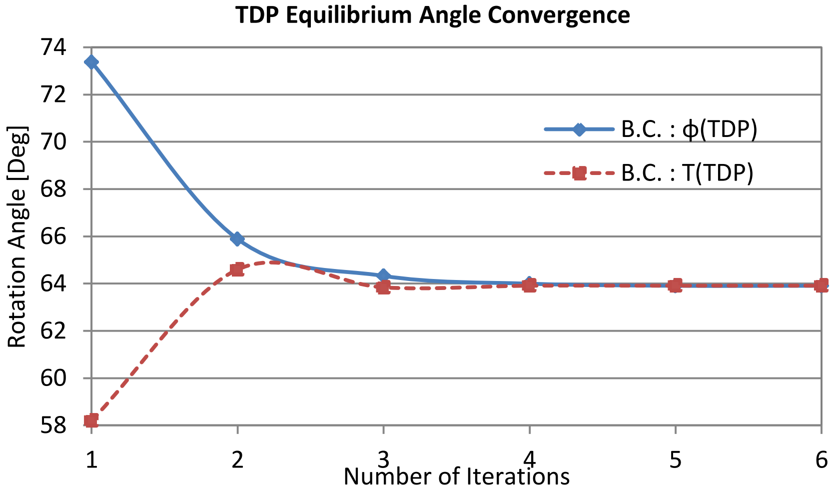


**Figure 6-32 TDP Equilibrium Angle Convergence – ILS 2400m from stinger tip**

As it can be seen in both cases the ILS equilibrium state (ILS and TDP angle) is converged at the same solution either using the touchdown point angle or torque as boundary condition. The slip length convergence is shown in Figure 6-33.

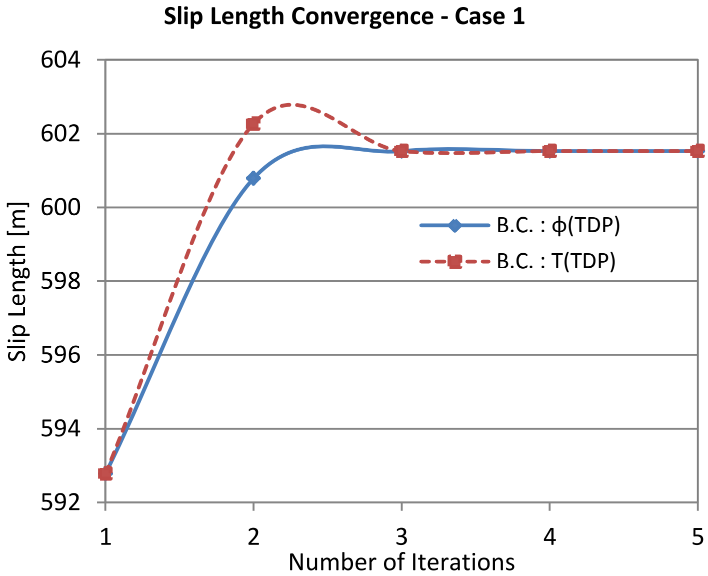


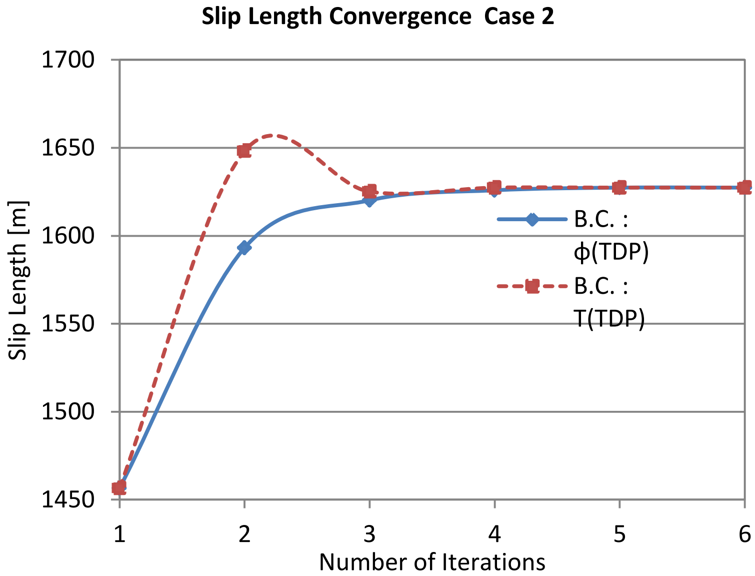


**Figure 6-33 Slip length convergence for two cases**

The large difference in the value of slip length between the two cases can be explained by the large difference in the value $\Delta\varphi_{eq}$ which at the 1$^{st}$ case is around 6.48$^{o}$ whereas at the 2$^{nd}$ case is around 47.56$^{o}$ (7.34 times higher). Taking into account equation 7.12, the slip length obtained at the case N$^{o}$1 shall be $\sqrt{7.34} \approx 2.709$ times than that one of case N$^{o}$1.

The slip length converges to 601.52 meters for case N$^{o}$1 and to 1627.4 meters for case N$^{o}$2. Dividing the two numbers gives a ratio of 2.705 which is what is expected from the theory with a relative error of 0.14%. Having explained in detail and verified the procedure for the determination of the equilibrium state the next step is to model the rotation problem sequentially, taking into account the torque in the laid pipe.

### 6.6 Sequential Model

After the first installation step of the inline structure, the pipeline on seabed is no longer torque free, but has a residual torque, which can be derived from the pipe's rotation profile on seabed. The length of slip, driven by the torque at touchdown point, is now defined by the length over which the sum of the friction forces compensate the difference between the TDP torque on one side and the residual torque on the other side (see ).

$$T_{TDP} - T_{soil} \cdot L_{slip} = T_0$$

Assuming again that the torque profile at the seabed decreases linearly

$$T_{laid}(x) = a \cdot x + b$$

At the touchdown point (x=0), the torque is equal to the torque obtained by the pipeline rotation problem $T_{TDP}$ (see **Eq. 7.10**) and at $x = L_{slip}$ , the torque equals to $T_{laid}\left(L_{slip}\right) = T_0$, where $T_0$ the residual torque in the laid pipe at the end of the slip length, thus

$$T_0 = a \cdot L_{slip} + T_{TDP} \Rightarrow a = \frac{T_0 - T_{TDP}}{L_{slip}}$$

Based on the above, the equation for the laid torque, from which the rotation profile and the slip length will be defined is

$$T_{laid}(x) = \left(\frac{T_0 - T_{TDP}}{L_{slip}}\right) \cdot x + T_{TDP}$$

Because there is no explicit formulation for the residual torque $T_{laid}(x)$ (it is derived from the rotation profile values, which are stored as a result of pipe slipping in previous step of the process), the slip length is found by iteration. Technically, starting from touchdown point, the first location along the laid pipe where the residual torque and the soil friction are fully balancing the torque from TDP is the location where the pipe rotation stops. The rotation profile on the seabed can be written

$$\varphi(x) = \int_0^x \frac{T_{laid}(x)}{G \cdot I_t} dx = \frac{1}{G \cdot I_t} \int_0^x \left[\left(\frac{T_0 - T_{TDP}}{L_{slip}}\right) \cdot x + T_{TDP}\right] dx$$

Integrating the equation above

$$\varphi(x) = \frac{1}{G \cdot I_t} \left[\left(\frac{T_0 - T_{TDP}}{L_{slip}}\right) \cdot \frac{x^2}{2} + T_{TDP} \cdot x\right] \qquad [\mathbf{6.14}]$$

Taking into account that at the slip length position the sum of the friction forces compensate the difference between the TDP torque on one side and the residual torque on the other side,

$$T_{TDP} - T_{soil} \cdot L_{slip} = T_0$$

the expression for $\varphi(x)$can be expressed as

$$\varphi(x) = \frac{1}{G \cdot I_t}\left[T_{soil} \cdot \left(L_{slip} - \frac{x}{2}\right) + T_0\right] \cdot x$$

The absolute theoretical difference between the rotation angle at the touchdown point and the rotation angle and the end of slip length is

$$\Delta\varphi = \frac{T_{soil} \cdot L_{slip}^2}{2 \cdot G \cdot I_t} + \frac{T_0 \cdot L_{slip}}{G \cdot I_t}$$

The rotation profile along the seabed taking into account the rotation angle at the touchdown point $\phi_{TDP}$ can be found as follows

$$\varphi_{soil}(x) = (\varphi_{TDP} - \Delta\varphi) + \frac{1}{G \cdot I_t}\left[T_{soil} \cdot \left(L_{slip} - \frac{x}{2}\right) + T_0\right] \cdot x$$

A simplified illustration that shows the rotation angle and torque profile derived from the distributed soil friction when laid pipe is initially torque free can be seen in Figure 6-34.

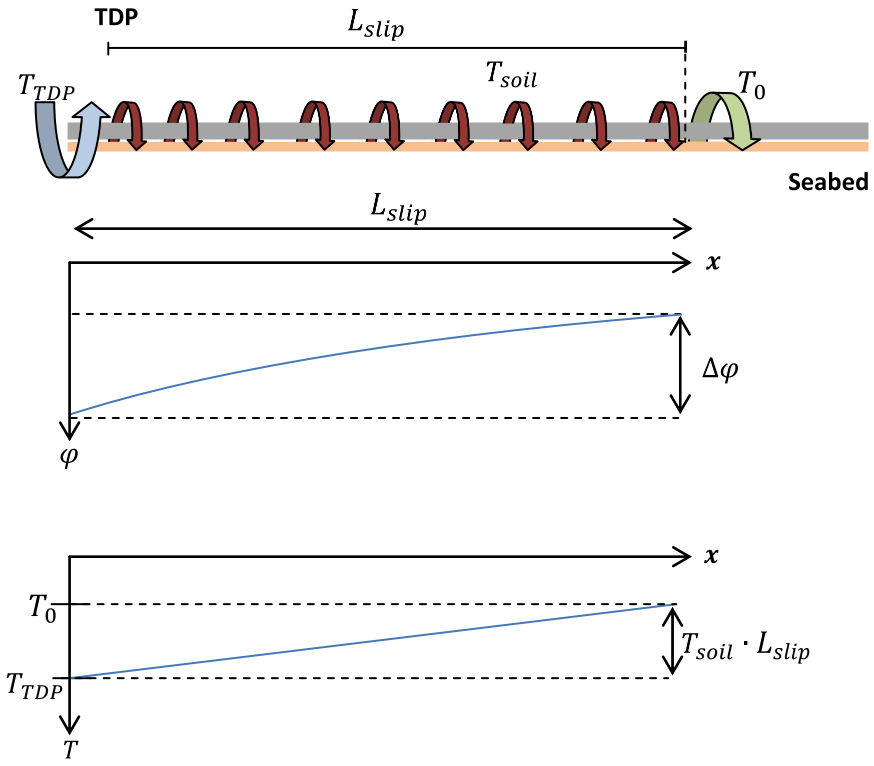


**Figure 6-34 Rotation angle and torque profile, accounting for residual torque on the seabed**

Similar as previously, finding the extent of pipeline rotation caused by the pipe torque at TDP implies finding the compatibility between the torque and roll angle at both sides of TDP. However, because of the existence of residual torque in the laid pipe, the procedure is slightly different and will be explained below.

1. Calculation the "post-ILS" catenary rotation profile for different values of $\delta\varphi$ with boundary conditions

$$(\mathbf{1})\ \phi_2(x_{ILS}) = \phi_{ILS,eq} \qquad (\mathbf{2})\ \phi_2(L) = \phi_{TDP} - \delta\varphi$$

   Where $\phi_{ILS,eq}$ is the equilibrium angle at the position of the inline structure (the procedure to determine $\phi_{ILS,eq}$ is described in detail Chapter 6.3.

2. Obtain the torque at the touchdown point based on equation

$$T_{TDP} = G \cdot I_t \cdot \phi_2'\left(x_{TDP}, \phi_{ILS,eq}\right)$$

3. Determination of the slip length $L_{slip}$ through an iteration procedure, by increasing the value of $x$ by a certain step size $dx$. The length of slip is found when

$$T_{TDP}(\Delta\varphi) = T_{soil} \cdot x + T_{laid}(x)$$

   For the value of $\delta\varphi$, the slip length has been found $L_{slip}(\delta\varphi)$ and the residual torque at that position $T_0(\delta\varphi) = T_{laid}\left(L_{slip}\right)$.

4. Compare the rotation angle at the touchdown point $\phi_{TDP} - \delta\varphi$ with the theoretical value $\varphi_{soil}(x)$ at the $x = 0$ based on the equation

$$\varphi_{soil}\left(L_{slip}\right) = \phi_0 - \frac{T_{soil} \cdot L_{slip}^2}{2 \cdot G \cdot I_t} - \frac{T_0 \cdot L_{slip}}{G \cdot I_t}$$

   In case that

$$\phi_{TDP} - \Delta\varphi = \phi_0 - \frac{T_{soil} \cdot L_{slip}^2}{2 \cdot G \cdot I_t} - \frac{T_0 \cdot L_{slip}}{G \cdot I_t}$$

   then $\delta\varphi = \Delta\varphi_{eq}$ and the equilibrium touchdown point angle is $\phi_{TDP,eq} = \phi_{TDP} - \Delta\varphi_{eq}$,

where $\phi_0$ is the rotation angle of the already laid pipe at the angle of slip.

Otherwise, another value of $\delta\varphi$ is picked and the same process is done, till the $\phi_{TDP,eq}$ is found.

The ILS descent along the suspended pipe is treated in a sequential way. At every step, the pipe pay-out is incremented with Δ (typically one pipe joint), giving a new position to the ILS. Then the pipe catenary and rotation profile are recalculated. For the rotation profile, the new boundary condition at TDP is assumed to be the rotation angle from previous step.

For every step, the new ILS equilibrium angle is calculated as detailed in Chapter 6.3, then the pipe slip at TDP, as described in Chapter 6.6. This iterative process for the calculation of the ILS equilibrium angle taking into account the pre-existing torque in the laid pipe is shown by the flowchart in Figure 6-35.

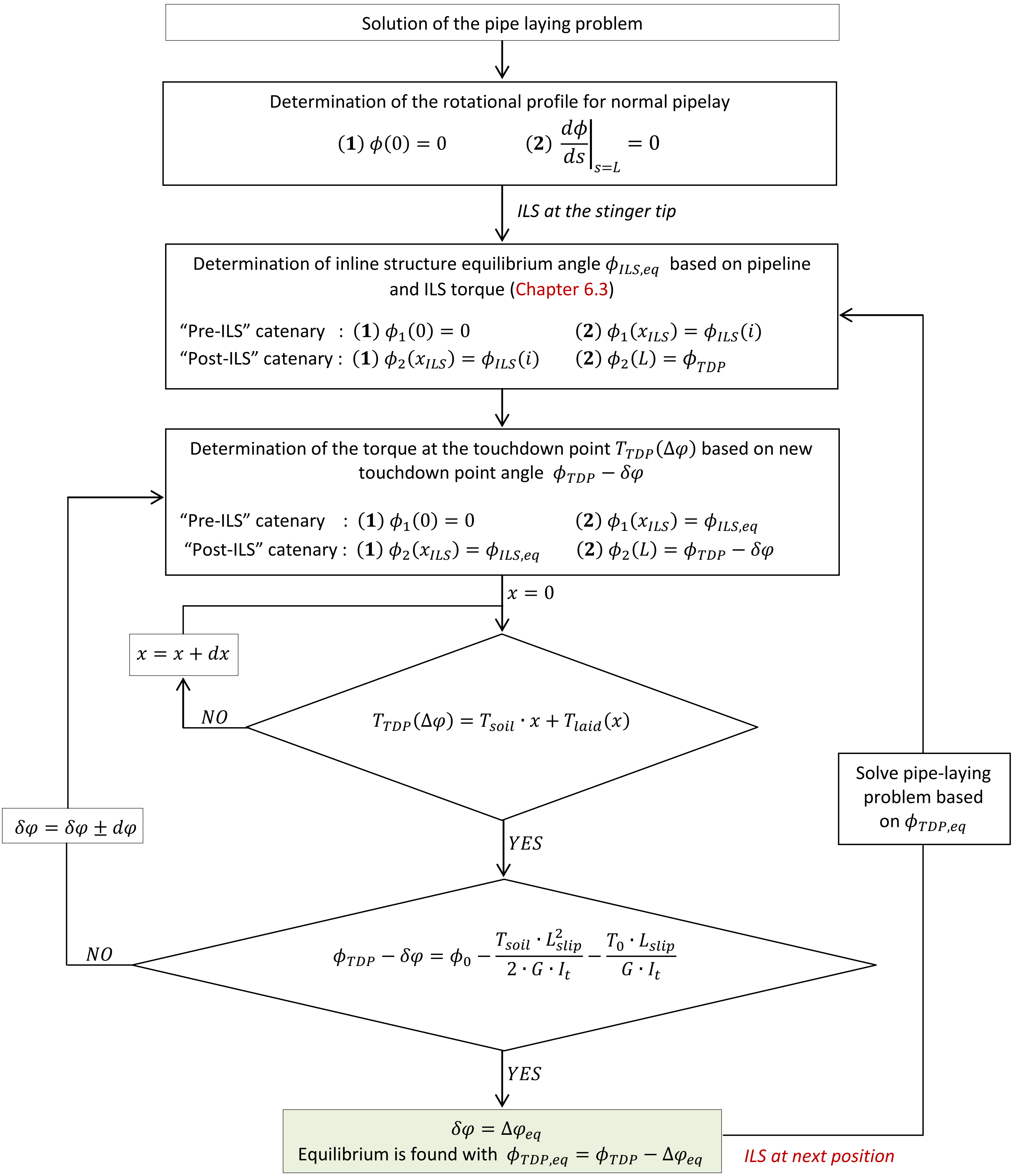


**Figure 6-35** **Process for slip determination with pre-existing torque in the laid pipe – Sequential Model**

## 6.7 Rotation Problem Analysis

The rotation phenomenon depends on many parameters which interfere with each other. The most important of them that will be investigated is the pipe-seabed interaction in terms of different values of soil friction, the effect of the mitigation measures (restrained and unrestrained buoyancy modules) for the decrease of rotation and the effect of the applied tension. A general description of how of these parameters affect the rotation phenomenon is given below.

In addition, the model depends on a number of numerical parameters, which may affect the accuracy and the computational time of the program. The most important of these numerical parameters that will be considered is the seabed step and the pipe pay-out at each installation step.

- **Soil friction effect**

The interaction between the pipeline and the seabed influences at the rotation of the pipe on seabed. Depending on the soil friction and taking into account the torque induced by the ILS at the touchdown point, the pipeline will slip in a different amount $(\Delta\varphi)$ and at different slip length $(L_{slip})$ at each installation step. That will have as a consequence a different touchdown point angle evolution during installation operation and a different inline structure landing angle. In order to investigate if the effect of the soil friction is considerable to the rotation phenomenon, three cases are examined, with a low, an intermediate and a high value of soil friction as shown in Table 6-5.

| Soil Friction [kNm/m] | | |
|---|---|---|
| 0.03 | 0.12 | 0.2 |

**Table 6-5 Soil friction values investigated**

- **Tension effect**

As mentioned in pipelay problem analysis, during operations there are two main criteria that have to be satisfied. Sagbend strain shall be below the acceptable limit (common value for the upper limit is 0.15% for static analysis) and tip separation - the distance between the pipeline and the stinger tip - shall be larger than 0.3 meters (depending on the project these values may be higher). Both of the sagbend strain and the tip separation depend on the applied tension. Higher applied tension has as a result lower sagbend strains and decreased sagbend curvature, a result that could lead to less rotation of the pipeline. At the same time, increased tension results in a longer suspended free span of the pipe which and consequently to lower torsional resistance and thus higher amount of rotation. In order to investigate the effect of the tension four different cases were conducted with different tip separation limit. It should be mentioned that higher values of tip separation limit require increased applied tension. The values used for the tip separation in the case studies are shown in Table 6-6

| Tip Separation [m] | | | |
|---|---|---|---|
| 0.3 | 1 | 2 | 3 |

**Table 6-6 Tip separation values investigated**

- **Buoyancy effect**

As described extensively in Chapter 6.3, when an inline structure is installed the most common mitigation measure in order to reduce the amount of rotation is the use of buoyancy modules. The effect of the magnitude of buoyancy module will be investigated taking into account its configuration (restrained – unrestrained buoyancy module) in combination with the other parameters.

Table 6-7 and Table 6-8 show the data used for the case study. The vessel used is Solitaire with a stinger configuration of L=140 meters (stinger length) and R=180 meters (stinger radius).
The residual radius of the pipe is R=1871m.

| | | |
|---|---|---|
| **Water Depth** | 2183 | $[m]$ |
| **Pipeline Diameter** | 20 | ["] |
| **Pipeline Wall Thickness** | 27.5 | $[mm]$ |
| **Field Joint Length** | 0.7 | $[m]$ |
| **Pipe Joint Length** | 12.2 | $[m]$ |
| **Pipeline Density** | 7850 | $[kg/m^3]$ |
| **Young`s Modulus** | 207000 | $[MPa]$ |
| **Anti-Corrosion Coating** | | |
| Thickness | 3.6 | $[mm]$ |
| Density | 921 | $[kg/m^3]$ |

**Table 6-7 Pipe, Coating & Environmental Data**

| | | |
|---|---|---|
| **ILS Submerged weight** | 14715 | $[N/m]$ |
| **C.o.G. distance above pipe centreline** | 0.9 | $[m]$ |
| **Yoke Length** | 5 | $[m]$ |

**Table 6-8 ILS Properties**

### 6.7.1 Soil Friction 0.12 [kNm/m] (Intermediate value)

- **Buoyancy Effect**

To investigate the buoyancy influence for the rotation phenomenon there were investigated the following cases

| Case | Buoyancy modules [-] | Buoyancy Force [t] | Configuration |
|---|---|---|---|
| **1** | 1 | 35 | Unrestrained |
| **2** | 1 | 35 | Restrained |
| **3** | 2 | 70 | 1 Restrained - 1 Unrestrained |
| **4** | 1 | 100 | Unrestrained |
| **5** | 1 | 100 | Restrained |

**Table 6-9 Buoyancy effect cases analysed**

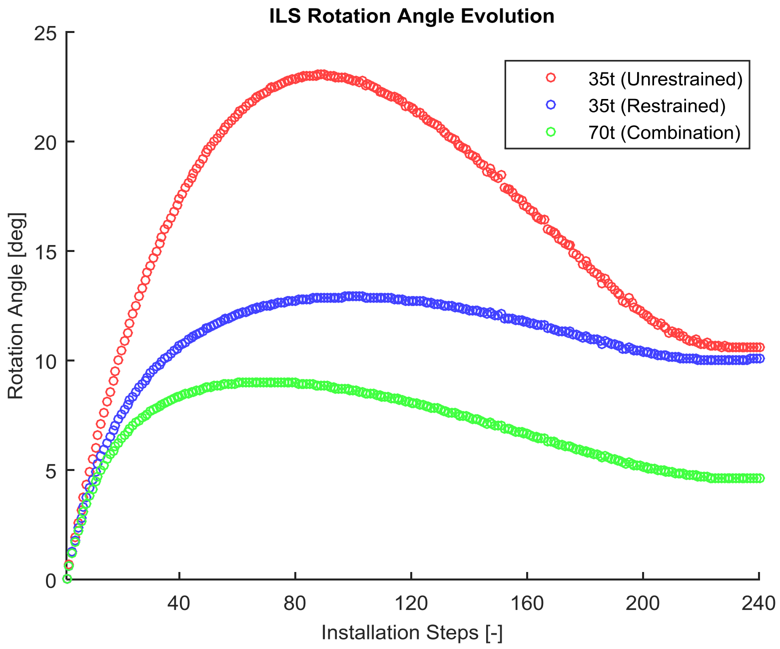


**Figure 6-36** **ILS rotation angle evolution during installation (Cases 1-2-3)**

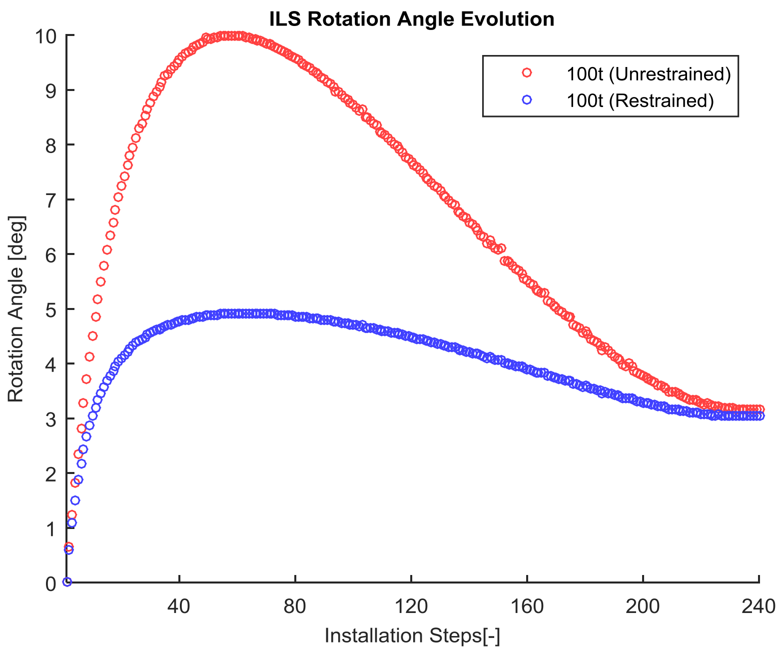


**Figure 6-37** **ILS rotation angle evolution during installation (Cases 3-4)**

As it can be seen from Figure 6-36 and Figure 6-37 the ILS landing rotation angle decreases with higher amount of buoyancy as it was expected. Specifically for the unrestrained buoyancy configuration ILS landing angle decreases from 10.62$^{o}$ (35t buoy) to 3.165$^{o}$ (100t buoy), 3.35 times lower landing angle, while for the restrained buoyancy configuration ILS decreases from 10.07$^{o}$ (35t buoy) to 3.04$^{o}$ (100t buoy) , almost 3.31 lower. The combination of two buoyancy modules (case 3) resulted to an ILS rotation angle of 4.61 $^{o}$.

Another fact that should be mentioned is that both for the case of 35t buoyancy and for that of 100t buoyancy there is not considerable difference at the ILS landing angles for the restrained and unrestrained configuration. For the 35t buoy (cases 1-2) the difference is $0.55^{o}$ while for the 100t buoy the difference is around $0.12^{o}$. That can be explained by the fact that the two different buoyancy configurations have the same effect close to touchdown point, where the pipe becomes almost horizontal.

In spite of the fact that the ILS landing angles are almost the same, for the unrestrained cases it is noticed that the maximum rotation angle reached during installation is much higher for both cases (35t and 100t). Specifically, for the case of 35t buoy the maximum rotation angle for the unrestrained configuration ($23.04^{o}$) is 1.78 times higher than that of the restrained configuration ($12.93^{o}$). The same behaviour is noticed also for the 100t buoy where the maximum for the unrestrained case is $9.992^{o}$ whereas for the restrained is $4.918^{o}$ (2.03 times higher).

These results can be explained by the fact that at the first installation steps, where the catenary has a steep configuration (angle of pipeline with horizontal is almost vertical - $\theta = 90°$) the effect of the buoy at the unrestrained configuration is reduced significantly (see Figure 6-15 and Figure 6-16) causing high rotation angles of the inline structure. As the installation process continues the buoy becomes much more effective resulting in a significant decrease of the rotation angle. For the restrained buoyancy configuration, the effect of the buoy is independent of the configuration of the pipeline, causing a much lower maximum rotation angle of the pipe and a smoother shape during the installation. Specific values of ILS landing and maximum angle are given in Table 6-10.

| Case | ILS landing angle [Deg] | ILS maximum angle [Deg] |
|---|---|---|
| 1 | 10.62 | 23.04 |
| 2 | 10.07 | 12.93 |
| 3 | 4.612 | 9.025 |
| 4 | 3.165 | 9.992 |
| 5 | 3.044 | 4.918 |

**Table 6-10 ILS landing and maximum angle for different buoyancy cases**

The touchdown point evolution angle for the 5 cases is shown in Figure 6-38 (Cases 1-2-3) and Figure 6-39 (Cases 4-5). As it can be seen the rotation angle evolution at the touchdown point has the same shape for all the cases. At the first installation steps, the reduction of the TDP angle is small because the catenary between the ILS and the TDP is large, thus the torque at the inline structure does not affect much the rotation of the touchdown point. As the catenary between the structure and the touchdown point becomes smaller during installation the torque at the ILS has an increasing effect to the touchdown point angle, resulting to a steady reduction of the TDP angle.

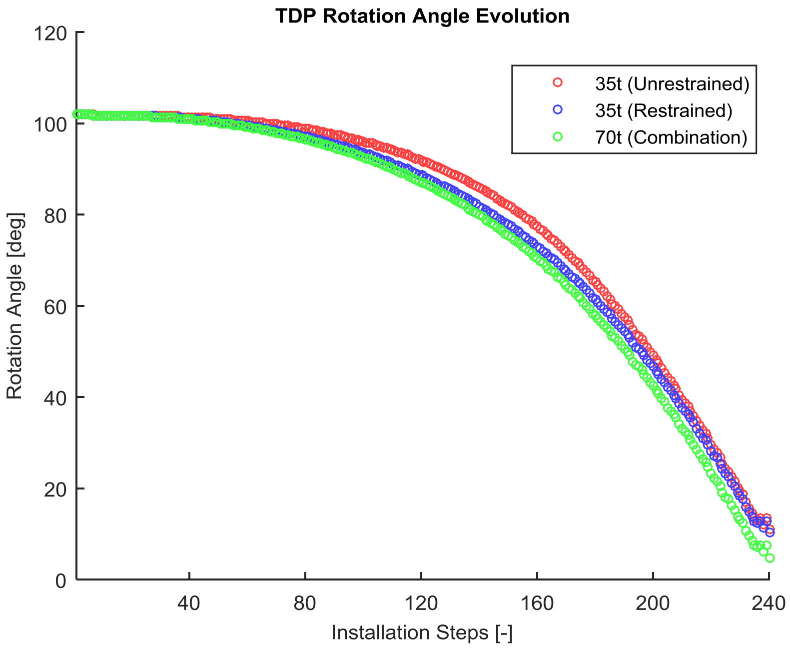


**Figure 6-38** TDP rotation angle evolution during installation (Cases 1-2-3)

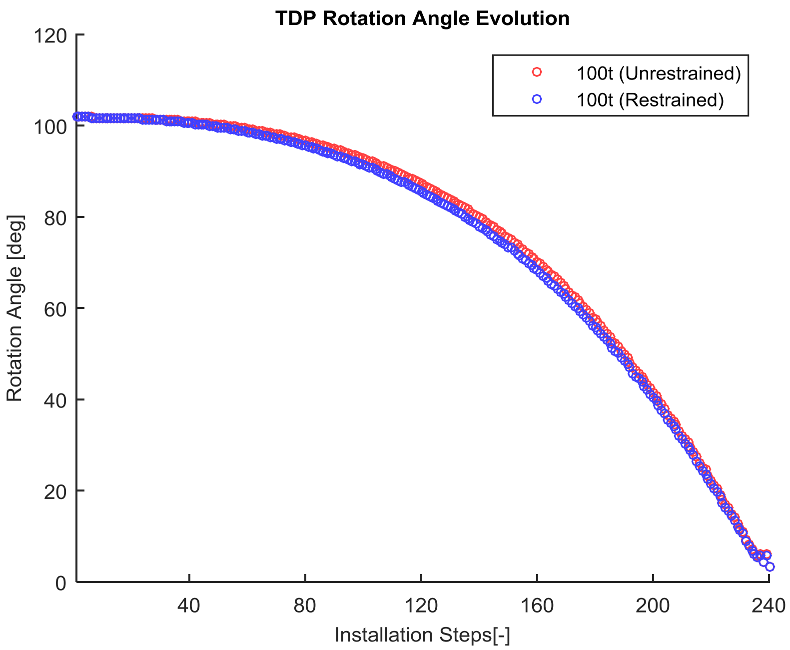


**Figure 6-39** TDP rotation angle evolution during installation (Cases 4-5)

Another important quantity is the torque evolution at the touchdown point. As mentioned in Chapter 6.5, the torque at the inline structure induces an amount of torque at the touchdown point. In the case of the unrestrained buoyancy configuration, the ILS torque is lower than that induced by the restrained at the beginning of installation, as it depends on the configuration of the pipe. When ILS moves further at the catenary during installation (where the pipe becomes gradually horizontal) its effect becomes gradually the same with that of the restrained buoy, thus the torque induced in both configurations are almost the same. During the last steps of installation, where the pipeline is almost horizontal, the ILS torque is dominated by the rotation angle of the structure. That can also be seen from the equations 6.7 and 6.8 for the

$$Unrestrained: \quad T_{buoy(un)} = F_{buoy} \cdot cos^2(\vartheta) \cdot sin(\phi_{ILS}) \cdot L_{yoke}$$

$$Restrained: \ T_{buoy(r)} = F_{buoy} \cdot cos(\vartheta) \cdot sin(\phi_{ILS}) \cdot L_{yoke}$$

When $\vartheta \approx 0° \Rightarrow cos(\vartheta) \approx cos^2(\vartheta) \approx 1$ ,so the higher rotation angle will result in higher torque at the touchdown point in the case of the unrestrained buoyancy configuration. The torque evolution can be seen in Figure 6-41 for the case of 100t buoyancy. Thus, the use of the restrained buoyancy has as a result lower landing rotation angle and lower torque at the touchdown point at the end of installation.

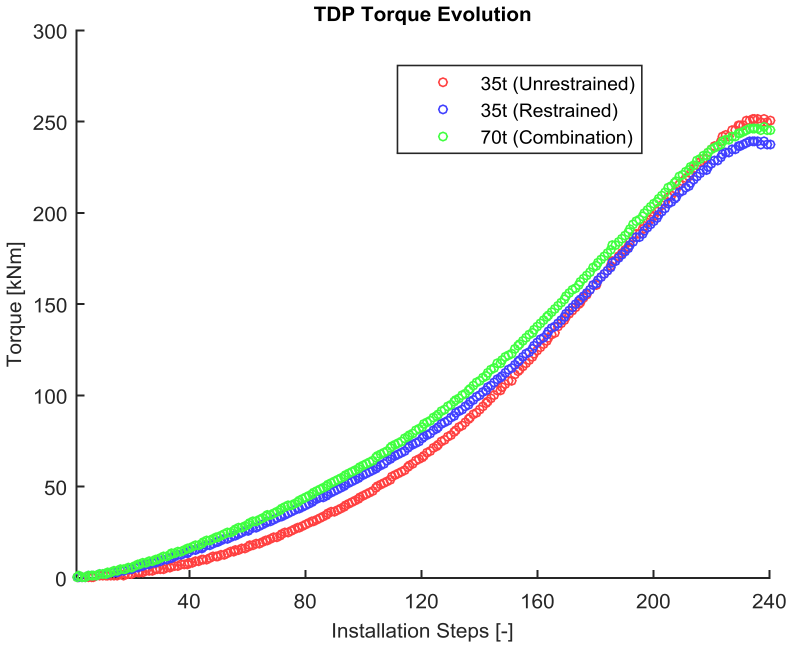


**Figure 6-40 Torque evolution during installation (Cases 1-2-3)**

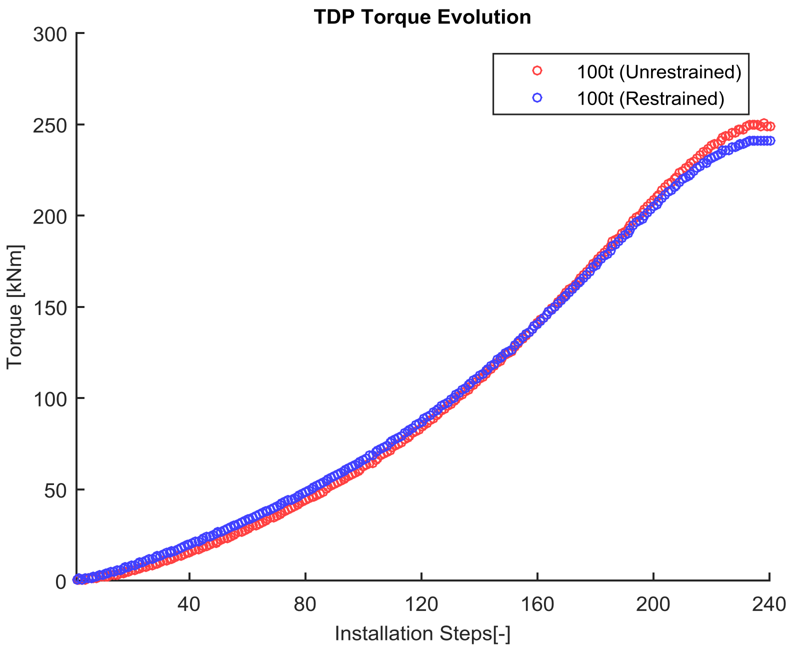


**Figure 6-41 Torque evolution during installation (Cases 4-5)**

Table 6-11 shows TDP torque at the touchdown point when inline structure is landed on seabed.

| Case | 1 | 2 | 3 | 4 | 5 |
|---|---|---|---|---|---|
| Torque $[kNm]$ | 250.4 | 237.3 | 245.6 | 240.8 | 248.7 |

**Table 6-11 TDP Torque when ILS is landed (Soil friction : 0.12 [kNm/m])**

The last parameter that will be analysed is the maximum slip length of the pipe during installation. When the unrestrained buoyancy configuration is used, as mentioned before the torque induced by the ILS to TDP is lower than that in the case of the restrained buoyancy configuration. As a result, at each step of the sequential model the residual torque $T_0$ at the already installed pipeline has a lower magnitude. Based on that, when the torque at the touchdown point for the case of the restrained and unrestrained configuration becomes almost the same, the length of the laid pipe which will counteract the $T_{TDP}$ will be larger in the case of the unrestrained configuration. That can also be seen from equation

$$T_{TDP} = T_{soil} \cdot x + T_0$$

For the same $T_{TDP}$ and $T_{soil}$ lower values of $T_0$ will have as a consequence larger values of x, thus length of slip, in order the equality to be met. That can be seen in also in Table 6-12.

| Case | 1 | 2 | 3 | 4 | 5 |
|---|---|---|---|---|---|
| Maximum slip length $[m]$ | 1472.59 | 882.9 | 840.71 | 931.46 | 440.71 |

**Table 6-12 Maximum slip length (Soil friction : 0.12 [kNm/m])**

- **Tension Effect Analysis**

As mentioned before tension has a considerable influence on the shape of the catenary. Higher tension will result to longer catenary and lower sagbend curvature and as a consequence the reduction of rotation along the catenary. In order to investigate the effect of tension same buoyancy is applied to all the cases (35t restrained buoyancy configuration). Higher values of tip separation, require higher amount of tension.

Figure 6-42 shows the evolution of ILS rotation angle during installation for different values of tip separation. As it can be seen, applying higher tension results in lower ILS rotation landing angle. Although the minimum tip separation for static analysis is 0.3 meters, in reality during actual installation operations the average tip separation is higher (over 1 meter) for possible vessel motions due to the environmental conditions, thus the result for 0.3meters can be considered conservative as it gives an overestimation of the landing rotation angle of the inline structure.

The same behaviour of the ILS angle is shown also for the touchdown point torque evolution during installation. Higher applied tension leads to lower values of torque resulting in a lower value of torque when the inline structure is landed. Figure 6-43 shows the torque profile at the touchdown point during installation.

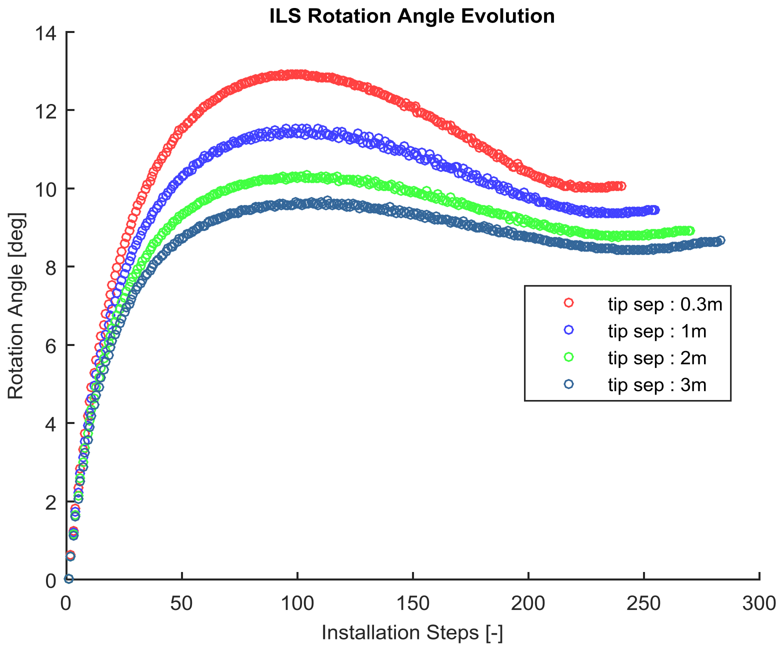


**Figure 6-42 ILS rotation angle evolution during installation for different tension**

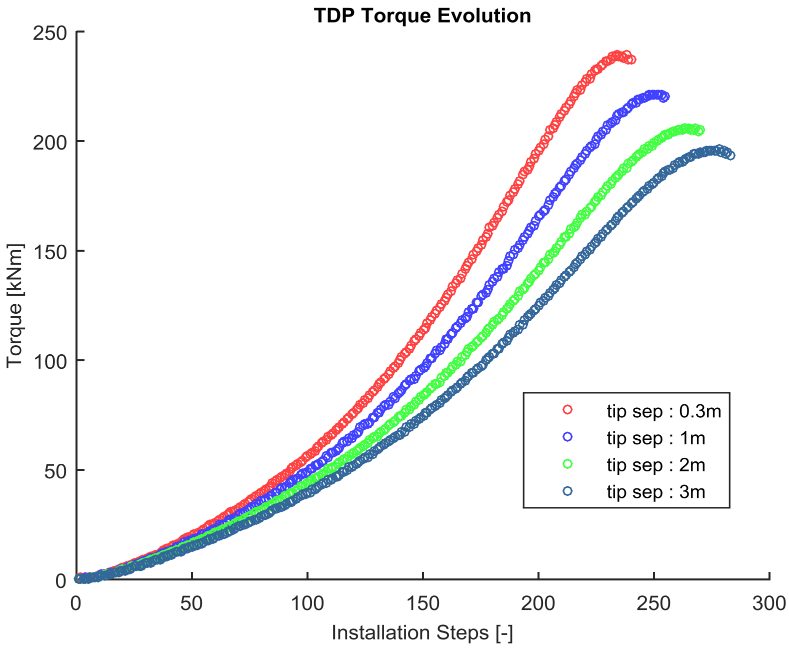


**Figure 6-43 Touchdown point torque evolution during installation for different tension**

Another important quantity is the bending strain during installation steps. As it can be seen from Figure 6-44. The bending strain is increasing during installation as the inline structure gradually approaches the seabed. This behaviour can be explained by the fact that the structure is much heavier and stiffer than the pipe and when it is at the curved sagbend area of the catenary causes the pipe to bend more. When the structure is at the steep part of the catenary (until step 100) there is not significant difference at the maximum bending strain between the four case studies, but as the installation proceeds, applying higher tension results in longer catenary and thus in lower values of bending strains.

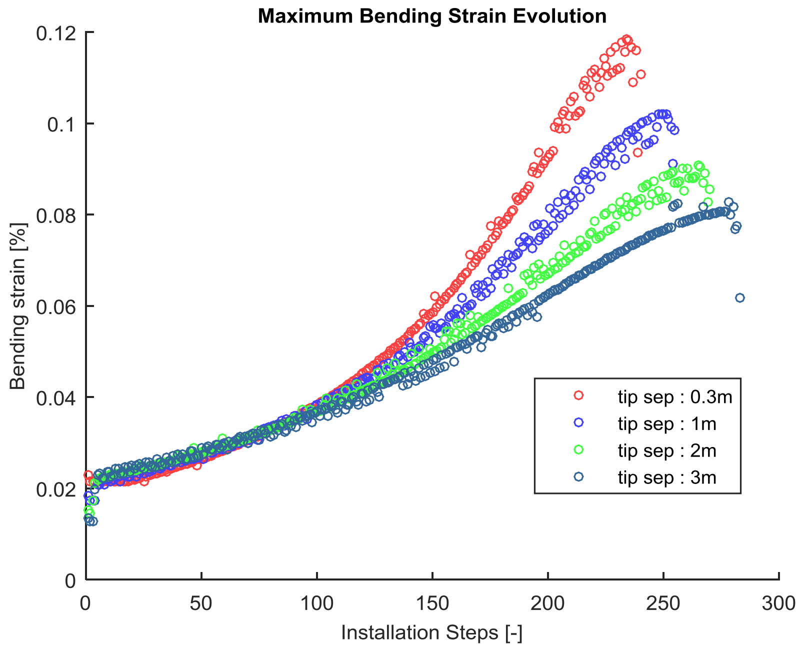


**Figure 6-44 Maximum bending strain evolution**

Table 6-13 summarizes the most important results obtained by the tension effect analysis.

| Case | ILS Landing Angle [Deg] | Maximum ILS Angle [Deg] | TDP Torque (ILS on seabed) [kNm] | Maximum Suspended Length [m] | Maximum Bending strain [%] | TDP Initial Rotation Angle [Deg] |
|---|---|---|---|---|---|---|
| 0.3m | 10.07 | 12.932 | 237.34 | 3079.13 | 0.118 | 101.823 |
| 1m | 9.448 | 11.533 | 220.76 | 3286.03 | 0.102 | 101.262 |
| 2m | 8.927 | 10.364 | 205.11 | 3470.45 | 0.091 | 100.522 |
| 3m | 8.661 | 9.686 | 193.61 | 3626.94 | 0.083 | 100.242 |

**Table 6-13 Results for different tension applied during inline structure installation (Soil friction : 0.12 [kNm/m])**

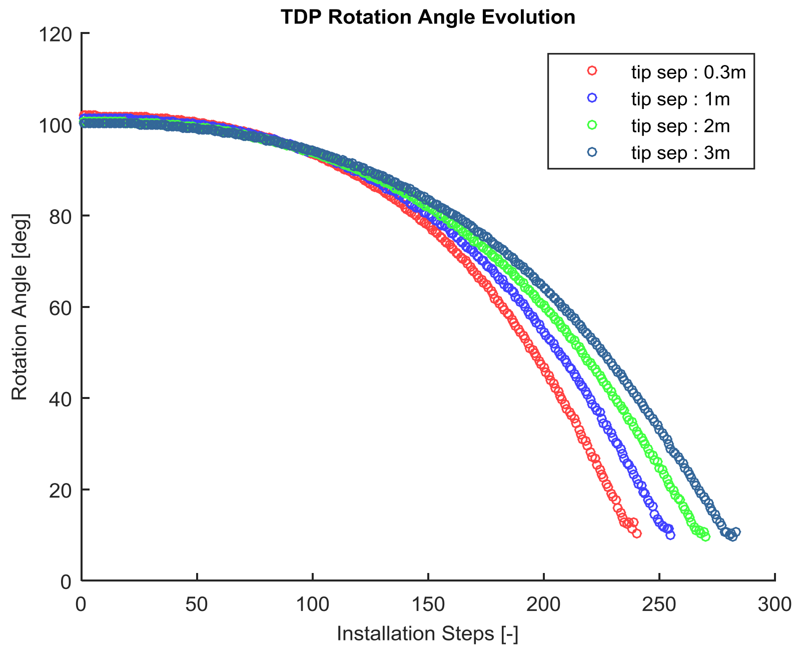


**Figure 6-45 TDP rotation angle evolution during installation for different tension**

### 6.7.2 Soil Friction 0.2 [kNm/m] (High Bound)

- **Buoyancy Effect Analysis**

To investigate how the high soil friction affects the rotation phenomenon there were analysed the same cases with respect to buoyancy as in the cases where soil friction was $0.03kNm/m$ and $0.12\ kNm/m$ (see Table 6-9) . Figure 6-46 shows ILS evolution angles for the 5 cases with soil friction of $0.12\ kNm/m$.

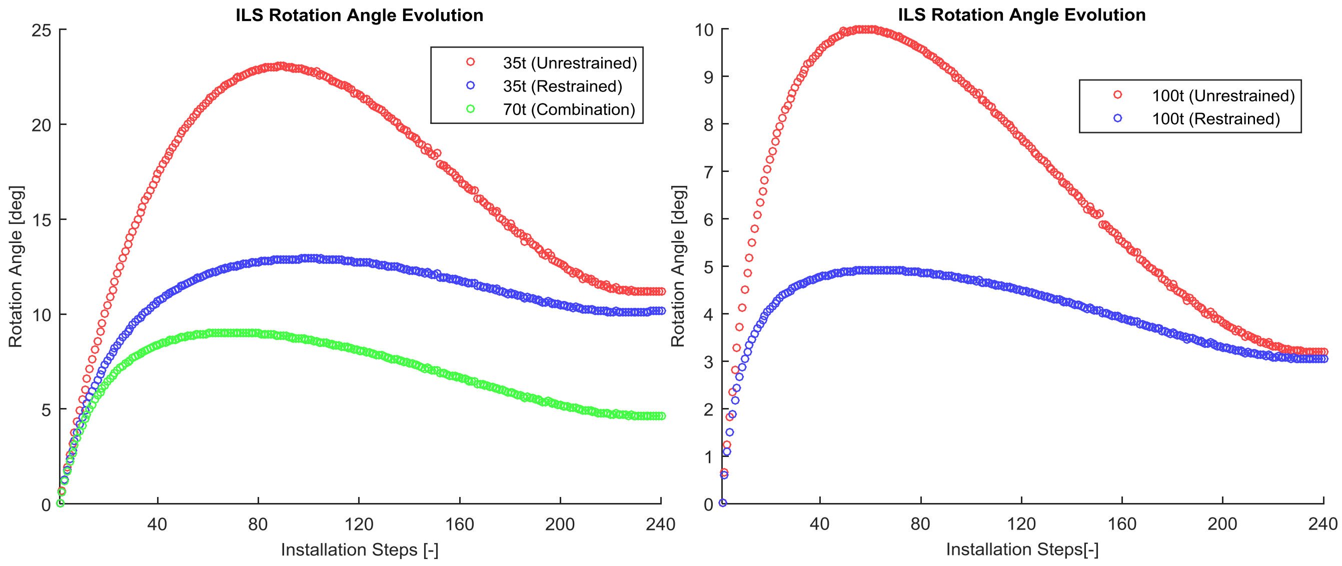


**Figure 6-46 ILS rotation angle evolution for different buoyancy (Cases1-5) – Soil friction : 0.2 [kNm/m]**

As it can be seen the ILS angle has identical evolution as in the cases of $0.12\ kNm/m$. It is noticed that the ILS landing angle is slightly higher for all the analysed cases which is a consequence of the higher constraint provided by the seabed to the pipe to rotate at each step. The largest difference is found for the unrestrained buoyancy configuration of 35t around 0.6$^{o}$ while for the other cases the difference is below 0.1$^{o}$. It should be mentioned that the soil friction seems to have no influence on the maximum rotation angle reached during installation for all the cases, with the maximum difference being around 0.02$^{o}$.

| Case | ILS landing angle [Deg] – S.F.:0.2 | ILS maximum angle [Deg] – S.F.:0.2 | ILS landing angle [Deg] – S.F.:0.12 | ILS maximum angle [Deg] – S.F.:0.12 |
|---|---|---|---|---|
| **1** | 11.22 | 23.06 | 10.62 | 23.04 |
| **2** | 10.15 | 12.94 | 10.07 | 12.93 |
| **3** | 4.652 | 9.026 | 4.612 | 9.025 |
| **4** | 3.197 | 9.993 | 3.165 | 9.992 |
| **5** | 3.054 | 4.919 | 3.044 | 4.918 |

**Table 6-14 Comparison between ILS landing and maximum angle for different values of soil friction**

As it can be seen, both in the case of the 35t of buoyancy and in the case of 100t the unrestrained configuration is most affected by the increase of the soil friction. That can be explained by the fact that the unrestrained buoyancy configuration becomes efficient at the last steps of installation and the rotation angle becomes highly dependent on the soil friction as the installation steps-time until the ILS reach the seabed are not sufficient for the reduction of the ILS rotation angle. On the other hand, in the case of the restrained buoyancy configuration the torque is accumulated gradually from the initial steps of installation as it efficient during the whole installation process. According to that, there is efficient time for the reduction of the ILS rotation angle independently of the soil friction.

The evolution of torque during installation has the same shape for all the cases. As it is expected the slightly higher rotation ILS landing angle has as a consequence a higher torque at the touchdown point at the last step of installation (see Table 6-15).

| Case | 1 | 2 | 3 | 4 | 5 |
|---|---|---|---|---|---|
| **Torque $[kNm]$ – S.F. :0.12** | 250.4 | 237.3 | 245.6 | 240.8 | 248.7 |
| **Torque $[kNm]$ – S.F. :0.2** | 263.6 | 240.2 | 247.3 | 241.9 | 252.5 |

**Table 6-15 Comparison between TDP torque when ILS is landed for different soil friction**

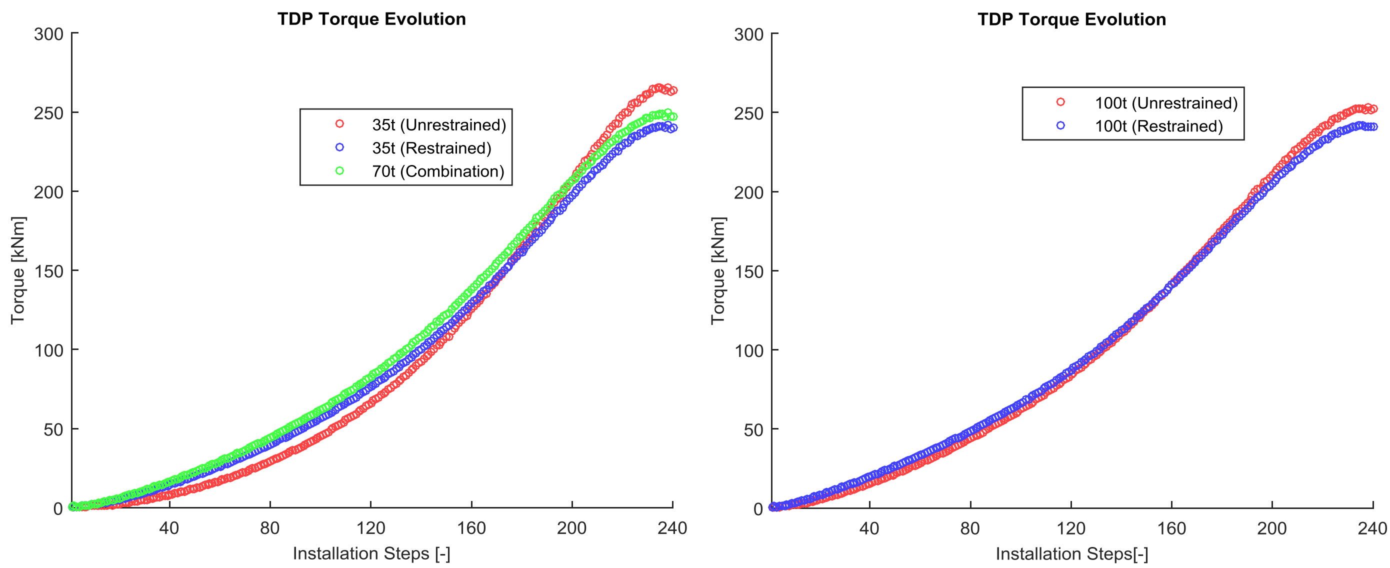


**Figure 6-47 Torque evolution during installation (Cases1-5) – Soil friction : 0.2 [kNm/m]**

As noted in the case of 0.12kNm/m soil friction, both for the case of 0.2kNm/m the unrestrained configuration resulted in lower maximum slip length during installation. It should be mentioned that the values of slip length are much lower than these obtained in the case of 0.12kNm/m of soil friction.

| Case | 1 | 2 | 3 | 4 | 5 |
|---|---|---|---|---|---|
| **Maximum slip length $[m]$** | 17.83 | 11.78 | 10.94 | 11.67 | 8.78 |

**Table 6-16 Maximum slip length (Soil friction : 0. 2 [kNm/m])**

- **Tension Effect Analysis**

As shown for the case of soil friction $0.12\ kNm/m$, the tension has a considerable influence on the ILS rotation angle during installation as well as on the maximum bending strains and the suspended length of the pipe . It was noticed that higher tension results in longer catenary and lower sagbend curvature and bending strain. As a consequence there is a reduction of rotation along the catenary. In order to investigate the effect of tension, same buoyancy is applied to all the cases (35t restrained buoyancy configuration).

Figure 6-48 and Figure 6-50 show the evolution of ILS rotation angle and TDP torque during installation for different values of tip separation for soil friction $0.2\ kNm/m$ . As it can be seen, the same behaviour is noticed as in the case with lower soil friction $(0.12\ kNm/m)$ . Applying higher tension leads to lower values of ILS rotation angle and touchdown point torque during installation. As a result the landing rotation angle of the inline structure as well as the torque at the touchdown point are lower for higher values of applied tension (larger tip separation).

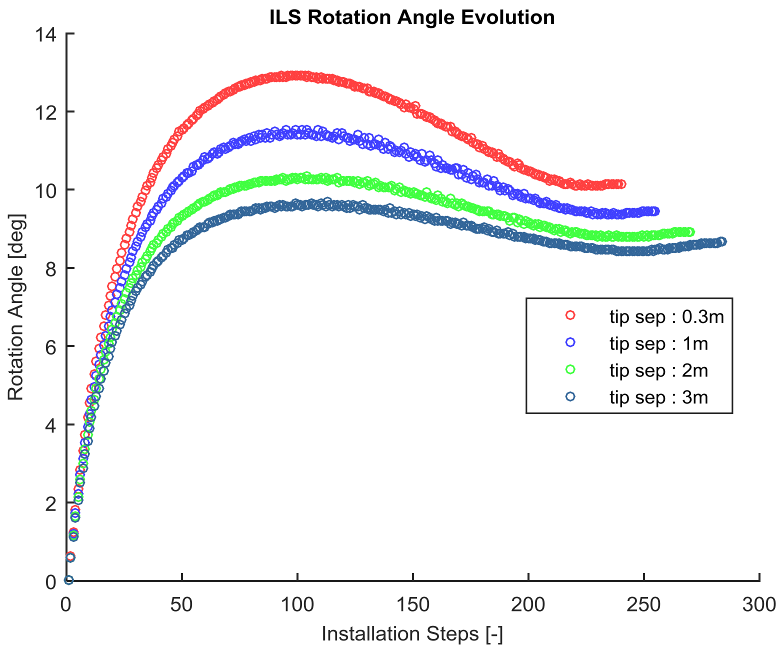


**Figure 6-48 ILS rotation angle evolution during installation for different tension**

Table 6-13 summarizes the most important results obtained by the tension effect analysis. It can be noticed that the maximum suspended length, the bending strain and the initial TDP rotation angle remain the same as in the previous case because the change of soil friction does not affect the pipelay results and the initial installation step.

| Case | ILS Landing Angle [Deg] | Maximum ILS Angle [Deg] | TDP Torque (ILS on seabed) [kNm] | Maximum Suspended Length [m] | Maximum Bending strain [%] | TDP Initial Rotation Angle [Deg] |
|---|---|---|---|---|---|---|
| 0.3m | 10.153 | 12.934 | 240.22 | 3079.13 | 0.118 | 101.823 |
| 1m | 9.459 | 11.535 | 221.07 | 3286.03 | 0.102 | 101.262 |
| 2m | 8.936 | 10.365 | 204.27 | 3470.45 | 0.091 | 100.522 |
| 3m | 8.662 | 9.687 | 194.71 | 3626.94 | 0.083 | 100.242 |

**Table 6-17 Results for different tension applied during inline structure installation (Soil friction : 0. 2 [kNm/m])**

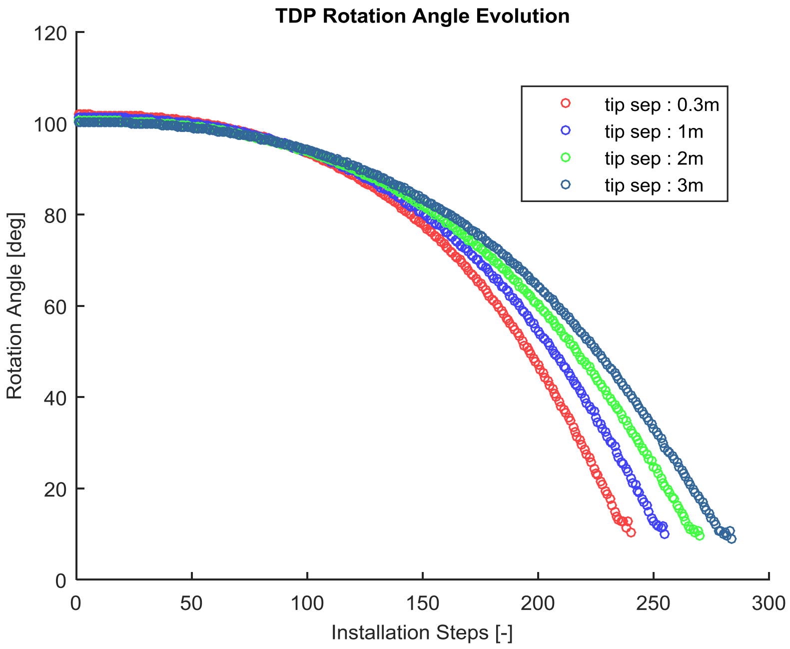


**Figure 6-49** **TDP rotation angle evolution during installation for different tension**

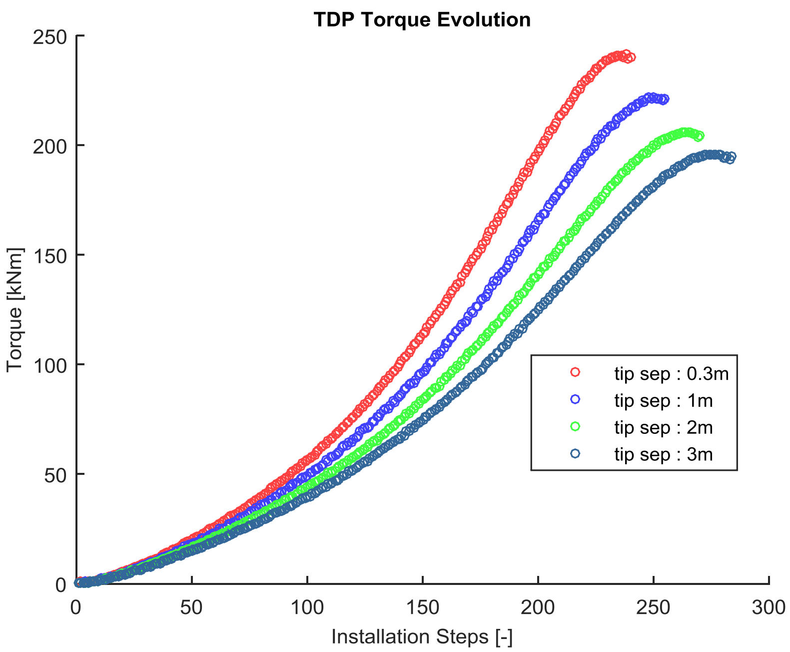


**Figure 6-50** **Touchdown point torque evolution during installation for different tension**

### 6.7.3 Soil Friction 0.03 [kNm/m] (Low Bound)

- **Buoyancy Effect Analysis**

Having analysed the buoyancy and tension effect for intermediate and high values of soil friction, it is interesting to investigate how the pipeline and the inline structure behave on non-stiff soils. For that reason the same cases with respect to buoyancy (see Table 6-9) were conducted with soil friction of 0.03 $kNm/m$. Figure 6-46 shows ILS evolution angles for the 5 cases.

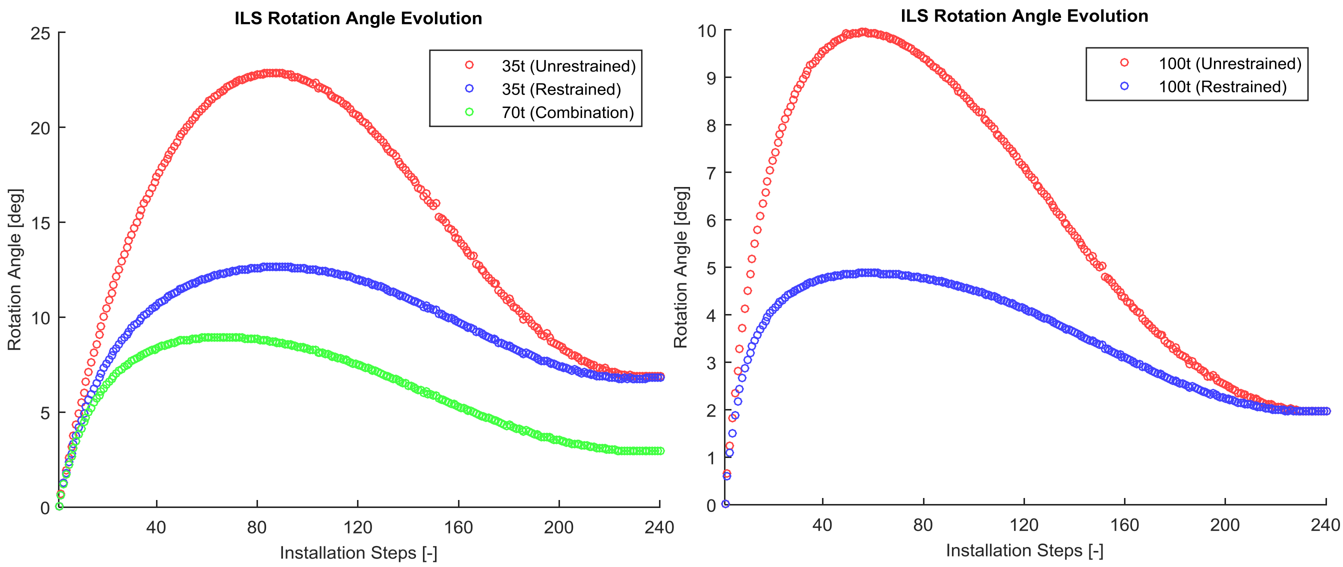


**Figure 6-51 ILS rotation angle evolution for different buoyancy (Cases1-5) – Soil friction : 0.03 [kNm/m]**

As it can be seen the ILS angle has identical evolution as in the cases of 0.12 $kNm/m$ and 0.2 $kNm/m$. It is noticed that the ILS landing angle is considerably lower for all the analysed cases which is a consequence of the low constraint provided from the seabed to the pipe to rotate at each step. The largest differences (see Table 6-18) are found for the unrestrained and restrained buoyancy configuration of 35t, 3.72$^{o}$ and 3.28$^{o}$ respectively. For large amount of buoyancy (cases 4 and 5) there is a difference of around 1.2$^{o}$ which is considered to be significant taking into account that the landing angles are small for these cases. In addition, the difference between the effect of the restrained and unrestrained buoyancy configuration becomes negligible for the landing rotation angle of the ILS in the case of low soil friction as in both cases of 35t (cases 1-2) and 100t (cases 4-5) the ILS landing angle differs of about 0.1 $^{o}$. Finally, the soil friction has no significant effect on the maximum ILS rotation angle during installation operation. The same was found also for the comparison between the cases of intermediate and high values of soil friction.

| Case | ILS landing angle [Deg] – S.F.:0.03 | ILS maximum angle [Deg] – S.F.:0.03 | ILS landing angle [Deg] – S.F.:0.12 | ILS maximum angle [Deg] – S.F.:0.12 |
|---|---|---|---|---|
| **1** | 6.90 | 22.84 | 10.62 | 23.04 |
| **2** | 6.79 | 12.64 | 10.07 | 12.93 |
| **3** | 2.942 | 8.941 | 4.612 | 9.025 |
| **4** | 1.974 | 9.943 | 3.165 | 9.992 |
| **5** | 1.965 | 4.874 | 3.044 | 4.918 |

**Table 6-18 Comparison between ILS landing and maximum angle for different values of soil friction**

The evolution of torque during installation has the same shape for all the cases as it can be seen from Figure 6-52.

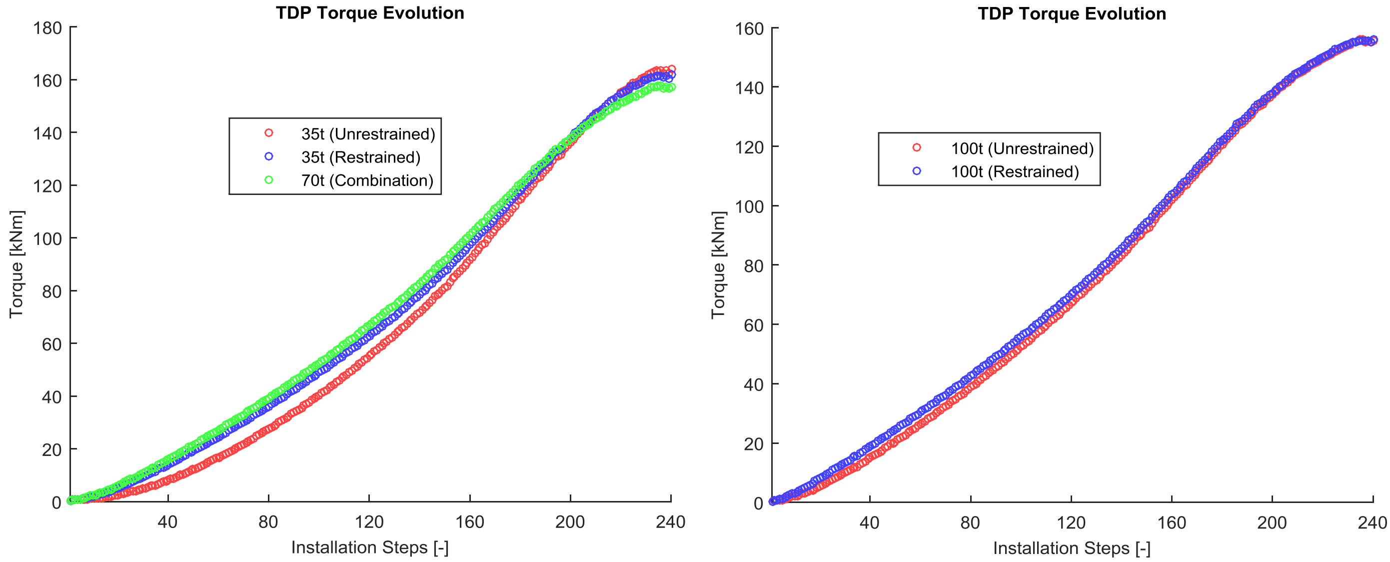


**Figure 6-52 Torque evolution during installation (Cases1-5) – Soil friction : 0.03 [kNm/m]**

As it is expected the lower rotation ILS landing angle has as a consequence a lower torque at the touchdown point at the last step of installation, when ILS is on seabed (see Table 6-19). Also, there is a considerable difference in the amount of torque around 85kNm in cases 1 and 3-5 and 78kNm in case 2.

| Case | 1 | 2 | 3 | 4 | 5 |
|---|---|---|---|---|---|
| Torque $[kNm]$ – S.F. :0.12 | 250.45 | 237.34 | 245.65 | 240.83 | 248.78 |
| Torque $[kNm]$ – S.F. :0.03 | 163.82 | 161.89 | 157.31 | 155.84 | 155.58 |

**Table 6-19 Comparison between TDP torque when ILS is landed for different soil friction**

For the case of low soil friction the maximum slip length is much higher than the previous two cases. Comparing with the case for 0.12kNm/m soil friction it is noted that the difference between the unrestrained and restrained configuration is not considered to be significant as there is a difference of 50m (case with 35t buoyancy) and 16m (case with 100t buoyancy). It is important to mention that for cases of low soil friction because of the large slip length additional attention should be taken for any structures which are already laid even they are away of the current touchdown point.

| Case | 1 | 2 | 3 | 4 | 5 |
|---|---|---|---|---|---|
| Maximum slip length $[m]$ | 5420.92 | 5370.66 | 5231.98 | 5085.19 | 5069.57 |

**Table 6-20 Maximum slip length (Soil friction : 0.03 [kNm/m])**

- **Tension Effect Analysis**

As shown for the case of soil friction $0.12\ kNm/m$ and $0.2\ kNm/m$, the tension has a noticeable influence for the ILS rotation angle during installation as well as for the maximum bending strains. It was mentioned that higher tension results to longer catenary and lower sagbend curvature and bending strain.

Figure 6-53 and Figure 6-55 show the evolution of ILS rotation angle and TDP torque during installation for different values of tip separation for soil friction $0.03\ kNm/m$ . As it can be seen for the lower value of soil friction $(0.03\ kNm/m)$ the increase of tension has no considerable effect at the landing angle of the ILS. As it can be seen from installation the value of landing angle fluctuates between 1.93° and 2.034° not showing a specific trend. The maximum ILS angle during installation has the same behaviour as in the cases with higher values of soil friction showing a gradual decrease for higher values of tension - tip separation (see Figure 6-53 and Table 6-21).

| Case | ILS Landing Angle [Deg] | Maximum ILS Angle [Deg] | TDP Torque (ILS on seabed) [kNm] | Maximum Suspended Length [m] | Maximum Bending strain [%] | TDP Initial Rotation Angle [Deg] |
|---|---|---|---|---|---|---|
| 0.3m | 6.791 | 12.636 | 159.16 | 3079.13 | 0.118 | 101.823 |
| 1m | 6.896 | 11.371 | 161.36 | 3286.03 | 0.102 | 101.262 |
| 2m | 6.635 | 10.230 | 152.41 | 3470.45 | 0.091 | 100.522 |
| 3m | 6.706 | 9.601 | 150.38 | 3626.94 | 0.083 | 100.242 |

**Table 6-21 Results for different tension applied during inline structure installation (Soil friction : 0. 03 [kNm/m])**

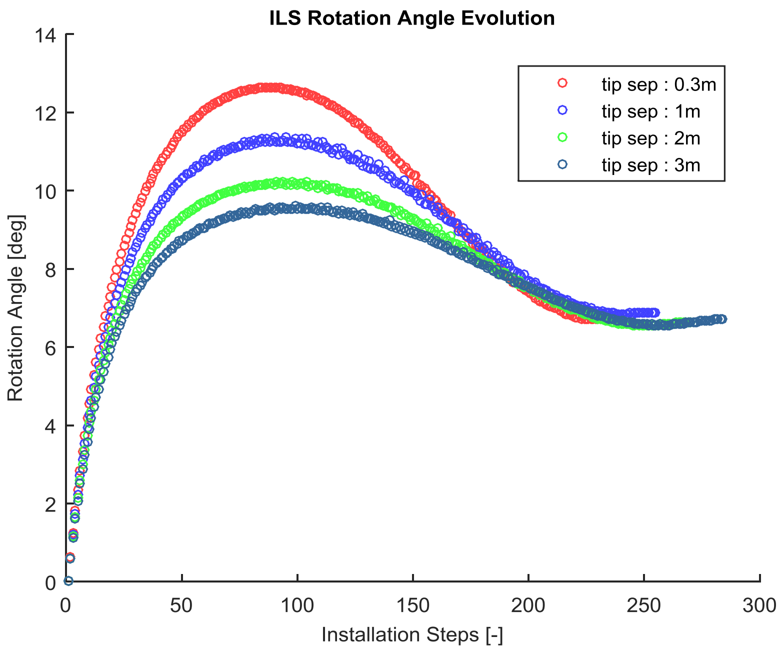


**Figure 6-53 ILS rotation angle evolution during installation for different tension**

The touchdown point angle evolution during installation for different values of tension is shown in Figure 6-54. It can be seen that for all the cases the touchdown point rotation angle has the same shape decreasing gradually until the last steps where presents some slight fluctuations for all cases. The tension has also an effect to the initial touchdown point rotation angle as it can be seen from Figure 6-54 and Table 6-21. Although the reduction of the initial TDP angle cannot be considered to be considerable  it verifies the fact that applying higher amount of tension results in lower values of rotation along the catenary for the pipeline in spite of the larger suspended length of the catenary.

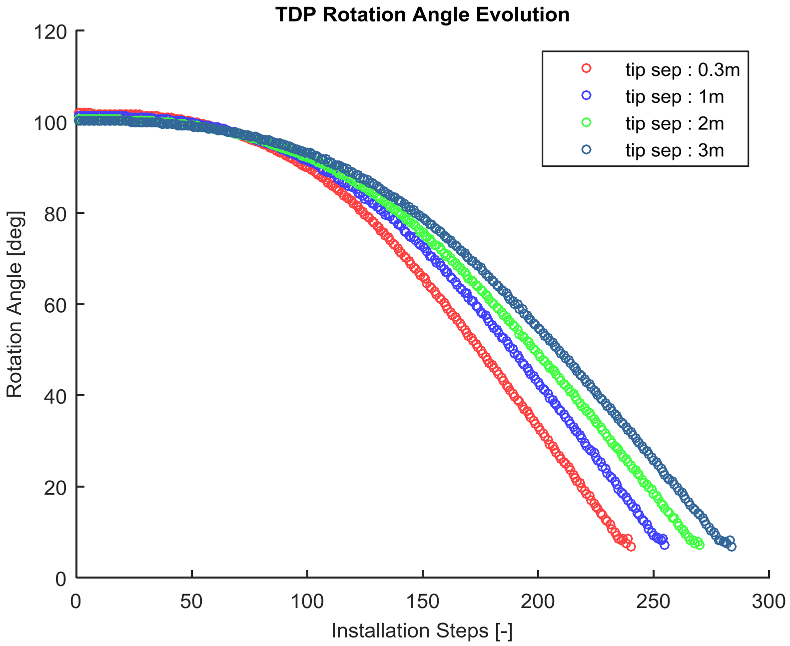


**Figure 6-54 TDP rotation angle evolution during installation for different tension**

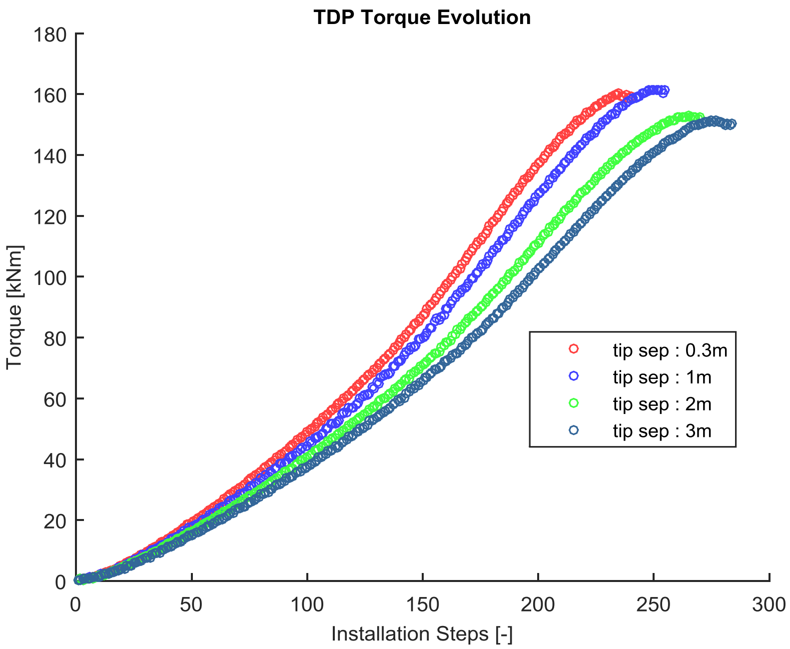


**Figure 6-55 Touchdown point torque evolution during installation for different tension**

### 6.7.4 Effect of numerical parameters

As it was mentioned at the beginning of the chapter, the two most important numerical parameters that will be considered are the seabed step and the pipe pay-out at each installation step.

Rotation and toque profiles are discretised along the catenary and on the seabed. Seabed step is a chosen parameter of the numerical model which describes the order of discretization of these profiles.

#### 6.7.4.1 Seabed Step Effect

In order to investigate if the effect of the seabed step is considerable to the rotation phenomenon, four cases are examined.

For the cases studied 35t buoyancy is used in restrained configuration, 012 kNm/m for soil friction and 0.3m for tip separation. Table 6-22 shows the inline structure landing and maximum angle during installation and the maximum slip length obtained using different values of seabed step.

| Seabed Step [m] | Quantity | | |
|---|---|---|---|
| | ILS Landing Angle [Deg] | Maximum ILS Angle [Deg] | Maximum Slip Length [Deg] |
| 0.01 | 10.070 | 12.932 | 882.91 |
| 0.1 | 10.050 | 12.931 | 882.9 |
| 0.5 | 10.010 | 12.931 | 849.5 |
| 1 | 9.979 | 12.930 | 849 |

**Table 6-22 Main rotation problem quantities for different values of seabed step**

As it can be seen, increasing the seabed step results in slightly different results for the quantities investigated. The parameter that is less affected by the seabed step is the maximum ILS angle during installation showing a divergence of 0.015% by increasing the seabed step from 0.01m to 1m. The ILS landing angle and the maximum slip length have a noticeable difference, especially for the case where the seabed step is 1m where the ILS landing angle is underestimated about 1% and the slip length about 3.7% with respect to the values obtained for the lowest value (0.01m).

The seabed step has negligible effect to the computational time but affects significantly the amount of data saved after the model is finished. Based on the above, it can be concluded that a value of seabed step of 0.1 meters can be considered to be as optimal for practical purposes and can give precise results. Further analysis can be done for different values of soil friction in order to investigate for different behaviour of the model.

#### 6.7.4.2 Pipe pay-out Effect

In order to investigate if the effect of the pipe pay-out is significant to the rotation phenomenon, three cases are examined. For the cases studied 35t buoyancy is used in restrained configuration, 012 kNm/m for soil friction, 0.3m for tip separation and seabed step 0.1m

Table 6-23 shows the inline structure landing and maximum angle during installation and the maximum slip length obtained using different values of seabed step.

| Pay-out [m] | Quantity | | |
|---|---|---|---|
| | ILS Landing Angle [Deg] | Maximum ILS Angle [Deg] | Maximum Slip Length [Deg] |
| 6.1 | 10.051 | 12.979 | 895.3 |
| 12.2 | 10.050 | 12.931 | 882.9 |
| 24.4 | 9.866 | 12.614 | 683.7 |

**Table 6-23 Main rotation problem quantities for different values of pipe pay-out**

As it can be seen from the table above pipe pay-out has a noticeable effect on the results, especially for the case of 24.4 meters where there is a relative difference of around 2% for the case of the landing and maximum ILS angle and 23.6% difference for the maximum slip length. The reason for that can be explained by the fact that the boundary conditions used in order to find the ILS and TDP equilibrium on each step depend on the pipe pay-out, so increasing significantly its value there it is needed an additional iteration procedure in order for the results to converge. Taking into account that the pipe pay-out affects significantly the computational time of the model and conducting a number of different comparisons in order to analyse its effect on the accuracy of the results it is proposed that the optimal value that gives reliable results in acceptable computational time for practical purposes, is 12.2 meters as the difference between the results in the first two cases is much lower than the accuracy required.

## 7.0 RESULTS DISCUSSION - CONCLUSIONS

In Chapter 6.7 a number of different cases were presented taking into consideration the effect of different parameters as the buoyancy effect, the soil friction and the tension.

Summarizing the results it can be concluded

- Applying the same amount of buoyancy for different values of soil friction, it was noticed that lower values of soil friction result in reduced inline structure landing angles. This behaviour was observed for all the cases studied independently of the amount of buoyancy (35t – 100t) and the configuration (restrained – unrestrained). This behaviour can be explained by the fact that for lower values of soil friction, the resistance provided from the seabed to the pipe is reduced and as a consequence, the already laid pipe is able to rotate more by the counteracting toque induced from the buoyancy modules. As it can be seen from Table 7-1 and Figure 7-1 there is a noticeable increase of ILS landing angle from the low (0.03kNm/m) to the intermediate (0.12 kNm/m) values of soil friction for all the cases studied and then the rate of increase decreases considerably from the intermediate to the higher bound (0.2kNm/m). In addition, it can be seen that the seabed friction has a more significant effect on the cases of low amount of buoyancy (cases 1-2).

  As far as the effect of buoy configuration is concerned, the restrained buoyancy configuration resulted to lower values of ILS landing angle, as it was expected, for all the cases independently of the soil friction and the amount of buoyancy. Both for the low and the high amount of buoyancy cases the difference between the two types of configuration becomes higher when the values of soil friction increase, as it can be seen from Figure 7-1, especially for the 35t buoyancy (low value).

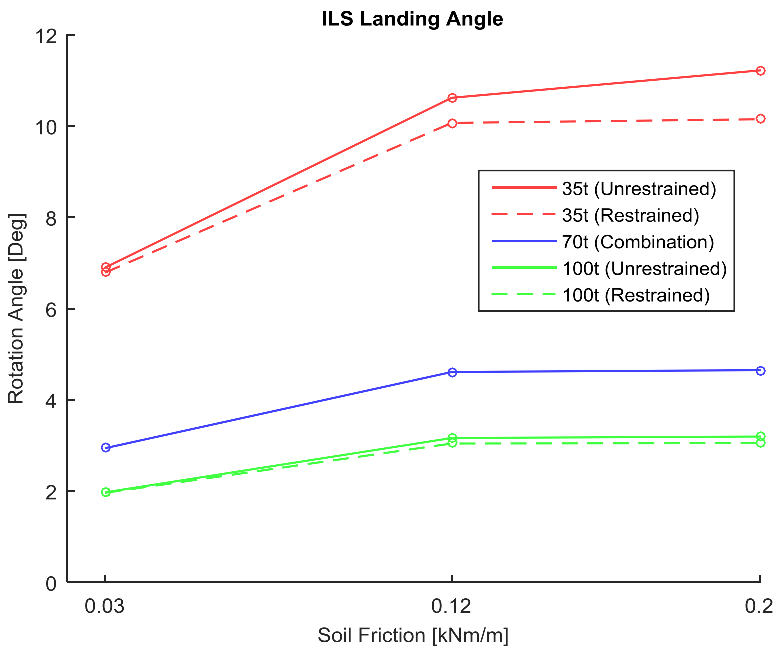


**Figure 7-1 ILS landing angle for different values of soil friction and buoyancy**

| Case | ILS landing angle [Deg] – S.F.:0.03 | ILS landing angle [Deg] – S.F.:0.12 | ILS landing angle [Deg] – S.F.:0.2 |
|---|---|---|---|
| **1** | 6.90 | 10.62 | 11.22 |
| **2** | 6.79 | 10.07 | 10.15 |
| **3** | 2.942 | 4.612 | 4.652 |
| **4** | 1.974 | 3.165 | 3.197 |
| **5** | 1.965 | 3.044 | 3.054 |

**Table 7-1 ILS landing angle for different values of soil friction and buoyancy**

- Another relevant quantity is the maximum rotation angle of the inline structure during installation. As it can be seen from Table 7-2 and Figure 7-2 the effect of soil friction to the maximum reachable ILS rotation angle during installation can be considered to be negligible for all the cases, independently of the amount or the configuration of the buoyancy. That can be explained by the fact that as shown in the Chapter 6.7 for all the cases the maximum ILS rotation angle is reached at the first installation steps, where the torque induced by the ILS to the laid pipe is relatively small and thus the soil friction has not yet considerable effect on the rotation phenomenon. In contrast with the ILS landing angle, the buoyancy configuration has a considerable effect on the maximum ILS rotation angle during installation. Specifically for the cases of low amount of buoyancy there is a difference around $11^{o}$ for all the values of soil friction, while for the cases 4 and 5 (100t buoyancy) the difference is around $5^{o}$ (see Table 7-2).

| Case | ILS maximum angle [Deg] – S.F.:0.03 | ILS maximum angle [Deg] – S.F.:0.12 | ILS maximum angle [Deg] – S.F.:0.2 |
|---|---|---|---|
| **1** | 22.84 | 23.04 | 23.06 |
| **2** | 12.64 | 12.93 | 12.94 |
| **3** | 8.941 | 9.025 | 9.026 |
| **4** | 9.943 | 9.992 | 9.993 |
| **5** | 4.874 | 4.918 | 4.919 |

**Table 7-2 Maximum ILS angle for different values of soil friction and buoyancy**

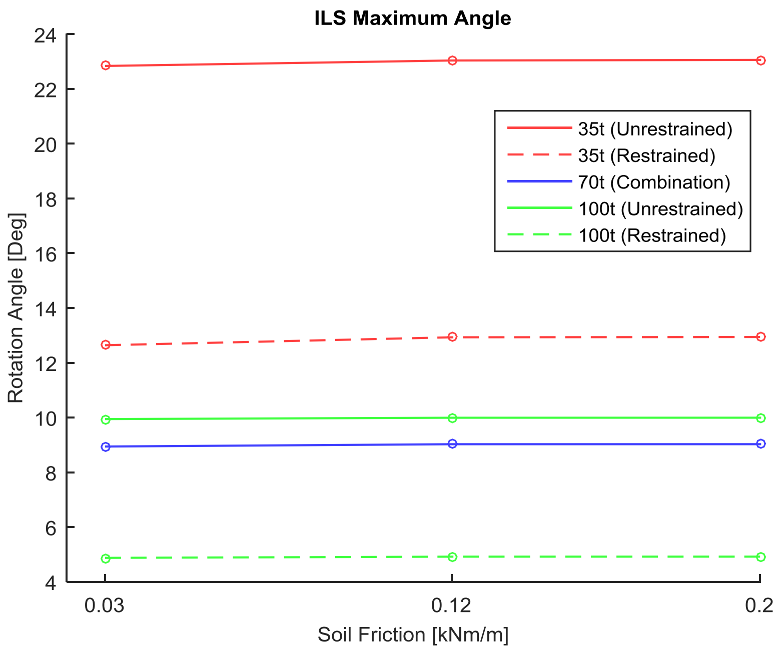


**Figure 7-2 Maximum ILS angle for different values of soil friction and buoyancy**

- For all the values of soil friction the effect of the applied tension was analysed for the rotation and the pipelay quantities. For all the cases studied, 35t of buoyancy were used in restrained configuration. As it can be seen from Figure 7-3 for the cases of the intermediate and the high value of soil friction, higher values of tip separation - tension result in lower values of ILS landing angles. That can be explained by the fact that higher tension results in lower sagbend strains, thus decreased sagbend curvature, and as a consequence lower amount of rotation. However it can be seen that as the tension increases the rate of decrease of ILS landing angle reduces showing that for a certain value of soil friction and buoyancy configuration there is a certain value of ILS landing angle that cannot be exceeded independently of the tension applied. For the case of soil friction 0.03kNm/m (low bound) the ILS landing angle does not show a specific behaviour as it fluctuates at around 6.7$^{o}$ showing that the tension has not considerable effect in the case of low soil friction.

| | **Tip Separation [m]** | | | |
|---|---|---|---|---|
| **Soil Friction [kNm/m]** | **0.3** | **1** | **2** | **3** |
| **0.03** | 6.791$^{o}$ | 6.896$^{o}$ | 6.635$^{o}$ | 6.706$^{o}$ |
| **0.12** | 10.07$^{o}$ | 9.448$^{o}$ | 8.927$^{o}$ | 8.661$^{o}$ |
| **0.2** | 10.153$^{o}$ | 9.459$^{o}$ | 8.936$^{o}$ | 8.662$^{o}$ |

**Table 7-3 ILS landing angle for different values of soil friction and tension**

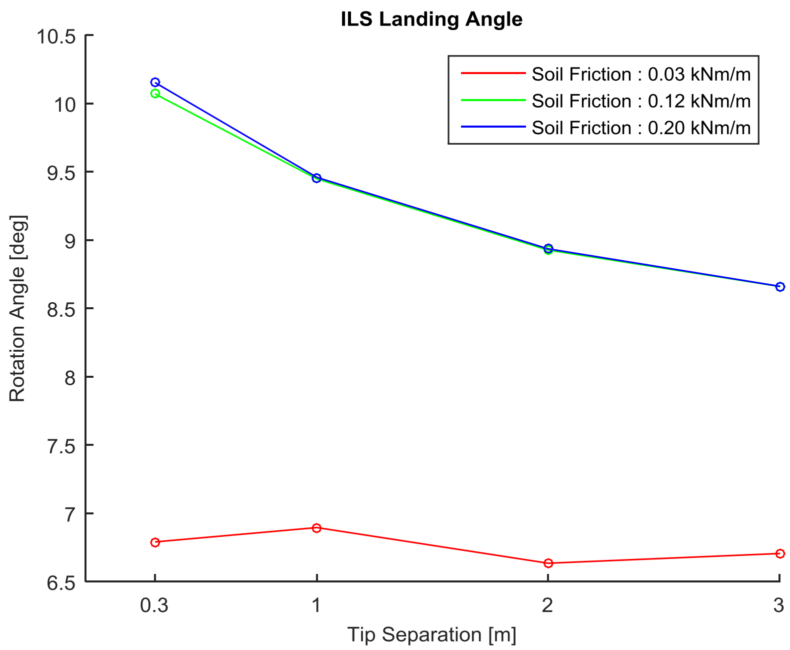


**Figure 7-3 ILS landing angle for different values of soil friction and tension**

The maximum angle of the in line structure during installation has the same behaviour for all the values of soil friction, decreasing for higher values of applied tension as it can be seen from Figure 7-4. Comparing with Figure 7-3 it can be concluded that the effect of tension is more considerable for the maximum ILS rotation angle during installation than for the ILS landing angle. In addition, the difference for the intermediate and the high values of soil friction is negligible for all the cases of applied tension.

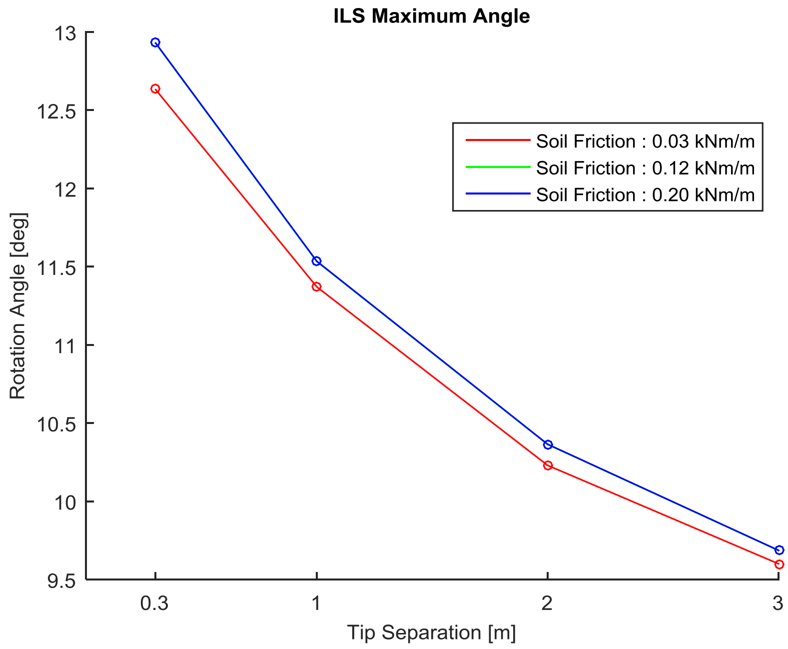


**Figure 7-4 ILS landing angle for different values of soil friction and tension**

| | **Tip Separation [m]** | | | |
|---|---|---|---|---|
| **Soil Friction [kNm/m]** | **0.3** | **1** | **2** | **3** |
| **0.03** | 12.636° | 11.371° | 10.231° | 9.601° |
| **0.12** | 12.932° | 11.533° | 10.364° | 9.686° |
| **0.2** | 12.934° | 11.535° | 10.365° | 9.687° |

**Table 7-4 ILS maximum angle for different values of soil friction and tension**

Applying higher amount of tension has also as a consequence the reduction of the maximum bending strains at the sagbend and the raise of the maximum suspended length as it can be seen from Figure 7-5 and Table 7-5.

| Maximum Bending strain [%] | Maximum Suspended Length [m] | Maximum applied top tension [kN] |
|---|---|---|
| 0.118 | 3079.13 | 4068 |
| 0.102 | 3286.03 | 4400 |
| 0.091 | 3470.45 | 4751 |
| 0.083 | 3626.94 | 5018 |

**Table 7-5 Maximum bending strain and suspended length during ILS installation for different values of tension**

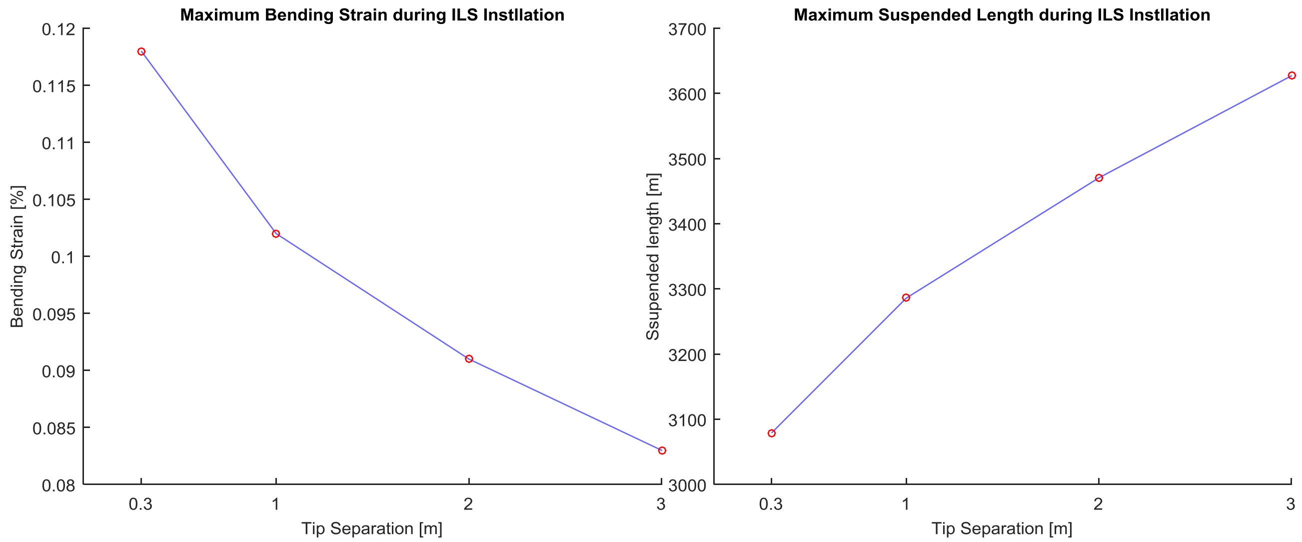


**Figure 7-5 Maximum bending strain and suspended length for different values of tension**

According to the results above, it can be concluded that the inline structure rotation angle is mainly dominated by the reduction of the bending strains and the decreased curvature along the pipeline for increased values of tension and not by the increase of the suspended length of the catenary.

- When the installation process starts, the initial touchdown point rotation angle is also affected by the tension applied. As shown before, there is a slight decrease of the TDP rotation angle by applying higher amount of tension, verifying the fact that higher tension results in lower values of rotation along the catenary.

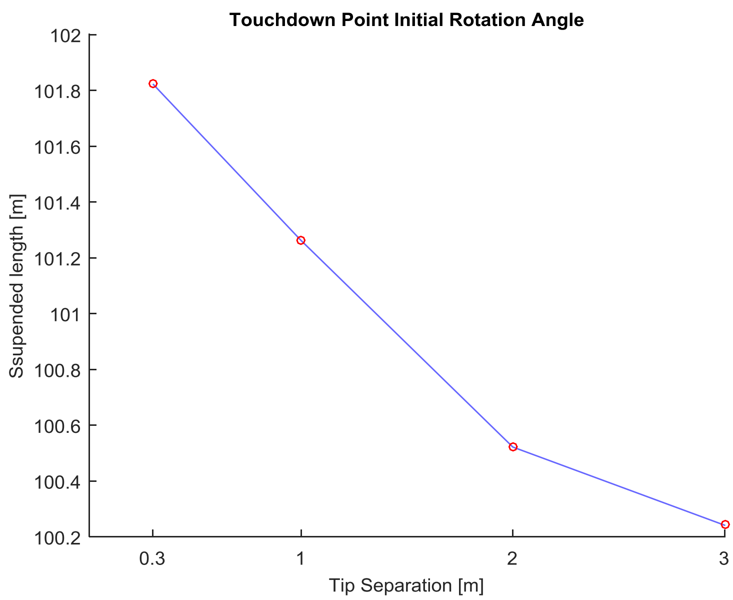


| Case | TDP Initial Rotation Angle [Deg] |
|---|---|
| 0.3m | 101.823 |
| 1m | 101.262 |
| 2m | 100.522 |
| 3m | 100.242 |

**Table 7-6 TDP Initial Rotation Angle**

**Figure 7-6 Touchdown point initial rotation angle for different values of tension**

As it can it can be seen the increase in tension resulted to a decrease of the initial touchdown point angle of around 1.6$^{o}$. Comparing with the ILS landing angle for different amount of tension (Figure

7-3 and Table 7-3) it is noticed that especially for the cases 0.12kNm/m and 0.2kNm/m the inline structure landing angle has a reduction of almost the same magnitude (1.41$^{o}$ and 1.49$^{o}$ respectively). According to that it can be concluded that the reduction of the ILS landing angle is mainly caused by the decrease of the initial touchdown point rotation angle. Thus an effective solution for the considerable reduction of the ILS landing angle would be the increase of tension a few kilometres before the inline structure installation, resulting in lower rotation angle of the already laid pipe and as a consequence in considerably decreased touchdown point angle when ILS is to be installed.

## 8.0 POTENTIAL ENERGY METHOD

In this chapter the potential energy method will be analysed for the derivation of the coupled differential equations which govern a pipeline segment subjected to bending, torsion and tension. The purpose of the chapter is to validate the results obtained from the energy minimization principle by solving the bending and the rotation problem simultaneously.

### 8.1 Derivation of coupled differential equations of motion

The total potential energy of a pipeline segment of length ds subjected to tension $T$ as shown in Figure 3-3 can be expressed as follows [17]

$$P = \int_0^L \frac{1}{2}EA[u'_{ax}(s)]^2 + \frac{1}{2}EI_b[\vartheta'(s)]^2 + \frac{1}{2}GI_t[\varphi'(s)]^2 - \frac{1}{2}\frac{TI_t}{A}[\varphi'(s)]^2 - \frac{1}{2}T\cdot(\theta)^2 + \rho Azds$$

where the first three terms describe the axial, bending and torsion energy. The fourth and the fifth term are second order terms related to the effect of tension for large deflection and rotation angles while the last term is the energy due the own weight of the pipe segment (z is the vertical displacement of a segment).

Taking into account the residual curvature due to the plastic deformation of the pipe on the stinger the curvature can be written with the same way as introduced in previous chapters, thus

$$\vartheta'(s) = \vartheta'(s) + k_r cos\varphi(s)$$

The potential energy can be written

$$P = \int_0^L \frac{1}{2}EA[u'_{ax}(s)]^2 + \frac{1}{2}EI_b[\vartheta'(s) + k_r cos\varphi(s)]^2 + \frac{1}{2}GI_t[\varphi'(s)]^2 - \frac{1}{2}\frac{TI_p}{A}[\varphi'(s)]^2 - \frac{1}{2}T\cdot(\vartheta)^2 + \rho Az\, ds$$

Expanding the squared term of the bending energy,

$$P = \int_0^L \frac{1}{2}EA[u'_{ax}(s)]^2 + \frac{1}{2}EI_b[\vartheta'(s)]^2 + EI_b\vartheta'(s)k_r cos\varphi(s) + \frac{1}{2}EI_b k_r^2 cos^2\varphi(s) + \frac{1}{2}GI_t[\varphi'(s)]^2 - \frac{1}{2}\frac{TI_p}{A}[\varphi'(s)]^2 - \frac{1}{2}T[\vartheta(s)]^2 + \rho Agz\, ds$$

In order to find equilibrium, the variation of the potential energy is set equal to zero:

$$\delta P = \int_0^L EAu'_{ax}\delta u'_{ax} + EI_b\vartheta'\delta\vartheta' + EI_b k_r cos\varphi\delta\vartheta' - EI_b\vartheta' k_r sin\varphi\delta\varphi - EI_b k_r^2 cos\varphi sin\varphi\delta\varphi + GI_t\varphi'\delta\varphi' - \frac{TI_p}{A}\varphi'\delta\varphi' - T\vartheta\delta\vartheta + \rho Agcos\vartheta\delta w + \rho Agsin\vartheta\delta u'_{ax}\, ds$$

Integration by parts gives (with zero integration constants from the boundary conditions):

$$\delta P = \int_0^L \delta P_1 + \delta P_2 + \delta P_3 \, ds$$

where the components of the energy potential can be written

$$\delta P_1 = (-EAu''_{ax} + \rho Ag sin\vartheta)\delta u_{ax}$$

$$\delta P_2 = \left(-GI_t\varphi'' - EI_b\vartheta' k_r sin\varphi - EI_b k_r^2 cos\varphi sin\varphi + \frac{TI_p}{A}\varphi''\right)\delta\varphi$$

The terms related to the variation of the rotation in bending plane $\delta\vartheta$ will be written with respect to $\delta w$. Taking into account $\delta\vartheta' = \delta w''$ (where w is the deflection of the beam) with integration by parts

$$EI_b\vartheta'\delta\vartheta' = EI_b w''\delta w'' = -EI_b w'''\delta w' = EI_b w''''\delta w$$

$$\begin{aligned} EI_b k_r cos\varphi\delta\vartheta' &= EI_b k_r (cos\varphi)'\delta\vartheta = -EI_b k_r \varphi' sin\varphi\delta\vartheta = -EI_b k_r \varphi' sin\varphi\delta w' \\ &= EI_b k_r (\varphi' sin\varphi)'\delta w \end{aligned}$$

$$T\vartheta\delta\vartheta = T\vartheta\delta w' = -T\vartheta'\delta w$$

Based on the above the expression for $\delta P_3$ becomes

$$\delta P_3 = (EI_b w'''' + EI_b k_r (\varphi' sin\varphi)' - T\vartheta' + \rho Ag cos\vartheta)\delta w$$

and taking into account that $w' = \vartheta$ the expression for $\delta P_3$ can be written

$$\delta P_3 = (EI_b\vartheta''' + EI_b k_r (\varphi' sin\varphi)' + T\vartheta' + \rho Ag cos\vartheta)\delta w$$

If the integral in the expression of $\delta P$ is to be zero for every variation $\delta u_{ax}, \delta\varphi \; and \; \delta w$, it should hold that:

$$EI_b\vartheta''' + EI_b k_r (\varphi' \cdot sin\varphi)' - T\vartheta' + \rho Ag cos\vartheta = 0$$

$$-GI_t\varphi'' - EI_b\vartheta' k_r sin\varphi - EI_b k_r^2 cos\varphi sin\varphi + \frac{TI_p}{A}\varphi'' =$$

$$-EAu''_{ax} + \rho Ag sin\vartheta = 0$$

Taking into account that the tension applied and the submerged weight can be written as

$$T = EAu'_{ax} \quad and \quad w_s = \rho Ag$$

the equations above can be written

$$EI_b\frac{d^3\vartheta}{ds^3} - T\frac{d\vartheta}{ds} + EI_b k_r \left(\frac{d\varphi}{ds} \cdot sin\varphi\right)' + w_s cos\vartheta = 0 \qquad [\mathbf{8.1}]$$

$$-\left(GI_t-\frac{TI_p}{A}\right)\frac{d^2\varphi}{ds^2}-EI_bk_r sin\varphi\ \frac{d\vartheta}{ds}-EI_bk_r^2 cos\varphi sin\varphi=0 \qquad [\mathbf{8.2}]$$

$$\frac{dT}{ds}=w_s sin\vartheta \qquad [\mathbf{8.3}]$$

Equations 7.1, 7.2 and 7.3 are the set of coupled differential equations which describe the motion of a pipe segment along the catenary subjected to bending and torsion under tension T. Following the same procedure by substituting the variable s with the dimensionless parameter ε, where

$$s=\varepsilon\cdot L\ where\ s\in[0,L]\ and\ \varepsilon\in[0,1]$$

the equations above become

$$\frac{EI_b}{L^3}\frac{d^3\vartheta}{d\varepsilon^3}-\frac{T}{L}\frac{d\vartheta}{d\varepsilon}+\frac{EI_b}{L^2}k_r\frac{d^2\varphi}{d\varepsilon^2}sin\varphi+\frac{EI_b}{L^2}k_r\left(\frac{d\varphi}{d\varepsilon}\right)^2 cos\varphi+w_s cos\vartheta=0$$

$$-\left(GI_t-\frac{TI_p}{A}\right)\frac{1}{L^2}\frac{d^2\varphi}{d\varepsilon^2}-\frac{EI_bk_r}{L}\frac{d\vartheta}{d\varepsilon}sin\varphi\ -EI_bk_r^2 cos\varphi sin\varphi=0$$

$$\frac{dT}{d\varepsilon}=w_sLsin\vartheta$$

Having formulated the coupled governing equations of a pipe segment along the catenary, the boundary conditions can be written as follows

$\vartheta(0)=0$ The pipeline angle at the touchdown point is zero.

$\left.\frac{d\vartheta}{d\varepsilon}\right|_{\varepsilon=0}=0$ The derivative of the angle (bending moment)at the touchdown point is zero.

$T(0)=T_h$ The tension at the seabed equals to the bottom tension (applied from the thrusters)

$\vartheta(1)=\vartheta_0$ The angle at the stinger tip equals to the departure angle.

$T(1)=T(st)$ The tension at the stinger tip equals to the axial top tension.

$\left.\frac{d\varphi}{d\varepsilon}\right|_{\varepsilon=0}=0$ The derivative of the rotation angle (torsion) at the touchdown point is zero.

$\varphi(1)=0$ The rotation angle at the stinger tip is zero.

In order to validate the results from the energy minimization principle, the same cases were conducted as these presented in Chapter 6.2. It should be mentioned that in this case the rotation and the bending problem is solved simultaneously based on the coupled equations presented above. In the case of the energy minimization principle the bending problem was solved firstly and the curvature obtained from its solution is used as an input for the rotation problem.

### 8.1.1 Case Study N°1

Figure 8-1 and Figure 8-2 show the rotation angle and the curvature evolution (and their difference) along the catenary obtained by the energy minimization method, where bending and the rotation problems are solved separately, and the potential energy method where the problems are solved simultaneously based on the coupled differential equations presented above.

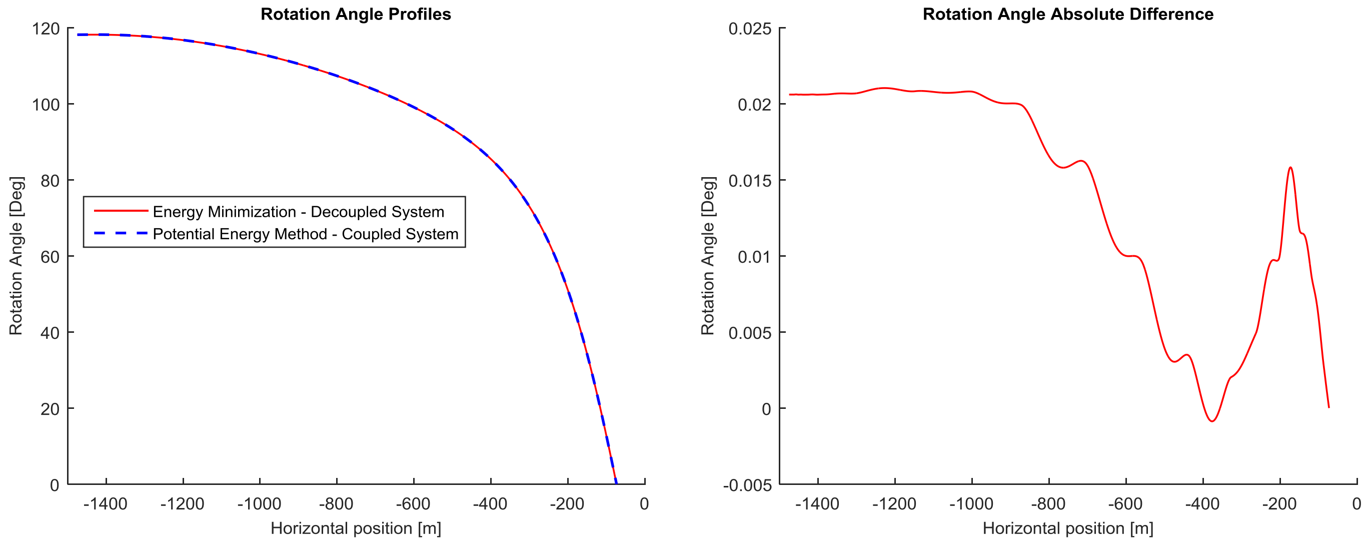


**Figure 8-1 Rotation angle & absolute difference (Residual Radius=511.1m)**

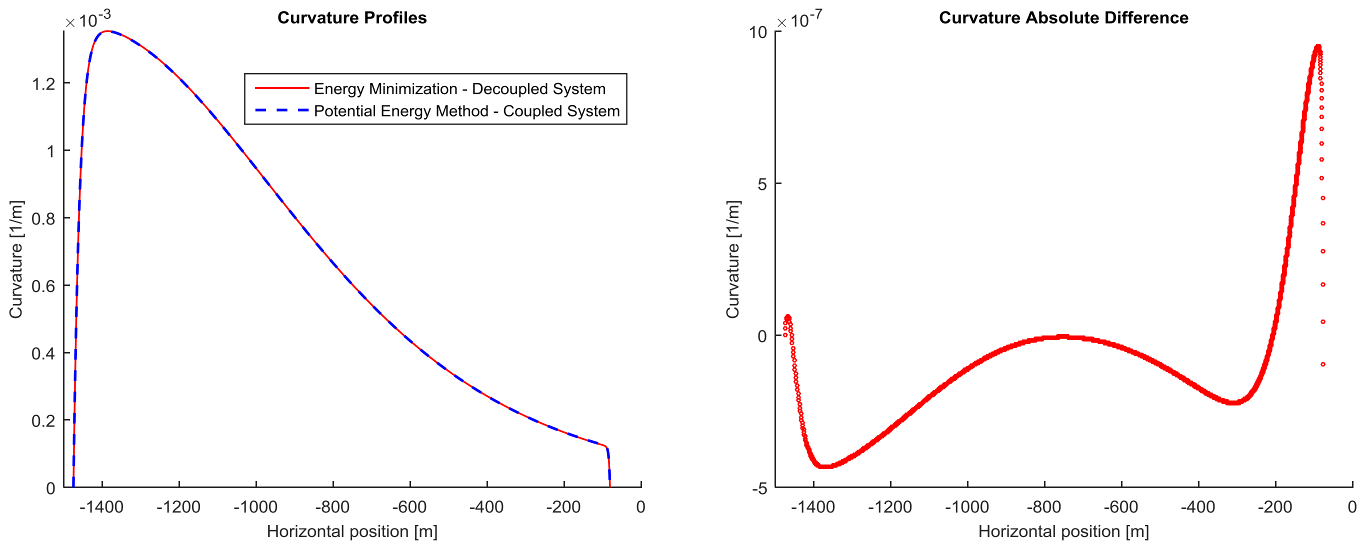


**Figure 8-2 Curvature evolution & absolute difference (Residual Radius=511.1m)**

As it can be seen the rotation angle difference between the two methods is lower than 0.025° along the catenary which can be considered to be negligible. The angle at the touchdown point given by solving the coupled differential equations based on potential energy method is 118.119° while from energy minimization principle the touchdown point angle was 118.099°. It should be noted that when the rotation becomes significant (after 400m from the stinger tip) the curvature obtained by the potential energy method is slightly lower than that obtained by energy minimization principle and that is caused by the fact that solving the bending and the rotation problems simultaneously, rotation is taken into account for the estimation of bending problem quantities resulting to lower values of curvature (see Chapter 5.2 for physical explanation).

### 8.1.2 Case Study N°2

Figure 8-3 and Figure 8-4 show rotation angle and curvature evolution (and their difference) along the catenary obtained by the energy minimization method and the potential energy method for the second case study.

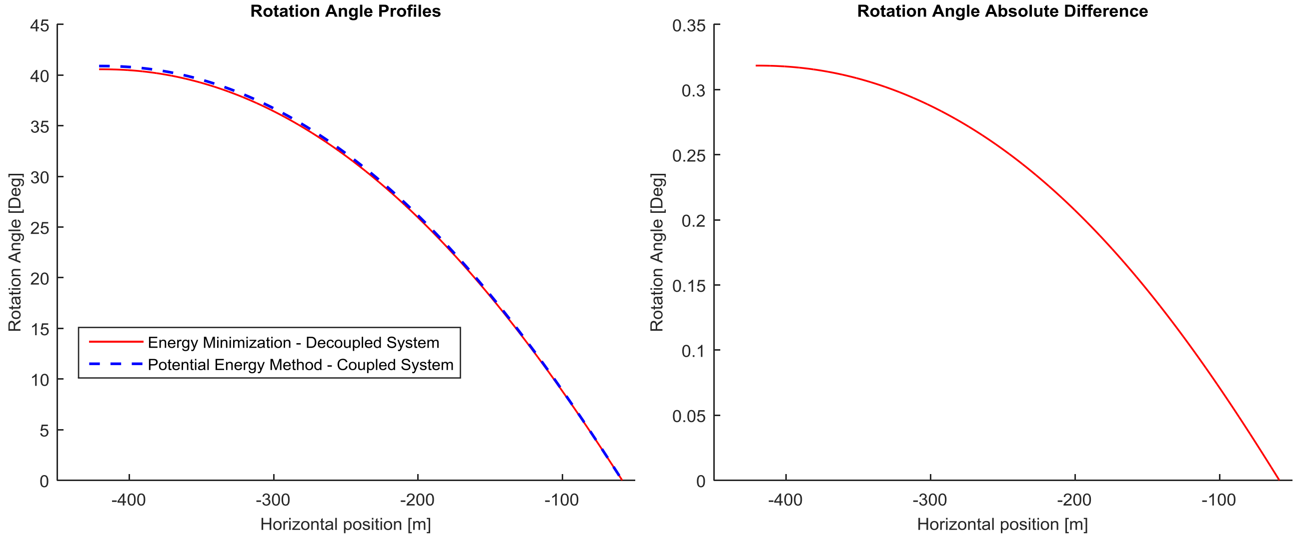


**Figure 8-3 Rotation angle evolution & absolute difference (Residual Radius=360.6m)**

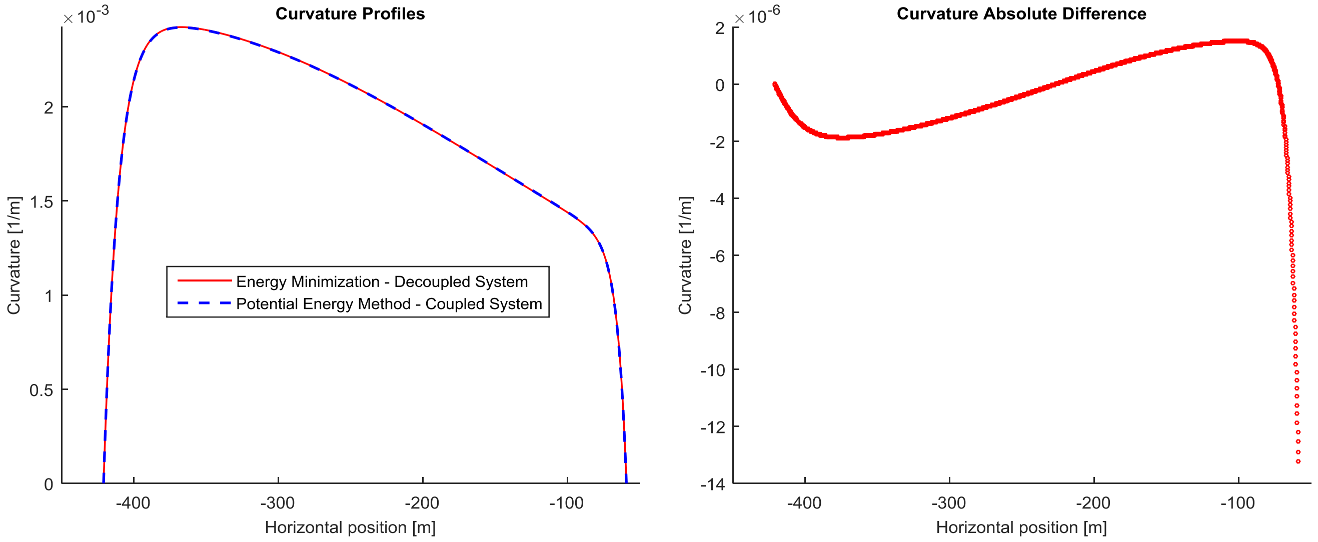


**Figure 8-4 Curvature evolution & absolute difference (Residual Radius=360.6m)**

At the second case the difference between the rotation angle along the catenary follows a smooth trend increasing gradually from 0 (stinger tip) to 0.32° around the area of touchdown point where this difference remains almost constant. The rotation angle at the touchdown point obtained by the potential energy method is 40.897° while based on energy minimization principle the touchdown point angle obtained was 40.578°. The curvature profile presents the same behavior at the sagbend region, with the energy minimization method overestimating the curvature as it does not take into account the residual curvature and the resulting rotation along the catenary.

### 8.1.3 Case Study N°3

Figure 8-5 and Figure 8-6 show rotation angle and curvature evolution (and their difference) along the catenary obtained by the energy minimization method and the potential energy method for the third case study.

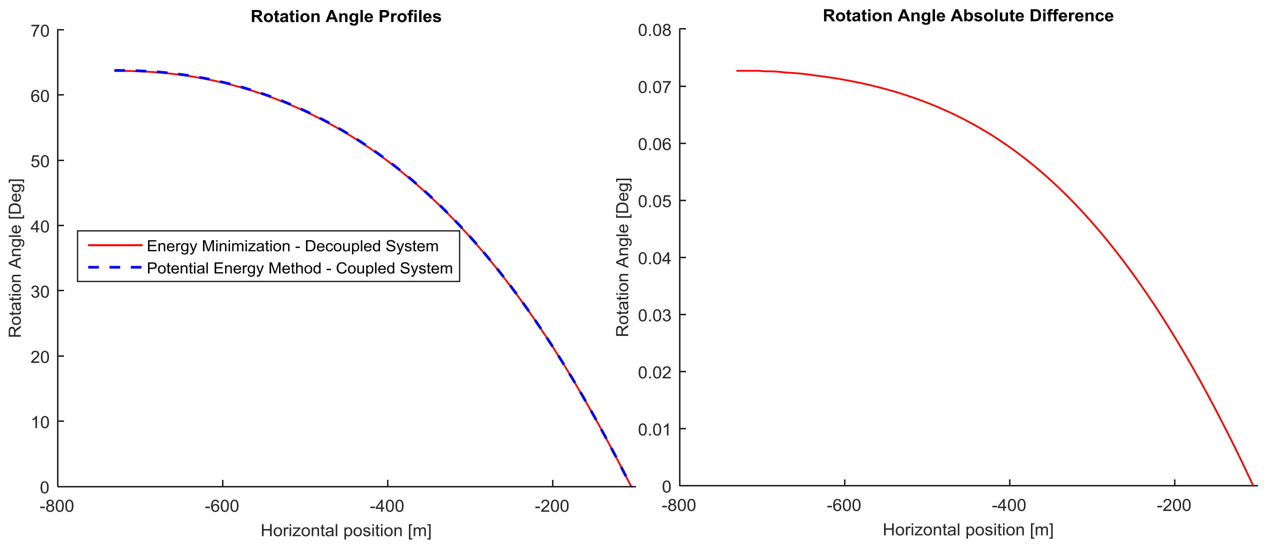


**Figure 8-5 Rotation angle evolution & absolute difference (Residual Radius=791m)**

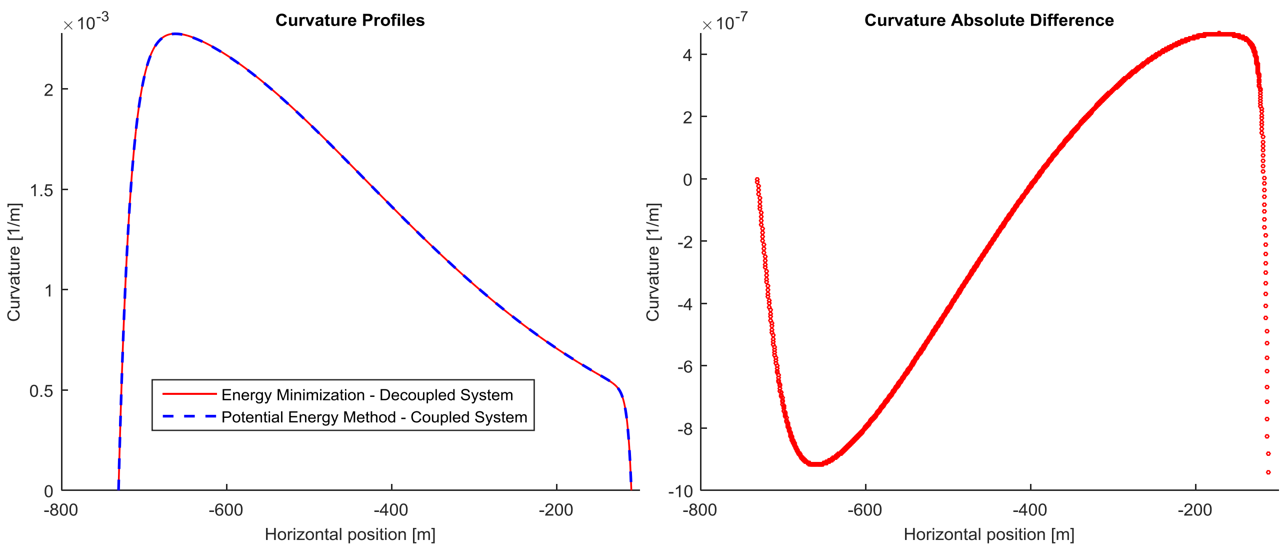


**Figure 8-6 Curvature evolution & absolute difference (Residual Radius=791m)**

At the third case the difference between the rotation angle along the catenary has the same shape as in the 2nd case, increasing gradually from 0 (stinger tip) to 0.07° around the area of touchdown point where this difference remains almost constant. The rotation angle at the touchdown point given by solving the coupled differential equations based on potential energy method is 63.771° while based on energy minimization principle the touchdown point angle obtained was 63.702°.

### 8.1.4 Case Study N°4

Figure 8-5 and Figure 8-6 show rotation angle and curvature evolution (and their difference) along the catenary obtained by the energy minimization method and the potential energy method for the third case study.

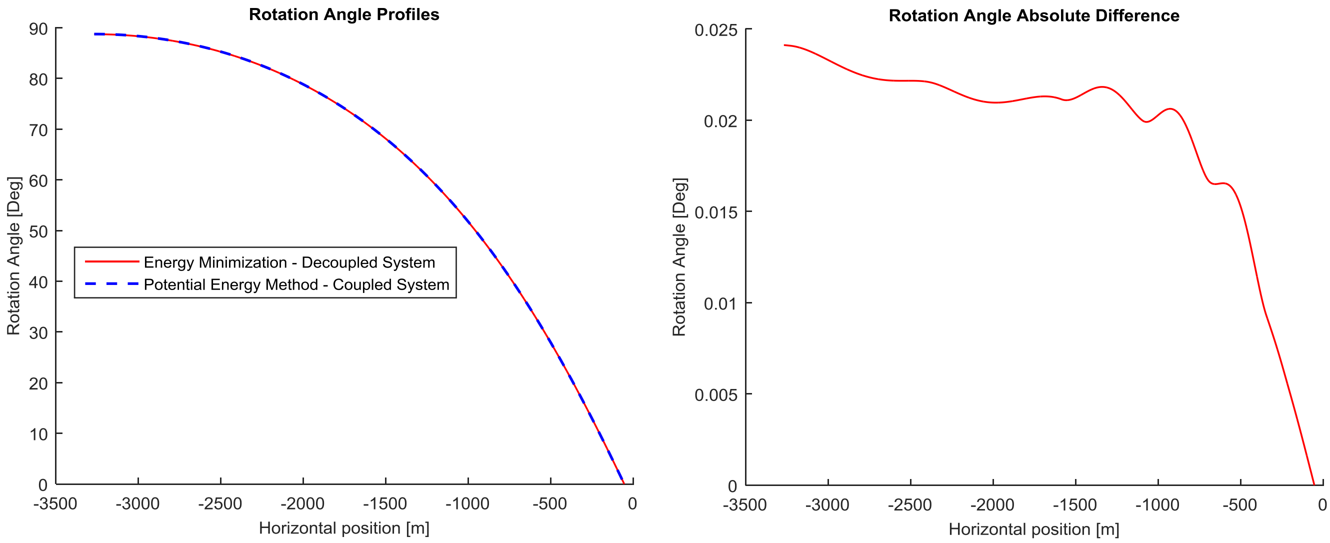


**Figure 8-7 Rotation angle evolution & absolute difference (Residual Radius=2262m)**

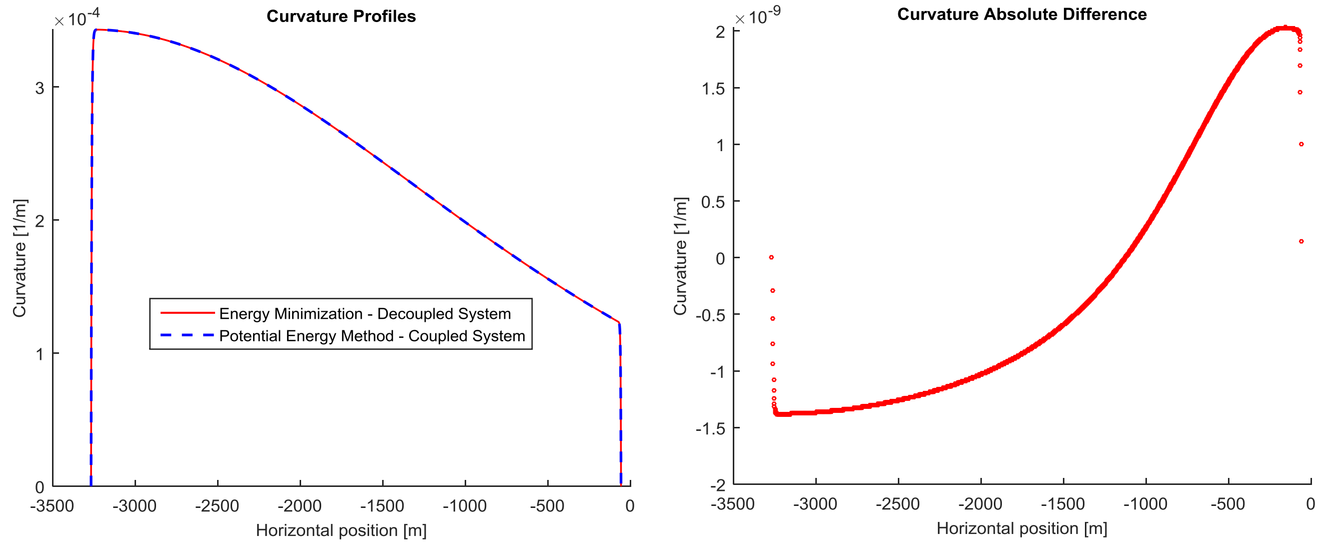


**Figure 8-8 Curvature evolution & absolute difference (Residual Radius=2262m)**

As it can be seen the rotation angle difference between the two methods is lower than 0.025° along the catenary. The angle at the touchdown point given by solving the coupled differential equations based is 88.759° while from energy minimization principle the touchdown point angle is 88.735°. For the largest part of the sagbend area the curvature obtained by the potential energy method is slightly lower than that obtained by energy minimization principle as rotation is taken into account for the estimation of bending problem quantities.

### 8.1.5 Results Analysis

Based on the comparisons between the energy minimization principle and the potential energy method can be concluded that the two methods lead to the same results with negligible differences for all the cases studied.

- **Curvature**

For all the cases the potential energy method resulted in lower values of curvature at the sagbend area. That can be explained by the fact that when the bending and the rotation problem are solved simultaneously the resulting pipe rotation is taken into account for the solution of the bending problem. For all the cases is shown that the influence of the torsion on bending is negligible. The order of the curvature difference is 3 to 4 times lower than the order of the actual values of curvature, thus the coupling effect has no significant effect on the problem. In addition, the highest difference between the two methods is noticed at the area of the stinger tip, where the derivative of the rotation angle $\frac{d\varphi}{ds}$ has its highest values and that can be explained by the additional coupling term

$$EI_b k_r \left(\frac{d\varphi}{ds} \cdot sin\varphi\right)'$$

in equation 7.1 which describes the bending problem.

- **Rotation Angle**

For all the cases studied the potential energy method, where the coupled differential equations for bending and rotation are solved simultaneously, resulted to slightly higher touchdown point angles than the energy minimization method. The largest differences between the rotation angle profiles were found for the cases of shallow waters (Case 2 – 200m and Case 3 – 600m) around 0.32$^o$ and 0.07$^o$ respectively at the touchdown point. For the other two cases the difference between the two methods reached a maximum of around 0.022$^o$ at the touchdown point. For all the cases studied the difference between the rotation angle along the catenary is zero at the stinger tip (boundary condition) and increases gradually until the touchdown point area where it remains constant. For the cases 2 and 3 the difference increases smoothly until the touchdown point as it can be seen from Figure 8-3 and Figure 8-5, whereas for the cases 1 and 4 are noticed some fluctuations along the catenary (see
Figure 8-1 and Figure 8-9). The difference in the rotation profile comes as a result of the difference in the curvature profile and is considered to be negligible.

Based on the results and the comparisons made it can be concluded solving the coupled differential equations using the potential energy method did not have considerable effect for any of the cases studied. The rotation and curvature profiles along the catenary as well as the rotation angle at the touchdown point presented minor differences which are not considered to be noticeable validating the results obtained from the energy minimization principle.

## 9.0 MODEL IMPROVEMENT - PIPE-SOIL INTERACTION

Instead of considering the soil to be purely rigid (pipelay problem) the pipeline can be considered as a beam laying on elastic foundation [2], [3]. The beam lies on elastic foundation when under the applied external loads, the reaction forces of the foundation are proportional at every point to the deflection of the beam at this point. This assumption was introduced first by Winkler in 1867. According to the Winkler model, the beam-supporting soil is modeled as a series of closely spaced, mutually independent, linear elastic vertical springs, defined by the seabed stiffness $k_s$, which provide resistance in direct proportion to the deflection of the beam.

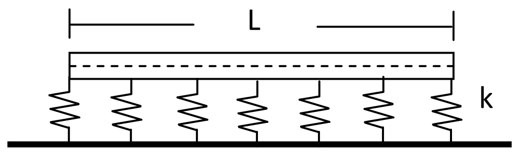


**Figure 9-1 Geometry of a beam on Winkler foundation**

Considering the pipe as a tensioned beam, the forces acting on a segment of pipeline laid on the seabed is shown in Figure 9-2.

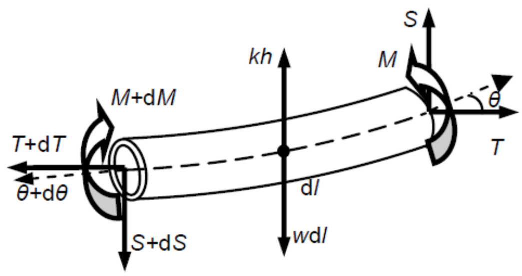


**Figure 9-2 Force sketch of segments of pipe on the seabed**

Based on the analysis of the acting forces the ordinary differential equation which governs the transverse motion of the tensioned pipe is

$$EI_b \frac{d^4y}{dx^4} - T_h \frac{d^2y}{dx^2} + k_s(y - D) = w_s$$

where $T$ is a constant tension, $k_s$ is the seabed stiffness and D the water depth. In order to solve the problem the equation has to become as follows

$$\frac{d^4y}{dx^4} - \frac{T_h}{EI_b}\frac{d^2y}{dx^2} + \frac{k_s}{EI_b}y = \frac{(w_s + k_s \cdot D)}{EI_b} \qquad [9.1]$$

The general solution of the nonhomogeneous differential equation can be expressed as a superposition of

$$y = y_c + y_p$$

where $y_p$ is a particular solution of Equation 8.1 and $y_c$ is the general solution of the homogeneous equation

$$\frac{d^4y}{dx^4} - \frac{T_h}{EI_b}\frac{d^2y}{dx^2} + \frac{k_s}{EI_b}y = 0$$

The general solution of the homogeneous equation can be written as

$$y = \sum_{n=1}^{4} \tilde{C}_n \cdot e^{(s_n \cdot x)}$$

Substituting in the homogeneous equation and following simple algebraic operations $y_c$ can be written

$$y_c(x) = c_1 e^{-\alpha x} cos(\beta x) + c_2 e^{-\alpha x} sin(\beta x) + c_3 e^{\alpha x} cos(\beta x) + c_4 e^{\alpha x} sin(\beta x)$$

where $c1$, $c2$, $c3$, and $c4$ are unknown coefficients, and

$$\alpha = \frac{1}{2}\sqrt{2\sqrt{\frac{k_s}{EI_b}} + \frac{T_h}{EI_b}} \quad and \quad \beta = \frac{1}{2}\sqrt{2\sqrt{\frac{k_s}{EI_b}} - \frac{T_h}{EI_b}}$$

Taking into account the inhomogeneous part of the solution the final expression of y becomes

$$y = D + \frac{w_s}{k_s} + c_1 e^{-\alpha x} cos(\beta x) + c_2 e^{-\alpha x} sin(\beta x) + c_3 e^{\alpha x} cos(\beta x) + c_4 e^{\alpha x} sin(\beta x)$$

It should be mentioned that, for the homogeneous equation for

$$\left(\frac{T_h}{EI_b}\right)^2 - 4\frac{k_s}{EI_b} < 0 \Rightarrow T_h < 2\sqrt{EI_b k_s}$$

no real solution can be obtained, so based on the problem the inequality

$$T_h \geq 2\sqrt{EI_b k_s}$$

have to be checked if it is satisfied.

The unknown coefficients will be found from the boundary conditions. The pipe laid on the seabed is modeled as a beam on the Winkler foundation. At long distance from TDP, the pipe on the seabed can be treated as a beam of infinite length. Considering the boundary condition at $x \to \infty$, where the embedment of pipe is only influenced by its self-weight, the value of *y* approximates the value

$$y = D + \frac{w_s}{k_s}$$

so the coefficients $c_3 \ and \ c_4$ shall be equal to zero.

$$y(x) = D + \frac{w_s}{k_s} + c_1 e^{-\alpha x} cos(\beta x) + c_2 e^{-\alpha x} sin(\beta x)$$

The displacement at y=0 can be assumed to be equal with D so

$$y(0) = D \Rightarrow c_1 = -\frac{w_s}{k_s}$$

Based on the fact that the pipeline approaches the seabed in horizontal position, angle θ=0, so

$$y'(0) = 0 \Rightarrow c_2 = \frac{\alpha}{\beta} \cdot c_1$$

So the final expression for the solution y is

$$y(x) = D + \frac{w_s}{k_s} + \left(-\frac{w_s}{k_s}\right) e^{-\alpha x} cos(\beta x) + \left(\frac{\alpha}{\beta} \cdot c_1\right) e^{-\alpha x} sin(\beta x) \qquad [\mathbf{9.2}]$$

The associated bending moment can be expressed as follows

$$M = EI_b \frac{d^2 y}{dx^2}$$

At the touchdown point, the seabed was considered to be infinitely stiff so the boundary condition was

$$B.C.: \left.\frac{d\theta}{ds}\right|_{s=0} = 0$$

Based on the Winkler model, the boundary conditions at the touchdown point (see Chapter 3.2.2) can be modified and can be expressed as follows

$$B.C.1: \theta(0) = \left.\frac{dy(x)}{dx}\right|_{x=0}$$

$$B.C.2: \left.\frac{d\theta}{ds}\right|_{s=0} = \left.\frac{d^2 y(x)}{dx^2}\right|_{x=0}$$

where function y is given by equation 7.1.

## 10.0 GENERAL CONCLUSION - RECOMMENDATIONS

The purpose of the thesis was to develop a model for accurately quantifying pipeline rotation during installation of inline structures with S-lay method. A sequential model was built based on mechanical principles and energy minimization approach in order to solve the pipelay and rotation problem simultaneously, identify the effect of plastic strains and residual curvature phenomenon and investigate rotation profile evolution during actual operations. The model includes also mitigation measures (buoyancy modules) and their effect in the reduction of total rotation as well as the effect of soil friction and applied tension.

The pipelay model, based on mechanical principles and nonlinear bending equation behaves with considerable accuracy for all the cases studied, independently of the input parameters as the water depth, the stinger configuration and for pipeline characteristics. The relatively higher errors at the boundaries (touchdown point and stinger tip) can be explained by the fact that the boundary conditions are not identical and can be improved by considering the seabed as a Winkler foundation and including in the model the overbend region respectively. The presence of these errors does affect the solution along the catenary for any of the cases studied. The model can be used for multiple pipe sections along the catenary as shown in Chapter 4.0.

The rotation problem of the pipeline was solved based on Lagrangian Minimization Method where the bending problem and the rotation problem are solved separately (decoupled system – Chapter 6.0) and based on Potential Energy Method where the two problems are solved simultaneously based on the coupled differential equations presented in Chapter 8.0. The two methods resulted in almost the same results for normal pipelay rotation problem with negligible differences for all the cases showing that the coupling has not considerable effect in the solution of the problem. Thus both of them can be used for the ILS sequential model to quantify accurately ILS rotation during installation.

Based on the above it is concluded that the model can be used as a reliable basis for the determination of pipelay and rotation quantities for pipeline and inline structure installations. The model can be easily modified with respect to the actual projects and can be further improved in order to be a fully developed tool in order to quantify rotation and ensure safety before the project execution.
Further improvements:

- Include overbend area in the model in order for the model to be fully independent of Offpipe & BendPipe.
- Consider the seabed as Winkler foundation and analyze its effect on pipelay and rotation problem.
- Include out of plane calculations of residual curvature and investigate the effect of out of plane deformations.

## 11.0 REFFERENCES


**[1]** Xia-Guang Zeng, Meng-Lan, Duan Che An, "Mathematical Model of Pipeline Abandonment and Recovery in Deepwater", Journal of Applied Mathematics, Volume 2014.

**[2]** F. Guarracino, V. Mallardo, "A refined analytical analysis of submerged pipelines in seabed laying", Applied Ocean Research 21, 1999.

**[3]** Feng Yuan, Zhen Guo, Lingling Li, Lizhong Wang, " Numerical Model for Pipeline Laying During S-lay", College of Civil Engineering and Architecture, Zhejiang University.

**[4]** Gong Shun-Feng, Chen Kai, Chen Yuan, Jin Wei-Liang, Li Zhi-Gang, Zhao Dong-Yan, "Configuration Analysis of Deepwater S-Lay Pipeline", 2011 Chinese Engineering Society and Springer, 2011.

**[5]** G.F. Clauss, H. Weede, A. Saroukh, "Offshore Pipe laying: Significance of Motions and Dynamic Stresses During Laying Operations", Technische U. Berlin, OTC 6760.

**[6]** Herman Perera, Donald Arnold, "Analytical Methods For Pipeline Installation", 21st Annual Convention Proceedings, 1992.

**[7]** SUBRATA K. CHAKRABARTI, "Handbook of Offshore Engineering" Offshore Structure Analysis, Inc. Plainfield, Illinois, USA.

**[8]** Gullik Anthon Jensen, " Offshore Pipe laying Dynamics", Doctoral thesis, Faculty of Information Technology, Mathematics, Norwegian University of Science and Technology, 2010.

**[9]** Won Young Yang, Wenwu Cao, Tae-Sang Chung, John Morris, "APPLIED NUMERICAL METHODS USING MATLAB", Wiley & Sons, Inc.

**[10]** Timmy Siauw , Alexander M. Bayen, " An Introduction to MATLAB® Programming and Numerical Methods for Engineers", Elsevier.

**[11]** L.F. Shampine, I. Gladwell, S. Thompson, "Solving ODEs with MATLAB", Cambridge University Press, 2003.

**[12]** Todd Young, Martin J. Mohlenkamp, "Introduction to Numerical Methods and Matlab Programming for Engineers", Department of Mathematics Ohio University, September 12, 2014.

**[13]** S.W. Rienstra, "Analytical Approximations for Offshore Pipe laying Problems", Mathematics Consulting Department, University of Nijmegen, The Netherlands, 1987.

**[14]** Robert C. Malathy, "OFFPIPE USER'S GUIDE, VERSION 2.05", November 1, 1996.

**[15]** A.V. Metrikine, "Dynamics, Slender Structures and an introduction to continuum Mechanics", Delft University of Technology.

**[16]** Geir Endal, Odd B. Ness and Richard Verley, “Behaviour of offshore pipelines subjected to residual curvature during laying ”, Statoil, Norway 1995 OMAE – Volume V, Pipeline Technology

**[17]** F.P. van der Meer : "Stability of Structures", CIE 5144 Lecture Notes, June 21, 2015

## APPENDIX A. Terminology

During pipelay operations specific terminology is used to clarify parts and angles of the pipe, stinger and barge.

**Tensioners**

Tensioners are the main element of the pipelay system. Their function is to hold the pipe in suspension between the end of the stinger and the seabed, by applying a constant tension to the pipe.

**Firing Line**

The firing line is the main line from where the pipe joints pass before they leave the vessel. It contains the welding, coating and non-destructive testing stations.

**Stinger**

Stinger is a steel construction attached on the end of the firing line on the front or stern of the vessel. The purpose of the stinger is guiding the pipeline in a pre-determined curve through the water to the seabed.

**Stinger radius**

The stinger radius is the radius of a circle formed by the pipe supports on the stinger.

**Lift-off point**

The lift-off point is the point from where the pipeline is no longer in contact with rollers on the stinger.

**Lift-off angle**

Is the angle of the pipeline, relative to the horizontal plane, at the point where the pipe is no longer in contact with the rollers on the stinger.

**Departure angle**

Is the angle of the pipeline, relative to the horizontal plane, at the stinger tip.

**Overbend**

Overbend is called the pipeline section where the pipe is bent up toward the sea surface. At the overbend region the pipe is guided by the stinger.

**Sagbend**

Sagbend is called the pipeline section where the pipe is bent down toward the seabed (part of the pipeline in suspension). This is between the inflection point and the touchdown point.

**Inflection point**

It is the transition point between the overbend of the pipeline and the suspended pipeline in the sagbend. At the inflection point the moment in the pipeline is zero.

**Bottom tension**

The bottom tension is the axial tension in the section of the pipeline where it touches the seabed.

**Touchdown point**

The touchdown point is the point where the pipeline touches the seabed.

**Vessel Force**

The vessel force, applied from the thrusters, is the force necessary to keep the pipeline under tension. This force is equal to the bottom tension.

## APPENDIX B. Comparison of main pipelay quantities (4 cases studied)

- **Case Study N°1**

The figures below show the evolution of axial tension and sagbend strains (total, bending, tensile) along the catenary for case study N°1.

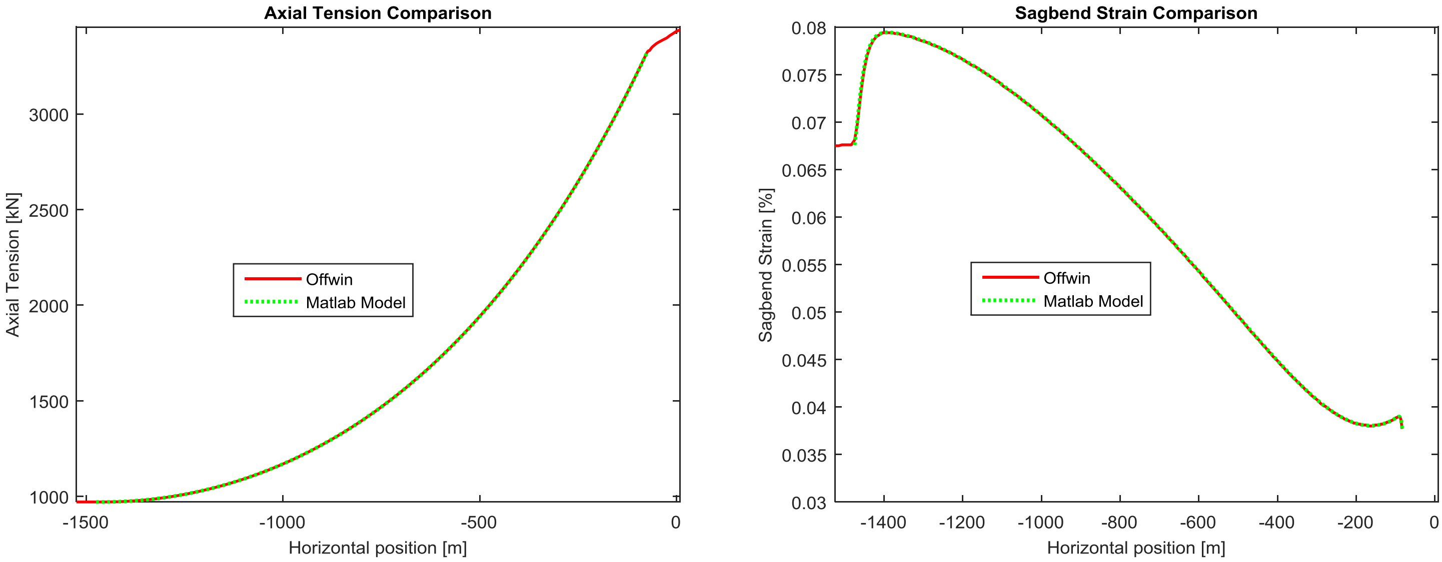


**Figure 11-1 Comparison of axial tension and sagbend strain along the catenary**

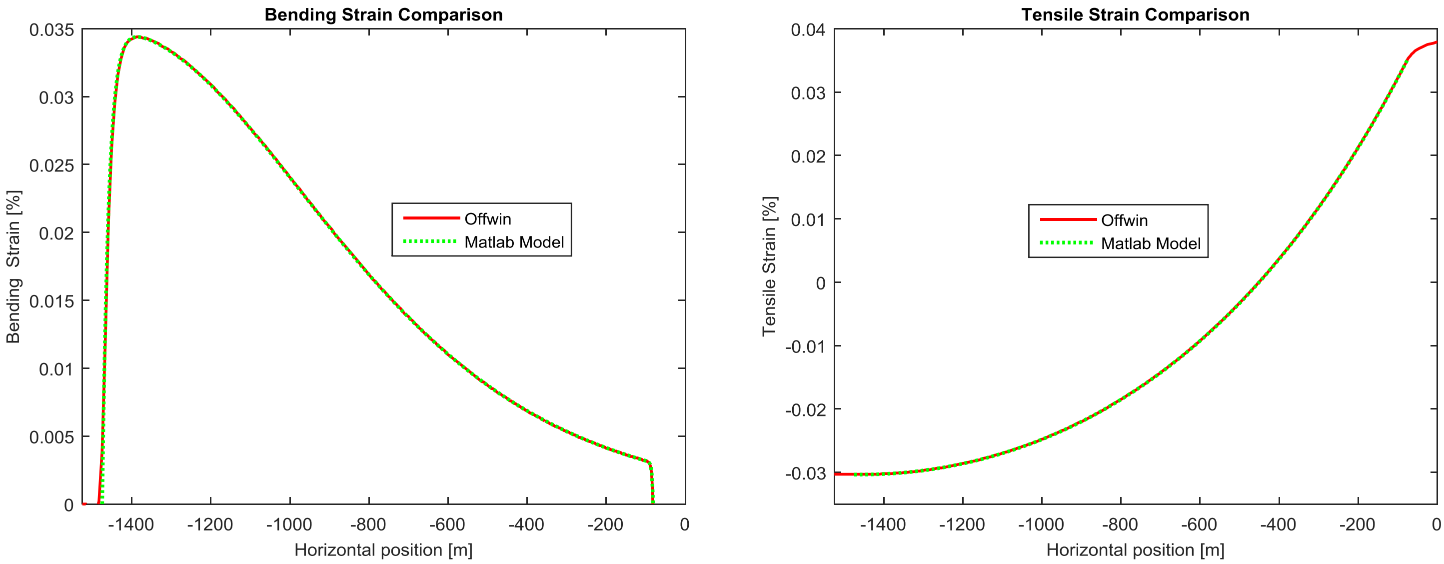


**Figure 11-2 Comparison of bending and tensile strain along the catenary**

As it can be seen Matlab model and Offwin results are in accordance both for the tension and for the strains evolution along the catenary. The negligible difference that can be seen at touchdown point for the bending (and as a consequence at the total strain) can be explained by the boundary condition that considers the seabed to be infinitely stiff.

- **Case Study N°2**

The figures below show the evolution of axial tension and sagbend strains (total, bending, tensile) along the catenary for case study N°2.

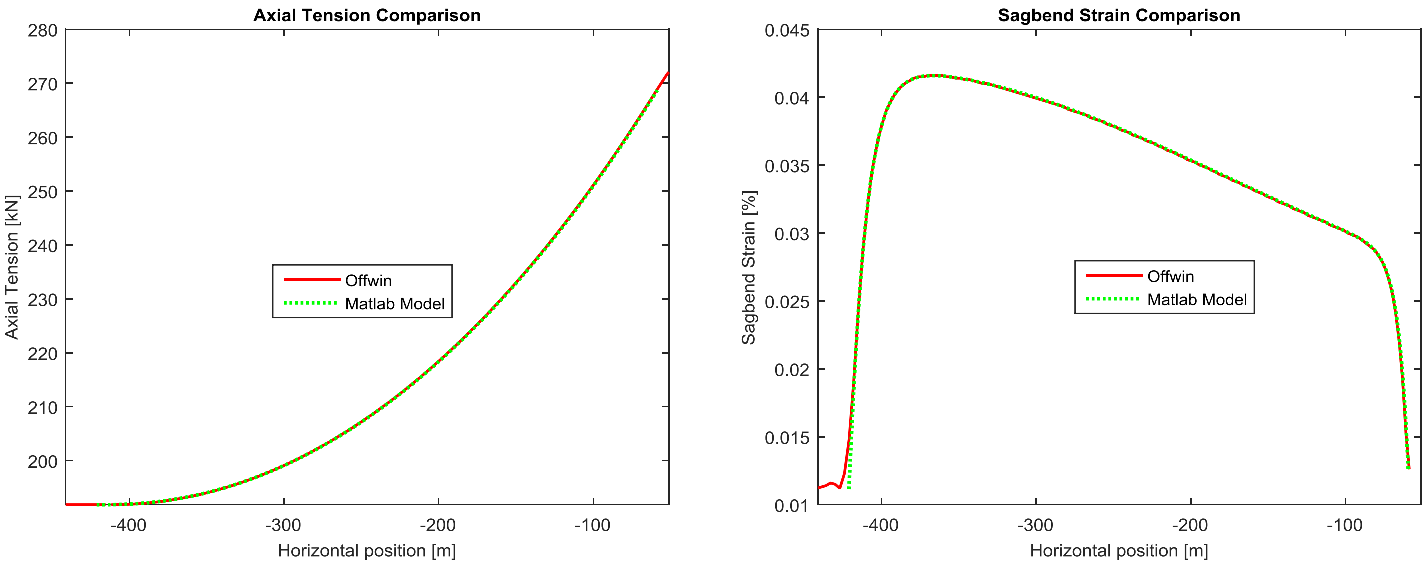


**Figure 11-3 Evolution of axial tension and sagbend strain along the catenary**

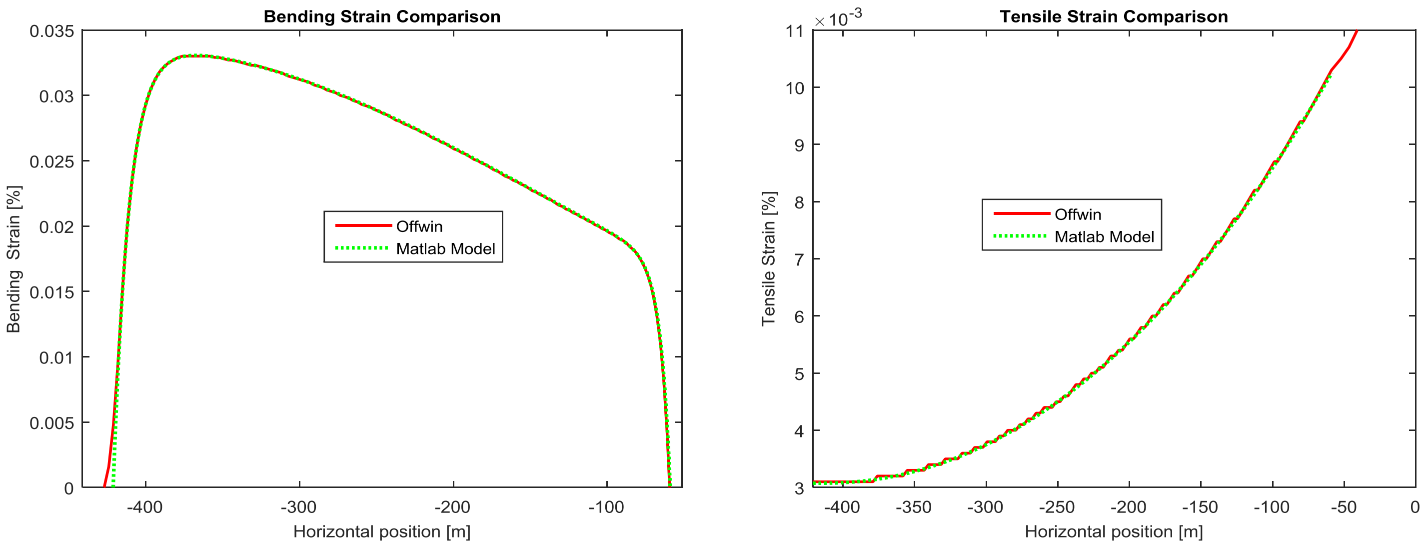


**Figure 11-4 Comparison of bending and tensile strain along the catenary**

As it can be seen from the figures above the evolutions of the axial tension and the strains are the same along the catenary. The steps that can be seen in tensile strain values of Offwin are present because of rounding to the 4th decimal from Offwin model.

- **Case Study N$^o$3**

The figures below show the evolution of axial tension and sagbend strains (total, bending, tensile) along the catenary for case study N$^o$3.

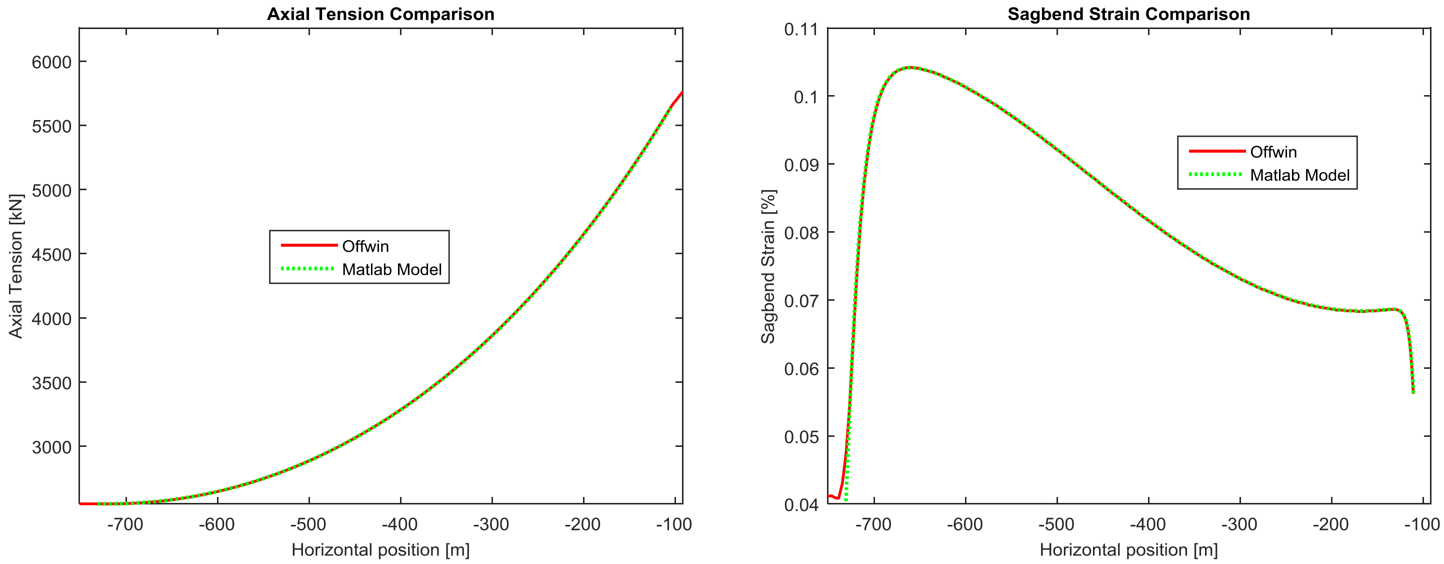


**Figure 11-5 Evolution of axial tension and sagbend strain along the catenary**

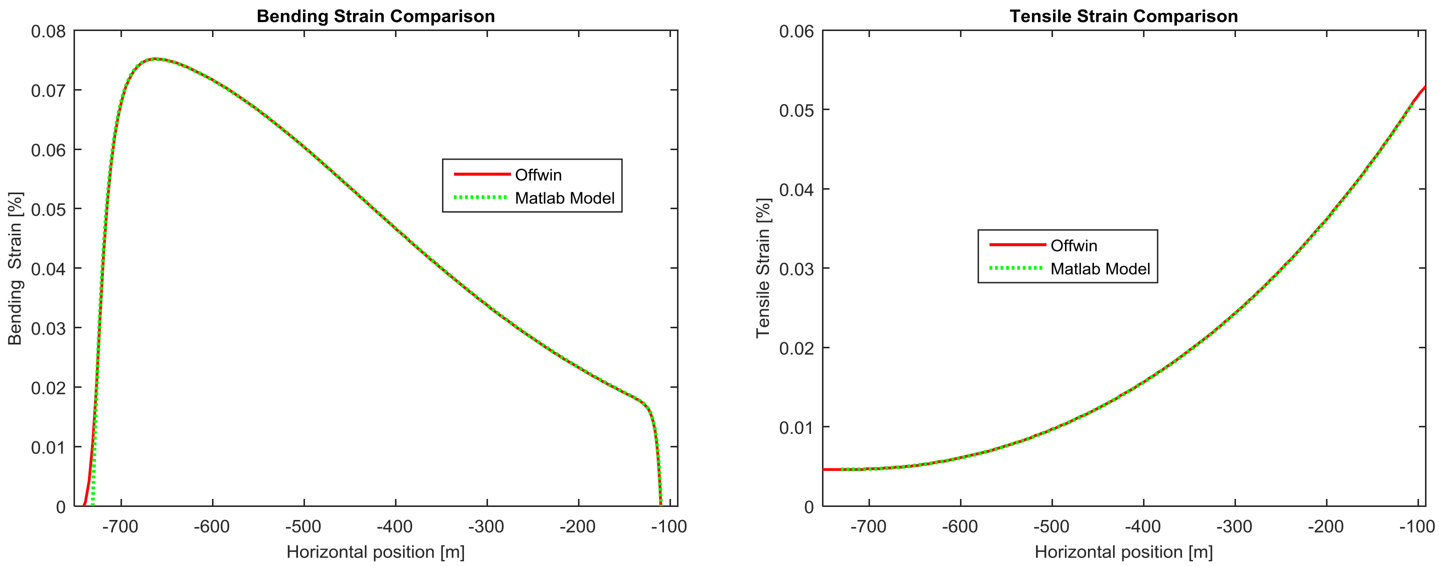


**Figure 11-6 Comparison of bending and tensile strain along the catenary**

- **Case Study N°4**

The figures below show the evolution of axial tension and sagbend strains (total, bending, tensile) along the catenary for case study N°3.

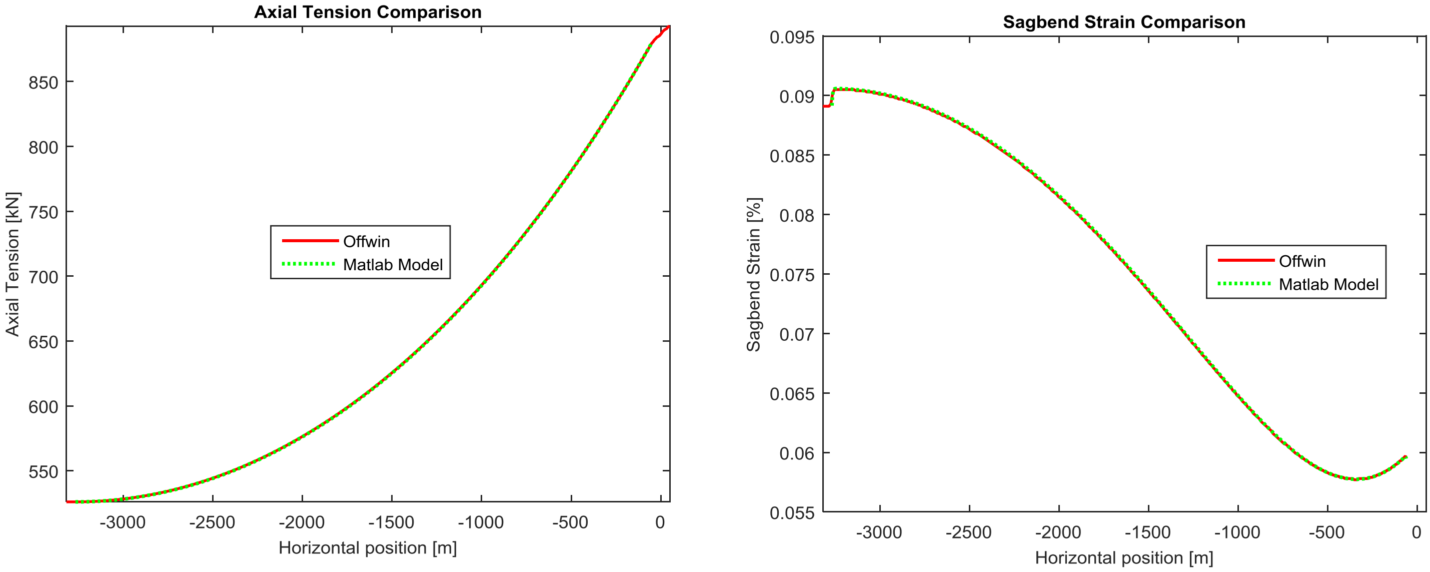


**Figure 11-7 Evolution of axial tension and sagbend strain along the catenary**

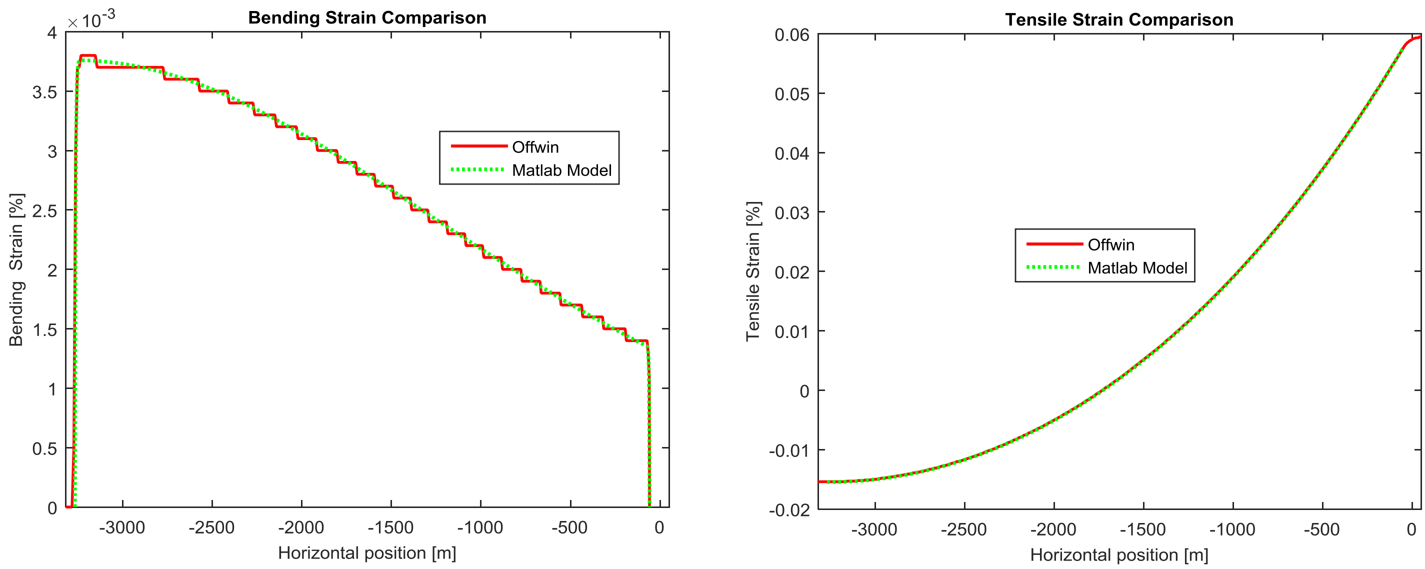


**Figure 11-8 Comparison of bending and tensile strain along the catenary**

As it can be seen from the figures above the evolutions of the axial tension and the strains are the same along the catenary. The steps that can be seen in bending strain values of Offwin are present because of rounding to the 4th decimal from Offwin model.